TWO COMPONENT FLUIDIZATION

by

Brian P. Le Clair
B.A.Sc., University of British Columbia, 1962

A THESIS SUBMITTED IN PARTIAL FULFILMENT OF THE

REQUIREMENTS FOR THE DEGREE OF

MASTER OF APPLIED SCIENCE

in the Department of

CHEMICAL ENGINEERING

We accept this thesis as conforming to the

required standard

Members of the Department of
Chemical Engineering

THE UNIVERSITY OF BRITISH COLUMBIA

January, 1964

In presenting this thesis in partial fulfilment of the requirements for an advanced degree at the University of British Columbia, I agree that the Library shall make it freely available for reference and study. I further agree that permission for extensive copying of this thesis for scholarly purposes may be granted by the Head of my Department or by his representatives. It is understood that copying or publication of this thesis for financial gain shall not be allowed without my written permission.

Department of CHEMICAL ENGINEERING

The University of British Columbia,
Vancouver 8, Canada.

Date Jan. 10, 1964

Abstract

Studies were made of the distribution of components, when two materials are fluidized in a liquid. The hypothesis tested was that the distribution of material is a function of the bulk density difference of the component beds. The component bed having the greatest bulk density will occupy the bottom of the total bed. It is possible for the bulk density of one material to be greater than the other at low velocities, and less than the other at high velocities. At some intermediate condition the bulk density difference between the two beds must be zero. This situation, called the inversion point, produces homogeneous mixing of the two components.

Mixtures of two materials for which an inversion was predicted by the stated hypothesis were tested. In the intermediate and turbulent flow regions inversions did not occur because macroscopic mixing destroyed the bulk density gradients being established. However, in the laminar flow region, where mixing was negligible, inversions did occur.

The quality of the inversion was affected as follows. For a sharp clear inversion of the two materials at the predicted velocity, the diameter ratio of the two groups of particles must be much greater than one and the density ratio (corrected for buoyancy) of the two groups of particles must be much less than one. Also of importance is the absolute density (corrected for buoyancy) of the particles.

Particle size distribution also appeared to strongly affect the quality of the inversion. These distributions set up bulk density gradients within the single component beds. This appeared to cause mixing of the two components and in some cases even formation of the two inverted beds before the predicted inversion velocity was reached.

The prediction of the bed expansion of mixtures was also studied. A correlation was developed on the assumption that each component of the mixture could be treated separately. The overall expansion thus would be the sum of the expansions of the individual components. There was very good agreement between values predicted by this method and experimental data. The method predicted expansion well for all degrees of mixing of the two components, but did not predict well when one of the components was near its minimum porosity for fluidization.

The empirical equations of Richardson and Zaki (4) for single component liquid fluidization expansions were checked. The values of the index "n" obtained from experimental data agreed within $\pm$ 5% of those calculated using the correlations. The equation developed by Richardson and Zaki for determining the free settling velocity of a single particle from extrapolated expansion data gave results which were within $\pm$ 15% of those obtained using the standard drag coefficient-Reynolds number plot for an isolated sphere.

Acknowledgement

I am indebted to Dr. Norman Epstein, under whose guidance this study was made, for his encouragement and assistance during the course of this project.

The assistance of Mr. R. Muelchen and the Workshop staff is appreciated for their proficiency at building the equipment to the specifications required.

I also wish to thank the National Research Council of Canada for financial assistance received, and the Department of Chemical Engineering at U.B.C. for additional support.

Table of Contents

Tables

List of Illustrations

Nomenclature

A - cross-sectional area of column, $ft.^2$

b' - index in Lewis and Bowerman equation, dimensionless.

C' - modified orifice meter coefficient, $\frac{\mu}{\rho}\sqrt{\frac{\rho}{p_1 - p_2}}$, where μ is in centipoises and the rest engineering units.

C" - modified orifice meter coefficient, $\frac{\mu}{\rho}\sqrt{\frac{\rho}{p_1 - p_2}}$, all engineering units.

D - column diameter, ft.

d - average particle diameter, ft., mm.

F_g - gravitational force, lb-force.

F_D - drag force, lb-force.

g - acceleration of gravity, $ft./sec.^2$

g_c - Newton's law conversion factor, (ft.) (lb.)/(lb-force) $(sec.^2)$

k - variable constant, dimensionless.

k' - constant in Lewis and Bowerman equation, dimensionless.

k" - constant containing liquid properties and k, $\frac{kg^{1/m}}{\rho^{(m-1)/2}\,\mu^{2-m}}$, dimensional.

L - vertical distance in a fluidized bed, ft.; vertical distance between a base position in the bed and an elevated position, ft.

M - weight of solid particles in a fluidized bed, lbs.

m - state-of-flow-index, dimensionless.

n - Richardson and Zaki index, dimensionless.

p - fluid pressure, $lb\text{-force}/ft.^2$

Δp_F - frictional pressure loss in a fluidized bed, $lb\text{-force}/ft.^2$

P - P ratio, $(\Delta p_F/L)_1/(\Delta p_F/L)_{theoretical}$, dimensionless.

Q - volumetric flow rate, $ft.^3/sec.$

R_e - particle Reynolds number, $\frac{dV_s\rho}{\mu}$, dimensionless.

r - particle diameter ratio, d_1 / d_2 , dimensionless.

t - time of efflux for fluid in viscometer tube, sec. .

V - velocity of fluid, ft./sec. .

V_o - free settling velocity of a particle, ft./sec. .

V_i - superficial liquid velocity when Richardson and Zaki plot is extrapolated to $\epsilon = 1.0$, ft./sec. .

V_p - velocity of particle in a fluidized bed, ft./sec. .

V_s - superficial liquid velocity, ft./sec.

V_{slip} - slip velocity between particle and fluid, ft./sec. .

v - volume of a fluidized bed fraction, $ft.^3$.

v_T - total volume of fluidized bed, lbs. .

W_m - weight of solids mixture in fluidized bed, lbs. .

w - weight of a specific fraction of solids in fluidized bed, lbs. .

γ - density corrected for buoyancy ratio, $(\rho_{s1} - \rho)/(\rho_{s2} - \rho)$, dimensionless.

ϵ - porosity of fluidized bed, dimensionless.

ϵ_{mf} - minimum porosity for fluidization, dimensionless.

ϵ_m - average porosity of mixture, dimensionless.

μ, μ_f - viscosity of fluid, lb./(ft.)(sec.) .

μ_ϵ - viscosity of fluidized suspension, lb./(ft.)(sec.) .

ρ, ρ_f - density of fluid $lb./ft.^3$.

ρ_ϵ - density of fluidized suspension, $lb./ft.^3$.

ρ_B - bulk density of fluidized bed, $lb./ft.^3$.

ρ_s - density of solid particles, $gm./cm.^3$, $lbs./ft.^3$.

ϕ - weight fraction of a solid component of a mixture.

subscripts

1, 2, A, B - specific fluidized beds of particles; 1 and 2 also denote upstream and downstream taps, respectively, on flowmeters.

i - any individual fluidized bed fraction.

O - free settling conditions.

F - frictional; also denotes gravitational units of force.

T - test section based on empty tube.

INTRODUCTION

Fluidization is a process widely used in industry, but the theory and techniques for design of liquid fluidization equipment and processes are not fully understood at the present time. Thus a sound program based on theoretical development and experimentation must be carried out to develop reliable design criteria.

The present work was formulated to study liquid fluidization of two component mixtures of solids, for example, a mixture of lead and steel fluidized by water. The two materials would have specified diameter and density ratios such that inversion of the materials will occur at some overall porosity above the minimum fluidization porosity.

Consider a fluidized bed composed of material A and material B such that $\rho_{SA} > \rho_{SB}$ and $d_B > d_A$. For particular ratios of ρ_{SA}/ρ_{SB} in conjunction with specified ratios of d_B/d_A, the fluidized bed will respond in the following way to changes in superficial liquid velocity. At low flow rates the fluidized bed will be made up of two layers, one above the other, such that all the heavy small particles will form a fluidized assemblage at the bottom of the column quite distinct from the light large ones which have formed an assemblage above the small heavy particles. Similarly at high velocities the fluidized bed will again be composed of two distinct strata, but now the large light particles will be at the bottom and the heavy small particles will be at the top of the bed. At some intermediate velocity between the two extremes inversion occurs. The inversion mode has been defined as the point of changeover, or the point of homogeneous fluidization of the two species of particles.

Inversion of the sort described above can occur because of the nature of particulate fluidization. Wilhelm and Kwauk (1) have described

particulate fluidization, usually but not always synonymous with liquid fluidization, as characterized by the separation of individual particles much in the manner of a gas. A mean free path can be observed, and the length of the path is found to increase with velocity." Thus liquid fluidization is observed to be an ordered expansion of the particles in the bed, without rapid large scale circulation and mixing of particles. Because of this, the position of the particles in a fluidized bed will be governed almost exclusively by drag and gravitational forces, on which the inversion phenomenon is based.

Qualitative observations of inversions have been described by two earlier workers, namely, Hancock (2) and Jottrand (3). Hancock (2) in 1936 discussed and described inversions of the type described above. The observations made were:

(1) At similar velocities in a column of fluidized mixed sands, the bulk density, ρ_B , developed by the bed increases from the top downwards, whereas with a uniform sand the bulk density is uniform down the bed.

(2) If one uniform sand has a particular bulk density at a particular liquid velocity, then it is possible for another uniform sand of a different solid density to develop the same bulk density at the specified liquid velocity if the size of its particles is suitably related to the particle size of the former particles.

(3) When two uniform sands develop the same bulk densities at a particular liquid velocity, the total mixture behaves as one uniform bed.

Jottrand (3) has observed a similar phenomenon but, as with Hancock, no quantitative measurements were recorded. In Jottrand's work a special case involving one component fluidized and the other unfluidized is reported. The conclusion drawn by Jottrand was, however, equivalent to

that drawn by Hancock, namely that, the primary factor governing classification in fluidized beds is the average bulk density developed by each of the components of the mixture fluidized seperately.

In order to correlate data obtained on two component fluidization, the literature was searched to determine the best method for measuring particle concentrations at various locations in the bed. Most liquid fluidization data have been correlated by bed expansion (ϵ vs. V_s) and differential pressure gradient ($\Delta p_F / L$ vs. V_s) through the bed. Analysis showed that the bulk density difference between two sections of a bed was equivalent or at least proportional to the difference in differential frictional pressure gradient between the sections. Therefore measurements of frictional pressure loss profiles could be used to determine bulk density profiles and hence longitudinal particle distributions, in a fluidized bed.

THEORY

A. Free Settling Velocity of a Particle

If a particle is falling under the influence of gravity in a fluid medium, the particle will accelerate to a constant terminal velocity, V_o. This velocity is dependent on the diameter, shape and density of the particle and the properties of the fluid through which it is falling. The constant terminal velocity will be achieved when the buoyancy-corrected gravitational accelerating force, F_g, is counterbalanced by the resisting upward drag force, F_d. For spheres,

$$F_g = \frac{\pi}{6} d^3 (\rho_s - \rho) g_c \qquad 1$$

and

$$F_D = \frac{1}{8} C_D \rho \pi d^2 V^2 \qquad 2$$

On equating F_g and F_D of equations 1 and 2, the drag coefficient, C_D, is then given by

$$C_D = \frac{4 d g_c (\rho_s - \rho)}{3 V_o^2 \rho} \qquad 3$$

The particle drag data can be represented in terms of a plot similar to the friction factor - Reynolds number plot for presenting pipeline pressure drop data. The drag coefficient is plotted against the Reynolds number based on a characteristic particle dimension and on the relative velocity between the particle and the fluid medium. The drag coefficient - Reynolds number curve has been divided into three regions, the Stokes' Law or laminar range, the intermediate region, and the Newton or turbulent region. In each region the curve has been approximated by a straight line. For the individual ranges C_D may be approximated as follows.

Stokes' Region

$$Re_0 < 0.3$$

$$C_D = 24/Re \qquad 4$$

$$V_0 = \frac{g(\rho_s - \rho)\, d^2}{18\mu} \qquad 5$$

Intermediate Region

$$0.3 < Re_0 < 500$$

$$C_D = 18.6\, Re^{-0.6} \qquad 6$$

$$V_0 = \frac{0.152\, d^{1.14} g_c^{0.714} (\rho_s - \rho)^{0.714}}{\mu^{0.428}\, \rho^{0.285}} \qquad 7$$

Newton Region

$$500 < Re_0 < 500{,}000$$

$$C_D = 0.44 \qquad 8$$

$$V_0 = \left[\frac{3\, g_c d\, (\rho_s - \rho)}{\rho}\right]^{0.5} \qquad 9$$

Generalizing, it can be stated that the drag force F_D is given by the following equation:

$$F_D = k\, V_0^m d^m \mu^{2-m} \rho^{m-1} \qquad 10$$

At low values of Reynolds number, where fluid resistance is independent of density, m equals 1.0, but this index increases to 2.0 at high values of the Reynolds number, where fluid resistance is independent of viscosity. Equating equations 1 and 10, we obtain a generalized equation for the free settling or terminal velocity of fall of a particle:

$$V_0 = \frac{k(\rho_s - \rho)^{1/m} d^{(3-m)/m} g^{1/m}}{\rho^{(m-1)/2} \mu^{2-m}} \qquad 11$$

The constant, k, in the equation varies from $\frac{1}{18}$ in the Stokes' region to $\sqrt{\frac{4}{3} \times \frac{1}{0.44}}$ in the Newton region, for a spherical particle.

B. Bed Expansion Correlations

Numerous equations have been developed for correlating bed expansion data, but there does not seem to be much agreement among workers as to which correlation is best. At the present time, the most comprehensive and easiest correlations to apply are the simple power functions relating porosity and superficial liquid velocity. Various studies reported in the literature on the velocity - voidage relationship in multiparticle systems are analysed in the following sections.

Happel (6) developed an equation for expansion relationships, by using the Navier-Stokes' equations without the inertial terms to describe the motion of multiparticle systems. The model of a fluidized or sedimenting bed was that of a number of cells, each consisting of a spherical particle at the center enclosed by a spherical envelope of fluid. The volume of fluid within the envelope was such that the porosity of a cell was equal to the overall porosity of the bed, and the envelope itself was assumed to behave like a free surface. That is, to obey the condition of zero shear stress at the fluid-fluid boundary. Disturbances caused by particles were confined to the cell in which they were associated. The relationship developed on these postulates is given by

$$\frac{V}{V_0} = \frac{3 - 4.5(1-\epsilon)^{1/3} + 4.5(1-\epsilon)^{5/3} - 3(1-\epsilon)^2}{3 + 2(1-\epsilon)^{5/3}} \qquad 12$$

This equation provides good agreement with experiment at very high and very low voidage, and at low Reynolds numbers, but is poor outside of these regions.

Hawksley (7) developed an equation based on the following proposals: (1) What is important is not the fluid density or viscosity but the suspension density and viscosity. (2) The relative velocity between fluid and particles is V_s/ϵ . Thus the fluidized bed density and viscosity are given by the following equations:

$$\mu_\epsilon = \mu_f \exp\left[4{\cdot}1(1-\epsilon)/(0{\cdot}64+\epsilon)\right] \qquad 13$$

$$\rho_\epsilon = \rho_s(1-\epsilon) + \epsilon\rho_f \qquad 14$$

Substitution of equations 13 and 14 into the Stokes' Law equation gives

$$V_s = \frac{(\rho_s-\rho)gd^2\epsilon^2}{18\mu \exp\left[4{\cdot}1(1-\epsilon)/(0{\cdot}64+\epsilon)\right]} \qquad 15$$

so that

$$\frac{V_s}{V_0} = \frac{\epsilon^2}{\exp\left[4{\cdot}1(1-\epsilon)/(0{\cdot}64+\epsilon)\right]} \qquad 16$$

The agreement of this equation with experimental data is again good at low Reynolds numbers but not at high Reynolds numbers.

Richardson and Zaki (4) have developed an equation based on the dynamic equilibrium of individual particles as a function of the fluidized bed and apparatus properties. The equation is based on a dimensional analysis development to determine the variables which are important and how they are grouped, and a comprehensive group of experiments to determine the powers on the various functional groups. Dimensional analysis anticipated the following groupings:

$$\frac{V_s}{V_o} = f\left[\frac{dV_s\rho}{\mu}, \frac{d}{D}, \epsilon\right] \qquad 17$$

The expansion equation developed was the following:

$$\frac{V_s}{V_i} = \epsilon^n \qquad 18$$

where V_i is the velocity obtained by extrapolating the log-log plot of superficial liquid velocity versus porosity to a porosity of one. The power n is a function of both the flow regime and the apparatus:

$$n = 4{\cdot}65 + 19{\cdot}5(d/D) \qquad Re_o < 0{\cdot}2 \qquad 19$$

$$n = \left[4{\cdot}45 + 18(d/D)\right] Re_o^{-0{\cdot}1} \qquad 0{\cdot}2 < Re_o < 200 \qquad 20$$

$$n = 4{\cdot}45\, Re_o^{-0{\cdot}1} \qquad 200 < Re_o < 500 \qquad 21$$

$$n = 2{\cdot}39 \qquad Re_o > 500 \qquad 22$$

Also, it has been shown by Richardson and Zaki that the following relationship holds:

$$\log V_o = \log V_i + d/D \qquad 23$$

The correlations of Richardson and Zaki have been subjected to rigorous tests by comparing them with extensive liquid fluidization data from numerous literature sources. Excellent agreement has been obtained, according to Leva (5). These correlations are the most reliable method of predicting expansion of liquid fluidized beds and are valid virtually up to $\epsilon = 1.0$.

Lewis and Bowerman (8) developed an equation of the form

$$\frac{V_s}{\epsilon} = V_0(k'\epsilon^{b'}) \qquad 24$$

where k' and b' are specific constants. This equation is intended to take into account the effects that particles may exert on each other. As these effects should decrease as interparticle spaces increase, the occurrence of bed voidage in the relationship shown above appears to be reasonable. In the absence of wall effect, when according to equation 23 $V_0 = V_i$, equation 24 is obviously equivalent to equation 18 with b' equal to n-1.

C. Frictional Pressure Drop in a Fluidized Bed

The frictional pressure drop relationship in a fluidized bed is developed from the supposition that the particles in a fluidized bed are entirely supported by the fluid. That is, the weight gradient of the solid bed is equal to the frictional pressure gradient through the bed caused by mass flow:

$$\Delta p_F = \frac{M g}{A \rho_s g_c} (\rho_s - \rho) \qquad 25$$

or

$$\frac{\Delta p_F}{L} = (\rho_s - \rho)(1 - \epsilon)\frac{g}{g_c} \qquad 26$$

These equations were experimentally corroboratedfor numerous solids fluidized in liquids by Wilhelm and Kwauk (1). Most of Wilhelm and Kwauk's data agree with the theoretical equation within 5%. The results of Richardson and Zaki (4) tend to indicate that the above equation holds for beds composed of particles which have a relatively low density and in which the particle to column diameter ratio is small.

For beds composed of large particles or very heavy particles, channeling, bridging and other aggregative effects occur and equation 26 does not agree too well with experiment. Figure 1 shows a graph relating the frictional pressure drop across a particulately fluidized bed with velocity through the bed. Also shown is a diagram of the pressure drop per unit length through a fluidized bed.

D. Stratification and Classification

An important problem which had not been worked on extensively in the past is stratification and classification in particulately fluidized beds composed either of one material or of a number of materials. Work in the field of stratification by size is being carried on at the present time in this department and should provide some useful information.

Richardson and Zaki (4) showed that if a fluidized bed is composed of particles of two distinct size ranges, then the small particles will form a bed on top of the bed of large particles, and there will be a distinct interface between the two beds. In a fluidized bed composed of a continuous range of particle sizes the solids will tend to arrange themselves so that the greatest amount of fines will be in the upper part of the bed. Verschoor (9) observed that stratification of particles will occur even for very narrow size ranges (100 to 120 mesh). Andrieu (10) systematically studied stratification by size in water-fluidized beds and found that the porosity of the fluidized bed increased from the bottom to the top of the fluidized bed, a conclusion which he deduced from the observed decrease in the pressure gradient and hence the apparent or bulk density of the fluidized bed. This finding is consistent with Hancock's (2) first observation, previously discussed.

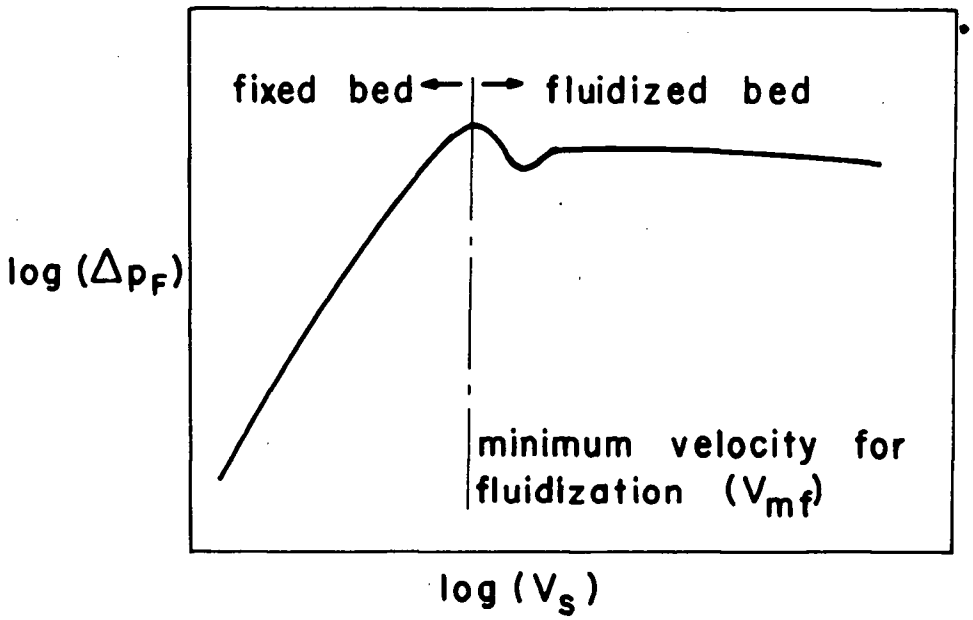

Figure 1a. Typical Fluidization curve relating frictional pressure loss across fluidized bed to superficial liquid velocity.

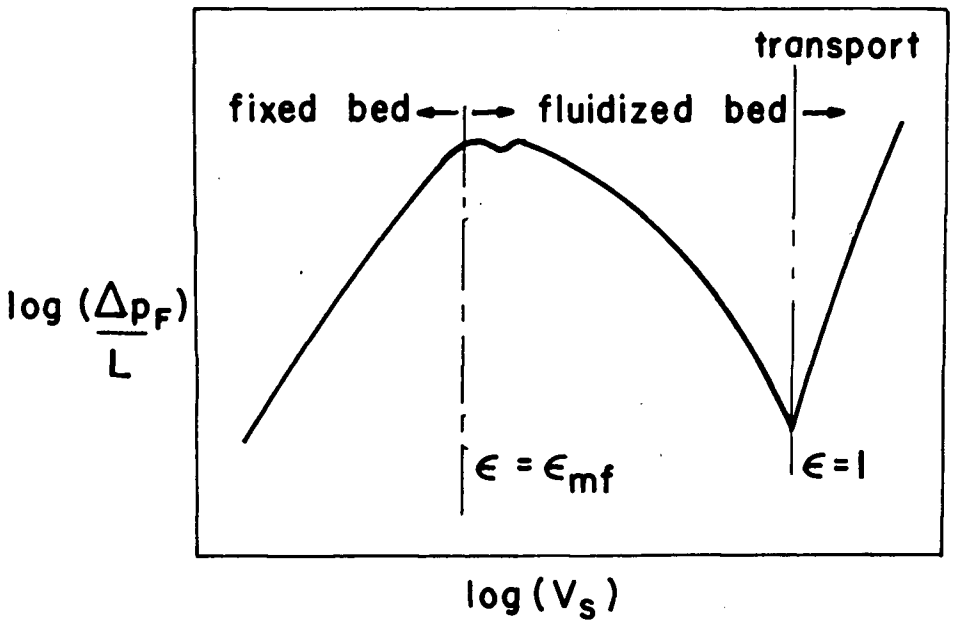

Figure 1b. Typical fluidization curve relating frictional pressure loss per unit height across a bed of particles to superficial liquid velocity.

E. Theoretical Derivation for Inversion

The driving force for segregation or stratification of two groups of particles in a particulately fluidized bed is assumed to be the difference in bulk density of the beds formed by each group of particles when they are individually subjected to the given superficial liquid velocity. The bulk density of a fluidized bed is given by

$$\rho_B = (1-\epsilon)\rho_s + \epsilon\rho \qquad 27$$

The difference in bulk density between two beds composed of particles 1 and 2, respectively, is therefore

$$\rho_{B1} - \rho_{B2} = (1-\epsilon_1)(\rho_{s1}-\rho) - (1-\epsilon_2)(\rho_{s2}-\rho) \qquad 28$$

Many bed expansion functions exist, but the simplest equation and that which represents empirical data best over the whole range encountered is that of Richardson and Zaki (4), which is

$$V_s = V_i\,\epsilon^n \qquad 29$$

or from equation 23,

$$V_s = 10^{-d/D} V_0\,\epsilon^n \qquad 30$$

The free settling velocity is given by equation 11, which is

$$V_0 = k''(\rho_s-\rho)^{1/m}\, d^{(3-m)/m} \qquad 31$$

Combining equations 30 and 31,

$$V_s = 10^{-d/D}\, k''(\rho_s-\rho)^{1/m}\, d^{(3-m)/m}\, \epsilon^n \qquad 32$$

As particles 1 and 2 are subjected to the same superficial liquid velocity, it follows that

$$k_1'' 10^{-\frac{d_1}{D}} (\rho_{s1}-\rho)^{\frac{1}{m_1}} d_1^{\frac{3-m_1}{m_1}} \epsilon_1^{n_1} = k_2'' 10^{-\frac{d_2}{D}} (\rho_{s2}-\rho)^{\frac{1}{m_2}} d_2^{\frac{3-m_2}{m_2}} \epsilon_2^{n_2} \qquad 33$$

If the assumption is made that both groups of particles fluidized within the same flow régime, that is, in a given region of Re_o (e.g. the Stokes' region or the Newton region), then $k_1'' = k_2''$, $m_1 = m_2$ and $n_1 = n_2$. These conditions can be approximately produced experimentally. Also if it can be assumed that the particles are small relative to the column diameter, then $10^{(d_2-d_1)/D^n}$ is equal to 1.0 approximately. Simplifying equation 33 accordingly,

$$\epsilon_2 = \epsilon_1(\gamma)^{1/mn}(r)^{(3-m)/mn} \qquad 34$$

where $\gamma = (\rho_{s1}-\rho)/(\rho_{s2}-\rho) \quad < 1$, and $r = d_1/d_2 \quad > 1$.

Substituting equation 34 back into 28 we have

$$\rho_{B1}-\rho_{B2} = (\rho_{s1}-\rho)\left[(1-\frac{1}{\gamma}) - \epsilon_1(1-\frac{r^{(3-m)/mn}}{\gamma^{(mn-1)/mn}})\right] \qquad 35$$

Inspection of equation 35 will reveal the following information:

(1) suppose that

$$1-\frac{1}{\gamma} < \epsilon_1(1-\frac{r^{(3-m)/mn}}{\gamma^{(mn-1)/mn}}) \qquad 36$$

The bulk density of bed 1 will then be less than the bulk density of bed 2, and the latter will occupy the bottom section of the column with bed 1 above it. This is classification by density.

(2) suppose that

$$1-\frac{1}{\gamma} > \epsilon_1(1-\frac{r^{(3-m)/mn}}{\gamma^{(mn-1)/mn}}) \qquad 37$$

The bulk density of bed 2 will be less then the bulk density of bed 1, and thus bed 2 will occupy the top of the column with bed 1 in the bottom section.

(3) suppose that

$$1 - \frac{1}{\gamma} = \epsilon_1 \left(1 - \frac{r^{(3-m)/mn}}{\gamma^{(mn-1)/mn}}\right) \qquad 38$$

The bulk density of bed 1 equals the bulk density of bed 2 and according to Hancock (2) there should be perfect mixing of the two sets of particles, producing one homogeneously fluidized bed. If this condition holds at a particular value of ϵ_1 , then for values of ϵ_1 less then this value, situation 1 will occur and bed 2 will be at the bottom and bed 1 at the top. Similarly for values of ϵ_1 greater than this particular ϵ_1 , situation 2 will occur. These situations are represented diagramatically by figure 2.

For situation 3 to occur, the bulk density difference must be equal to zero, and therefore by equation 35,

$$\epsilon_1 = \frac{1 - \gamma}{\gamma^{1/mn} r^{(3-m)/mn} - \gamma} \qquad 39$$

The corresponding value of ϵ_2 for this particular value of ϵ_1 is given by equation 34, or by applying the condition of zero bulk density difference to equation 28, which then simplifies to

$$\epsilon_2 = 1 - \gamma(1 - \epsilon_1) \qquad 40$$

Since the void fraction in a particulately fluidized bed can vary only from ϵ_{mf} to 1, a reversal from sorting to sizing will occur in such a

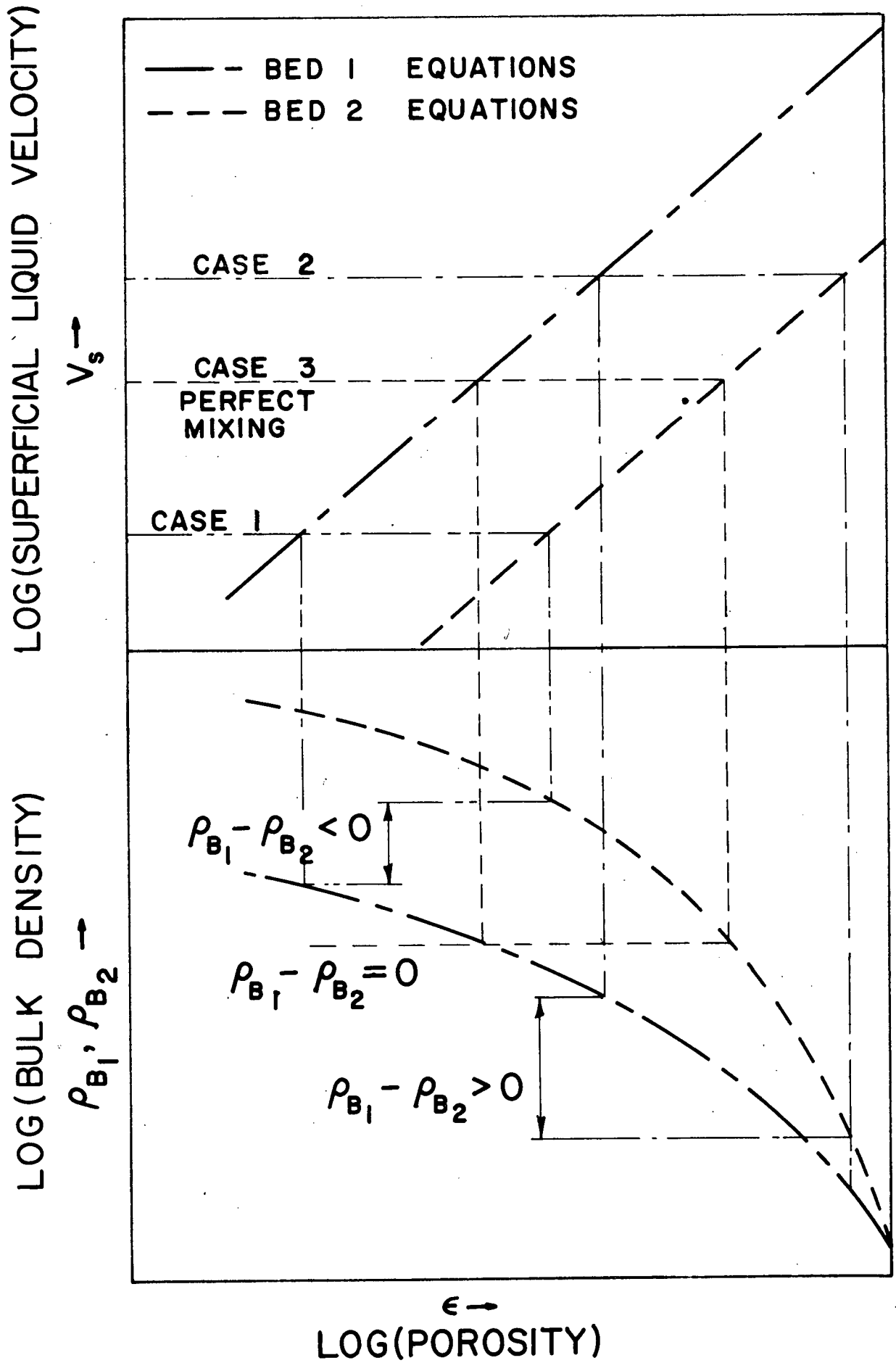

Figure 2. Prediction of Fluidized Bed Inversion

bed during its expansion only if r and γ are such that

$$\epsilon_{mf} < \epsilon_1 < \epsilon_2 < 1$$

where ϵ_1 and ϵ_2 are calculated from equations 39 and 34 (or 40) respectively. Beare (11) has produced a plot for the laminar or Stokes' region (m=1, n=4.65) relating inversion conditions with particular values of r and γ. This plot is given in Appendix I. A similar plot also appears for the Newton region (m=2, n=2.39) which can be compared to the laminar plot.

F. Mixed Bed Height Predictions

Numerous workers have correlated liquid fluidized bed expansion equations for uniform particles, but very little work has been done on correlating expansion data for fluidized beds composed of mixed sizes or beds composed of more than one solid material. Lewis and Bowerman (8) studied fluidized beds of non-uniform sized particles and found that the performance of the system could be accurately predicted from equations for the constant diameter spheres. This can be done by using the equations to calculate the performance for each narrow particle size fraction, then summing the contributions for all fractions to give the overall bed expansion. If a fluidized bed is composed of a number of different materials and it can be assumed that the fluidized bed is separated into distinct layers of different materials, then the contributions for each section can be similarly summed to give the overall average porosity of the mixture as a function of velocity.

Suppose a fluidized bed is composed of w_1 pounds of particles of density ρ_{s1}, w_2 pounds of particles of density ρ_{s2}, and so on. Then the volume of each section in the fluidized bed is given by the following

equation, in which the subscript i refers to any individual section i :

$$v_i = \frac{1}{1-\epsilon_i} \times \frac{w_i}{\rho_{si}} \qquad 41$$

The total volumes of the bed is the sum of the volume of the different sections.

$$v_T = \sum v_i = \sum \frac{1}{1-\epsilon_i} \times \frac{w_i}{\rho_{si}} \qquad 42$$

The average porosity of the mixture is the ratio of volume of liquid in the bed to the total volume of the fluidized bed.

$$\epsilon_m = \frac{\sum \frac{1}{1-\epsilon_i} \times \frac{w_i}{\rho_{si}} - \sum \frac{w_i}{\rho_{si}}}{\sum \frac{1}{1-\epsilon_i} \times \frac{w_i}{\rho_{si}}} \qquad 43$$

$$= \frac{\sum \frac{\epsilon_i}{1-\epsilon_i} \times \frac{w_i}{\rho_{si}}}{\sum \frac{1}{1-\epsilon_i} \times \frac{w_i}{\rho_{si}}} \qquad 44$$

The above equation should hold for a fluidized bed which is separated into layers, but not necessarily when the materials are mixed together. It is here postulated that equation (44) also applies to mixed beds. Thus the average porosity and the height of a fluidized bed of mixed species can be predicted from a knowledge of the porosity-velocity relationships of the individual components.

Hoffman, Lapidus and Elgin (12) have studied this aspect of fluidization and have proposed an equation for the overall bed expansion of a bed of mixed sizes. Their work is concerned with particles of the same material but different sizes, during the expansion of which the particles are completely segregated by size and do not mix. The equation they propose is equivalent to

$$\epsilon_m = 1 - \frac{1}{\sum \frac{X_i}{1-\epsilon_i}} \qquad 45$$

where $X_i = w_i / W_m$ = weight fraction of size i in the solid mixture. This equation is equivalent to equation 43 or 44 for constant density solids, but Elgin et al make the statement that it does not hold for fluidized beds when the layers mix.

The basic assumption underlying Elgin's work is that a unique relationship exists between the slip velocity and the hold up for any particulate system. The slip velocity is the relative velocity between the particles and the fluid and is given by

$$V_{slip} = \frac{V_s}{\epsilon} - \frac{V_p}{1-\epsilon} \qquad 46$$

For a batch-fluidized bed, $V_p = 0$ and the slip velocity is equivalent to the average interstitial velocity in the bed.

APPARATUS

A. General

The equipment was designed so that a wide range of flows could be pumped through the test section. A schematic diagram of the apparatus is displayed in figure 3. The equipment is an open system composed of two loops. The primary loop consists of the storage tank, pump and heat exchanger which maintains the fluid at room temperature. The secondary circuit consists of the flow- and temperature-measuring section and the test column.

(a) Pump

The test fluid is circulated by a Paramount close-coupled type U 1-3-2 pump driven by a 3 h.p. motor operating at 3450 rpm. The pump was provided with a John Crane mechanical seal to prevent air being sucked into the pump. The capacity of the pump is 60 U.S. gallons per minute against a total head of seventy feet of water and was supplied by Pumps and Power Limited, of Vancouver, B.C.

(b) Piping

The piping is 2-inch I.D., type L, Noranada copper seamless pipe, and the fittings used throughout were all copper or brass. All shut-off valves except the flow control valves are 2-inch brass gate valves. The two large control valves are globe valves and the small control valves are needle valves.

(c) Heat exchanger

The heat exchanger which removes heat generated by the pump is a seven-tube baffled, counter-current type. The cooling medium was on the shell side and the test fluid was in the tubes. In runs with low viscosity fluids the temperature of the effluent liquid was controlled by adjusting the cooling water throughput. With high viscosity fluids,

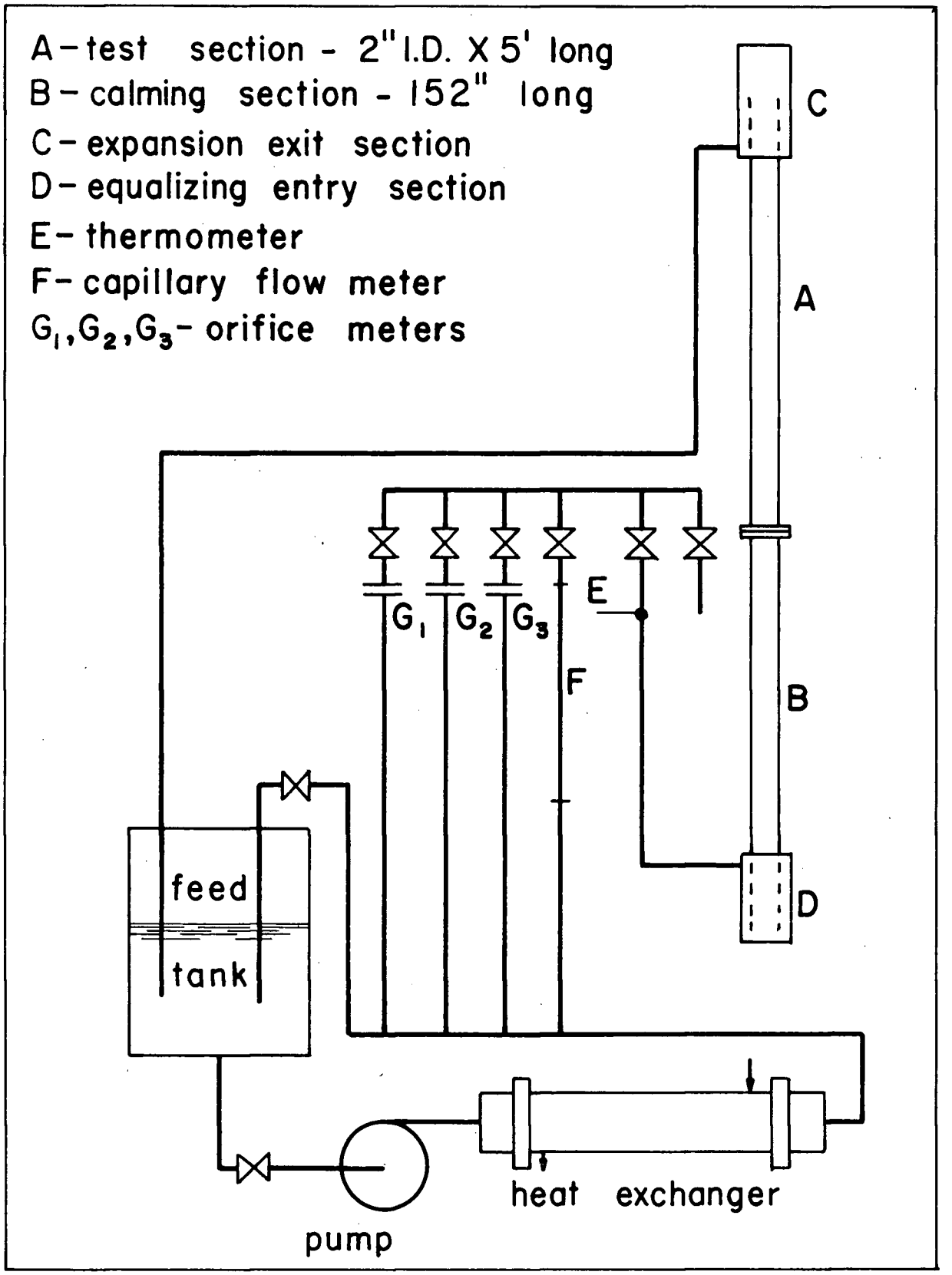

Figure 3. Schematic Diagram of Apparatus.

where the controlling resistance was on the tube side, the temperature was controlled by adjusting the flow through the primary circuit. Thermometer E in figure 3 was used to measure the efflux temperature to the test section.

(d) Flow Meters

The liquid-metering section consists of three sharp-edged orifice meter runs and a capillary flow meter. A calming length upstream of at least 50 diameters and downstream of at least 10 diameters was allowed on orifice meter runs, and all orifice meters were fitted with corner taps. The capillary flow meter consists of a 0.25-inch diameter, stainless steel tube 4'7" long with a calming length upstream, and downstream of 100 pipe diameters and 50 pipe diameters respectively. The pressure drop across the flow meters was measured by means of one of two manometers, a 60-inch air-filled inverted U-tube manometer for relatively small pressure drops, and a 30-inch mercury-filled U-tube Merian manometer for higher pressure drops. The tap leads from the meters are connected to a manifold system, so that the pressure drop across any meter may be measured by one or both manometers. Vents were provided at all high points to allow complete removal of air from the lines and mercury traps were fitted to the mercury manometer. Pertinent details as to sizes of orifices are given in table I.

Table I

Orifice Meter Sizes

Meter Run	Orifice Diameter inches	Run Diameter inches
1	0.85	2.0
2	0.40	1.0
3	0.20	0.5

(e) Test Fluids

The test fluid used for laminar flow runs was an aqueous solution of polyethylene glycol E-9000, supplied by Dow Chemical Company, of Midland, Michigan. For the intermediate region runs, water was used as the test liquid. These liquids were used because they meet the following requirements: they are (1) Newtonian, (2) non-corrosive, (3) stable and resistant to bacterial attack, (4) possess high viscosity at high glycol concentrations, are (5) transparent, and (6) are not toxic. The Newtonian properties of the polyethylene glycol solutions were checked by comparing the Stormer Viscosimeter (Ch.E.2002) curves for these solutions with those obtained for glycerol solutions. No non-Newtonian behaviour could be detected after the glycol solutions were violently stirred for a long time. To increase corrosion resistance, sodium dichromate and sodium hydroxide were added. These chemicals effectively stopped any corrosion but caused the glycol solution to turn a dark orange-brown color. The solution used was 40% by weight of polyethylene glycol in water, which had a viscosity of about 0.090 lb./ft.sec and a density of 67.4 lb./ft.^{3} at 70°F.

B. Test Section

The test section consisted of one of two test columns, an ordinary 2-inch I.D. and 5-foot long industrial Pyrex glass tube and a column constructed of perspex containing pressure taps at numerous positions up the column. The perspex column was also 2-inch I.D. and 5 feet long. A detailed schematic diagram of a pressure tap appeares in figure 4. Each pressure tap was connected into one of two headers in such a way that frictional pressure drop measurements could be made across alternate taps or from the bottom tap to any other tap. The headers were connected to a 100-cm. long 8-mm. glass U-tube containing carbon tetrachloride. A diagram of the differential pressure measuring system appears in figure 6.

The column attachment flanges were constructed so that the column could be aligned vertically, and so that the calming section and column joint could be properly aligned. It was found that the quality of fluidization was affected markedly by these two factors. Non-alignment of column and calming section caused large eddies and channeling in the fluidized bed. Large scale circulation up one wall of the column and down the other resulted from not having the column vertical.

The support for the fluidized bed was a 16 mesh stainless steel screen on top of which was a 2-inch deep fixed bed of lead spheres. The diameter of the spheres used in a particular run was determined by the size and density of the material being fluidized in the column during the run. If the lead spheres were too large, they caused channeling in the fluidized bed and if they were too small they fluidized and disrupted the bed being studied. The equalizing entry section consisted of a 152-inch long section of straight copper pipe and a concentric

annulus distributor to the straight pipe. A diagram of this distributor is shown in figure 5. The expansion exit section is a simple overflow from the 2-inch diameter pipe into a larger chamber. A diagram of this section is also shown in figure 5.

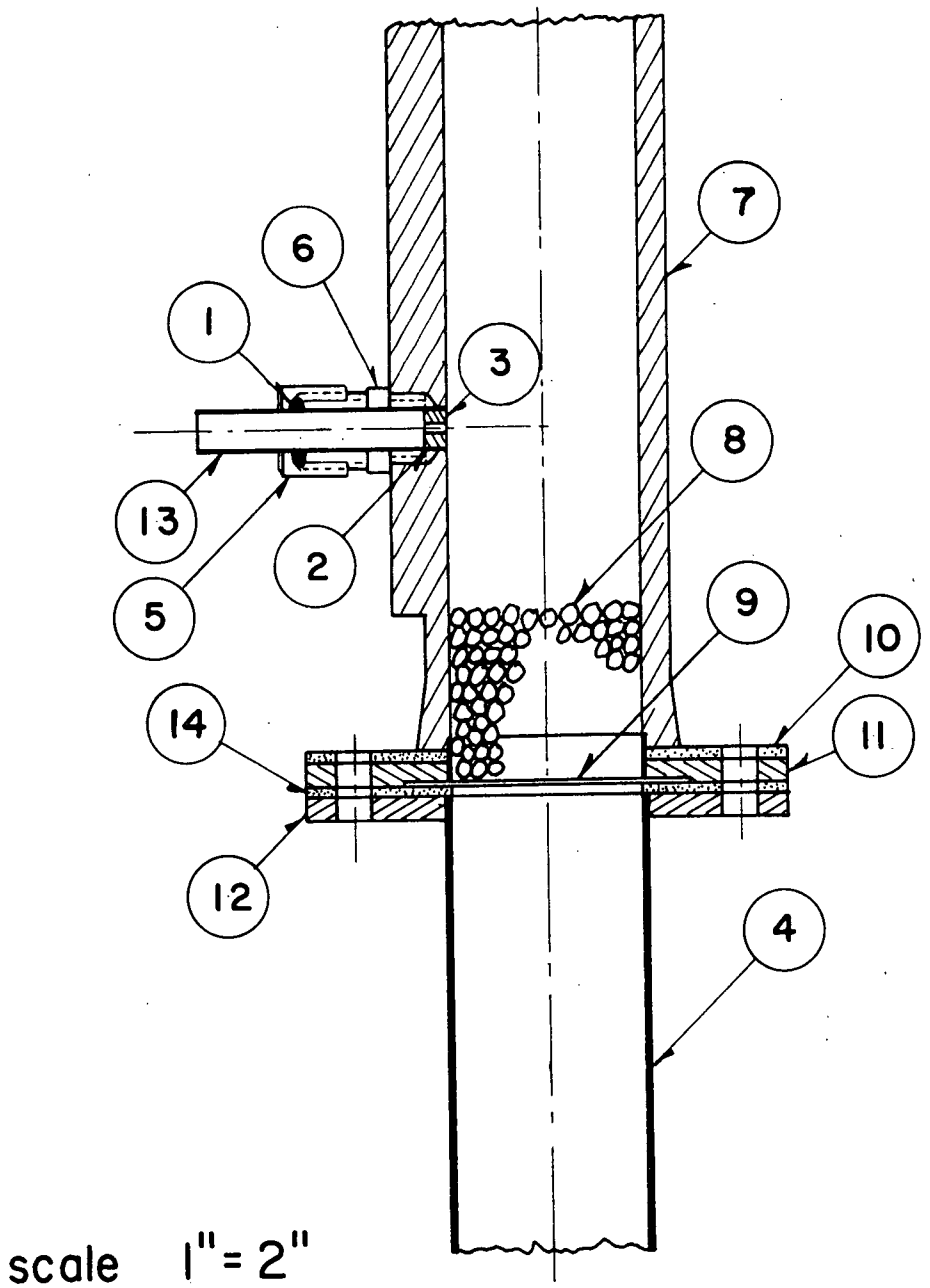

Figure 4. Schematic Diagram of a Sectional View of the Column.
(glass backing flange omitted)

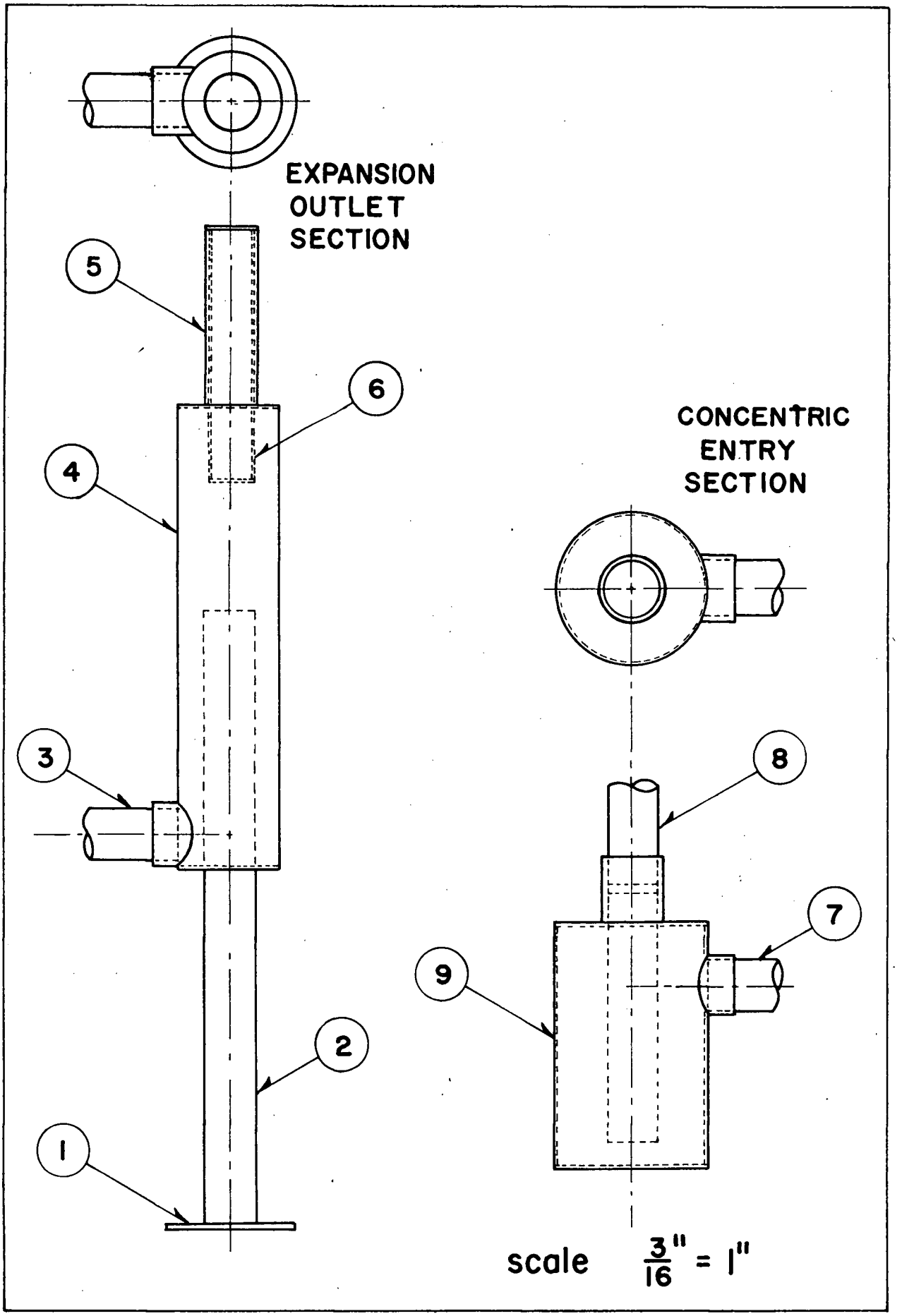

Figure 5. Diagram of Entry Section to and Exit Section from Column.

Key to Figure 4

1. plastic "O"-ring.
2. plug with 1/16" hole drilled through it.
3. 150 Tyler mesh screen covering pressure tap inlet.
4. 2-inch I.D. entry section to column.
5. 3/8" Imperial compression nut.
6. 1/4" pipe to 3/8" compression Imperial connector.
7. 2-inch I.D. perspex column.
8. packed bed of lead spheres.
9. 16 mesh stainless steel support screen.
10. rubber gasket.
11. brass adapter flange for support screen.
12. brass flange.
13. 1/4" inch I.D. copper tubing.
14. rubber gasket.

Key to Figure 5

1. brass connector flange.
2. 2-inch I.D. column extension.
3. 2-inch I.D. return line to storage tank.
4. 4-inch I.D. expansion section.
5. & 6. alignment apparatus for sampler used by B. Pruden (15).
7. 2-inch I.D. line from fluid metering section.
8. 2-inch I.D. calming section below column.
9. 6-inch I.D. expansion section.

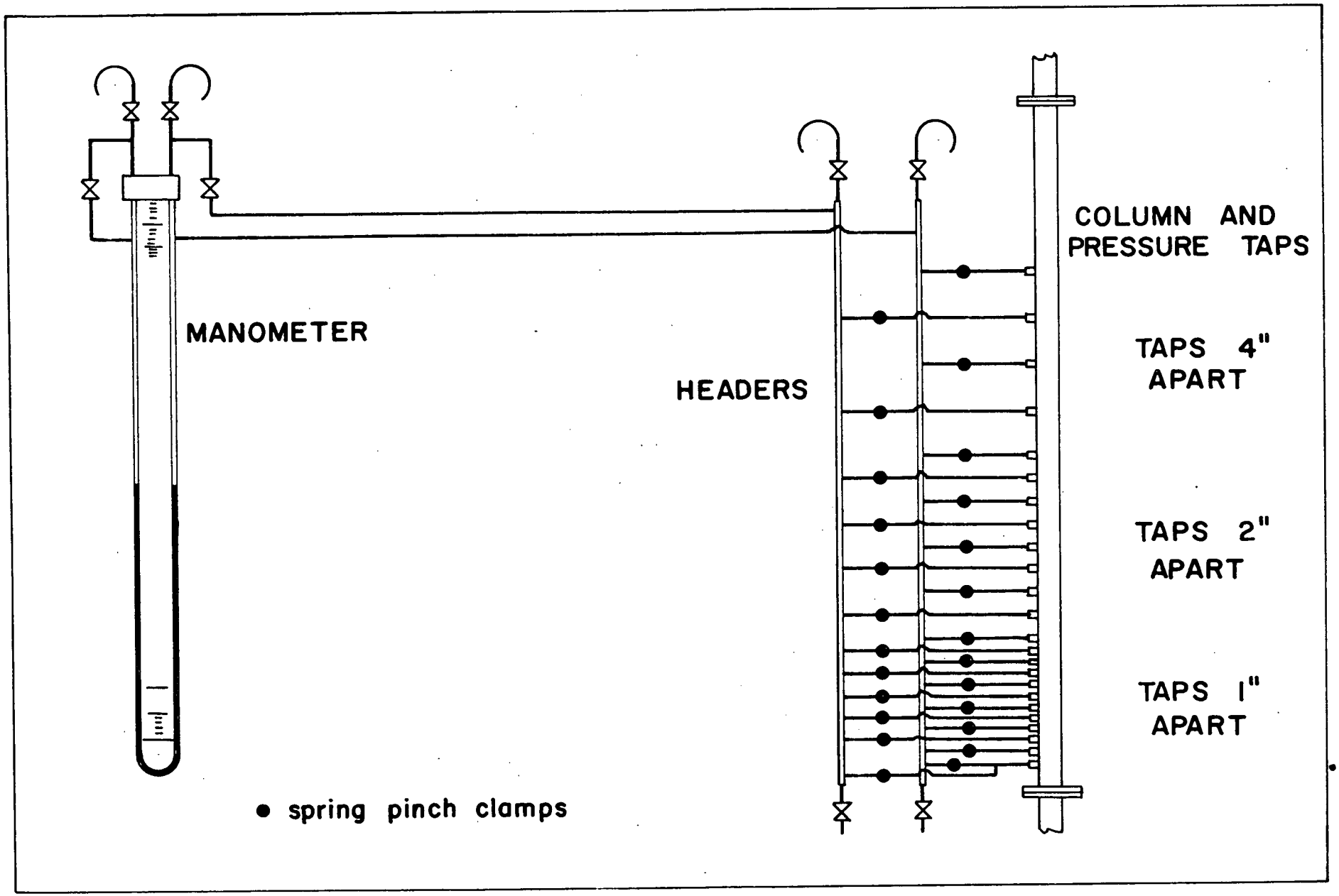

Figure 6. Diagram of Differential Pressure Measurement System.

EXPERIMENTAL PROCEDURES

A. Operating Procedure

For each mixture of solids tested the procedure was as follows. Each component was run separately to determine the single component properties; then the two components were mixed together and run to determine how the mixture fluidized. During each of the three runs for each particular mixture, expansion data and frictional pressure loss data were obtained. Visual observations of the bed were also recorded.

1. Expansion data.

At the various flow rates after equilibrium was obtained, the bed height, room temperature, fluid temperature and manometer readings were recorded. When the test fluid was polyethylene glycol the bed took about 5 minutes to come to equilibrium after the flow rate was changed. Water fluidized beds required a much shorter time to come to equilibrium.

2. Frictional pressure drop data.

At various liquid flow rates and bed heights, frictional-pressure drop profiles were determined by measuring the difference in pressure between various pressure taps and a base pressure tap. Manometers were bled before any readings were taken, to ensure that no air was in the lines. When the test fluid was polyethylene glycol, the manometer took about 15 minutes to come to equilibrium. The sample calculations presented in Appendix II for a particular mixture will give a good indication of how data were taken and how the results were obtained.

B. Orifice Meter Calibrations

The method used for calibration of the orifices and the capillary flow meter was as follows. At steady state conditions, when constant temperature and manometer readings prevailed, the time to collect fifty

pounds of fluid was measured. The capillary flow meter was calibrated only for high viscosity polyethylene glycol solutions; whereas the $\frac{1}{2}$-and 1-inch orifice meters were calibrated for both polyethylene glycol solutions andwwater. The data for the orifice meters has been plotted as C'/Re_T against Re_T , where $Re_T$is the fluid Reynolds number in the test section and

$$\frac{C'}{Re_T} = \frac{\mu}{\rho}\sqrt{\frac{\rho}{p_1 - p_2}} \qquad 47.$$

Least squares lines of the data were calculated. Maximum and mean deviations of the data from the least squares lines are given in Table 2. The calibration plots appear in Figures 7 and 8. The least squares equations for the orifices meters are given in Table 3.

The capillary flow meter was calibrated in the laminar flow range. According to theory, for flow in the laminar region, the friction factor times the Reynolds number should be a constant and equal to 16. The average of this product as determined from all calibration runs was actually 15.395. The main source of the discrepancy can be understood by reference to the equation for determining the product;

$$f \cdot Re_T = \frac{p_1 - p_2}{\mu Q}\left[\frac{\pi D^4}{8 L_m} g_c\right] \qquad 48.$$

Equation 48 shows that a slight error in the measurement of the capillary diameter will be greatly magnified in the $f \cdot Re_T$ product.

The maximum and mean deviations for the capillary flow meter are respectively +3.5% and $\pm$ 1.24%. The calibration equation developed for the meter by weighting the 80 data points equally is

$$V_s = 1.468 \times 10^{-6} \frac{p_1 - p_2}{\mu} \qquad 49.$$

Table 2

Accuracy of Flow Meter Correlations

meter	mean deviation	maximum deviation
½", glycol	± 2.3%	± 10%
1", glycol	± 2.9%	+ 9%
½", water	± 2.0%	+ 9%
1", water	± 2.9%	- 13%

Table 3

Least Squares Equations for Meters

Polyethylene glycol solution

½" meter $\log \frac{C'}{Re_T} = -0.9363 \log(Re_T) - 1.174$

1" meter $\log \frac{C'}{Re_T} = -0.9523 \log(Re_T) - 0.5574$

Water

½" meter $\log \frac{C''}{Re_T} = -1.0641 \log(Re_T) + 31.399$

1" meter $\log \frac{C''}{Re_T} = -1.018 \log(Re_T) + 1.848$

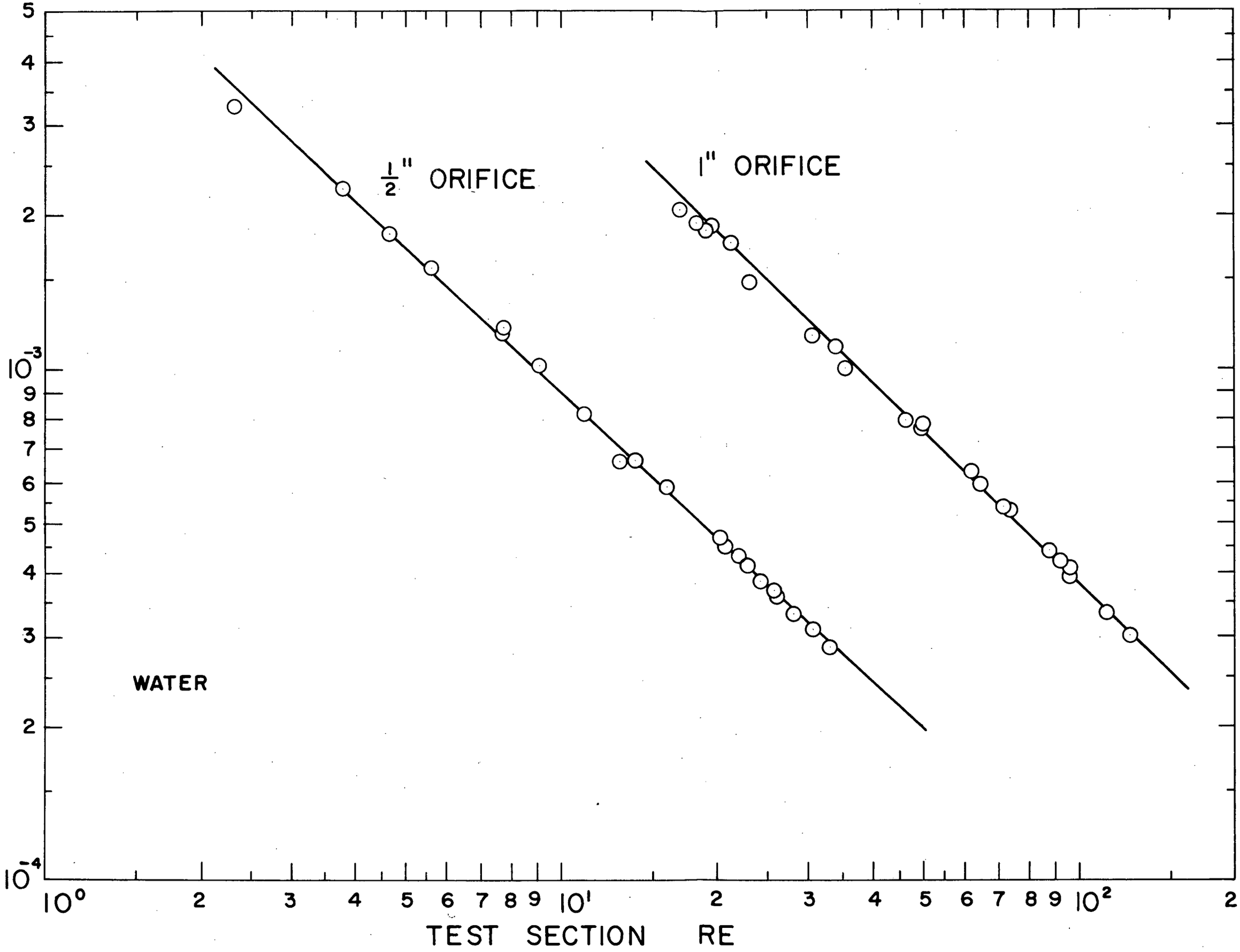

Figure 7. Flow-Meter Calibration Curve for Water.

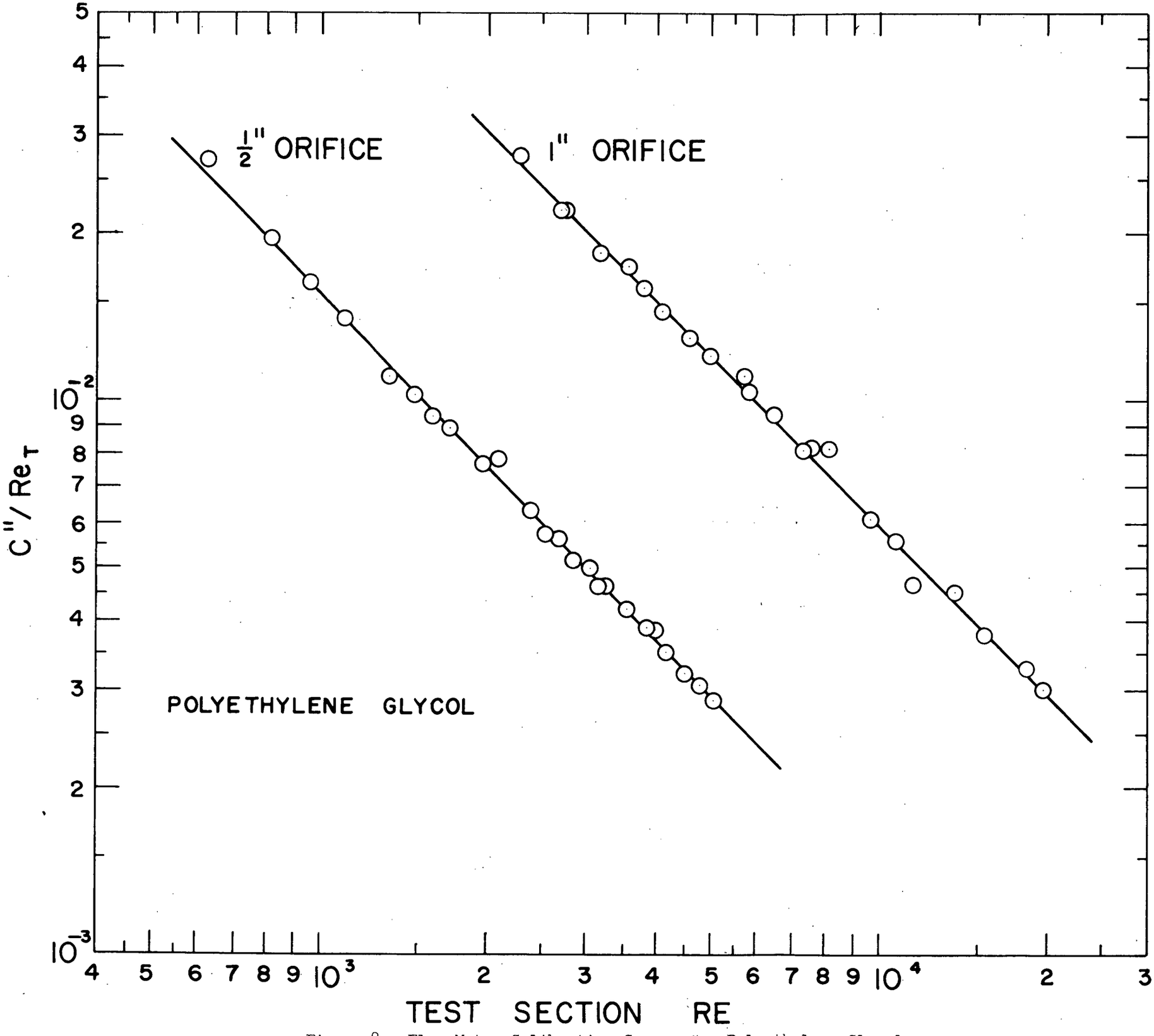

Figure 8. Flow-Meter Calibration Curves for Polyethylene Glycol.

C. Measurement of Viscosity and Density of Test Liquid.

The kinematic viscosity and fluid density of the test liquid were measured in a constant temperature oil bath with a precision scientific temperature controller capable of controlling within $\pm$ 0.1°F. Samples of the test liquid were taken at the end of each run, and during the run for some of the longer runs. Duplicate measurements at three temperatures, 70, 75 and 80°F., were made of the samples. These temperatures were chosen because they bracketed the temperature of the fluid in the test column for almost all the runs.

The density of the fluids was measured using the departmental set of standard hydrometers (Ch.E 1566). These hydrometers are standardized at 60°F., whereas the present experiments were conducted in the range of 68-80°F. The possible error due to the temperature effect was checked using a Westphal balance and distilled water was employed as an absolute standard. The hydrometers used were found to give the true density within $\pm$ 0.2%.

A Cannon-Fenske viscosimeter (R933, Size 300) tube was especially calibrated for measurement of the high viscosity polyethylene glycol solutions. The tube was calibrated by comparing the discharge time for a tube (C-8) previously calibrated by De Verteuil (13) with the time taken in the test viscosimeter. A precision of $\pm$ 0.1% was obtained. The procedure used for filling, cleaning and measuring times of efflux from tubes is given in the ASTM manual, D445-53T (14). For this tube, R933, within the recommended range of kinematic viscosities (50-200 centistokes), the viscosity in centistokes is given by

$$\upsilon = 0.2546\, t \qquad 50$$

where t = efflux time in seconds. The correction for kinetic energy is

negligible provided the efflux time is greater than 200 seconds, and was neglected in this case as the efflux times were of the order of 400 seconds.

D. Measurement of Particle Density.

Particle density was measured using a number of 25-ml. specific gravity bottles. Two random samples were taken from the bulk of the material and the particle density was measured by the following method. Measurements were obtained by first weighing the specific gravity bottle empty, next filling it two-thirds full of particles and weighing, then filling it completely and weighing and finally removing the particles and weighing the bottle full of water. From these weighings and the temperature in the laboratory, the volume and the weight of particles could be determined, and thus the density of the particles.

E. Sizing of Particles.

Two methods were used to measure the average diameter of the particles. For spherical particles greater than 2 mm., the micrometic method was used. After screening the particles through a series of sieves developed by B. Pruden (15), a random sample of 100 beads were measured using a micrometer. The diameter used for the beads was the average of 100 measurements. For beads of 2 mm. or greater the maximum deviation of the measured diameters from the average was about $\pm$ 5.0%.

For smaller beads and particles, the arithmatic average of two adjacent screen sizes was used. The procedure was as follows. About 500 grams of particles were screened between adjacent Tyler sieves of the 4th root series in a Ro-tap machine for 10-minute intervals. After the first screening, particles which remained between the two specified sieves were

collected and screened again. The second, third and fourth screenings were carried out on such particles only. Each screening was about 10 minutes long, after which the sieves were regularly cleaned. It was found that by about the fourth screening a negligible amount of material was passing through the smaller sieve.

EXPERIMENTAL RESULTS

A. Experiments with a Single Species

1. Bed Expansion Measurements

To be able to predict inversion and bed expansions of mixtures of two or more species of particles using single component equations and data, numerous runs were made with single component fluidized beds. For each experiment on fluidization of a particular species, curves were plotted of log V_s against log ϵ . Typical curves are shown in figures 13, 17, 21, 27, 28, 30, and the slopes and intercepts obtained are given in tables 4 and 5. The data were correlated in this form because of its simplicity and because Richardson and Zaki (4) have shown that it works quite well over the complete range of fluidization.

The results obtained for the slopes have been compared with values predicted by using the empirical equations of Richardson and Zaki in tables 6 and 7. The agreement is good in almost every case.

Tables 6 and 7 also compare free settling velocity, V_o , as computed from the experimental intercepts and equation 23, with V_o as calculated from the standard drag coefficient-Reynolds number correlations for free settling of spheres. Discrepancies between the respective values, which range as high as 30% but average less than 14%, could be due to the non-sphericity and non-uniformity of the particles.

Trial runs were made with a mixture of alundum and glass micro-bead (cataphote) particles to determine the effect on a fluidized bed of having another fluidized bed above or below the particular bed being studied. When the fluidized micro-bead bed was above the alundum bed the expansion curve for the alundum deviated slightly from the curve obtained when there was not any bed above. As can be seen in figure 9, the alundum bed is

Table 4

Summary of Fluidization Results for Particles in Water

No.	Particles d, mm.	Particles ρ_s, $\frac{gm.}{cm.^3}$	Particles Material	Re_o	V_o ft/sec	$\log(V_i)$	n	d/D	Figure
1	1.08	2.91	Ballotini	198	0.590	-0.250	2.56	0.021	29
2	0.767	3.95	Alundum	129	0.543	-0.280	2.87	0.015	27
3	0.645	3.95	Alundum	97.8	0.516	-0.310	2.95	0.013	28
4	0.912	3.95	Alundum	171	0.606	-0.235	2.76	0.018	31
5	1.83	2.92	Ballotini	511	0.904	-0.080	2.31	0.036	29
6	1.08	3.17	Crystalon	195	0.582	-0.256	2.77	0.021	27
7	0.542	4.50	Nickel-Glass	89.3	0.532	-0.285	3.02	0.011	30

Table 5

Summary of Fluidization Results for Particles in Polyethylene Glycol

No.	Particles d, mm	ρ_s $\frac{gm}{cm^3}$	Material	Re_o	V_o ft/sec.	$\log(V_i)$	n	d/D	Figure
8	0.456	8.90	Nickel	0.025	0.0236	-1.635	4.75	0.009	13
9	0.645	3.95	Alundum	0.031	0.0205	-1.700	5.36	0.013	17
10	2.28	2.73	Ballotini	0.507	0.0959	-1.063	4.59	0.045	13
11	1.08	2.91	Ballotini	0.077	0.0309	-1.530	5.13	0.021	17
12	3.15	7.83	Steel	5.97	0.770	-0.185	4.13	0.062	21
13	2.05	11.33	Lead	2.04	0.404	-0.433	4.19	0.040	21
14	0.542	4.50	Nickel-Glass	0.0168	0.0163	-1.800	4.84	0.011	24

Table 6

Comparison of Results with Richardson-Zaki and Free Settling Correlations. Water

No.	Re_o		V_o ft/sec.		n	
	Experiment	Correlation	Expt.	Correl'n	Expt.	Correl'n
1	198.0	210.0	0.590	0.626	2.56	2.53
2	129.1	144	0.543	0.606	2.87	2.83
3	97.8	102	0.516	0.538	2.95	2.97
4	171	198	0.606	0.701	2.76	2.80
5	511	537	0.904	0.951	2.31	2.38
6	195	218	0.582	0.651	2.77	2.72
7	89.3	82	0.532	0.487	3.02	2.98

Table 7

Comparison of Results with Richardson-Zaki and Free Settling Correlations. Polyethylene Glycol.

No.	Re_o		V_o ft/sec.		n	
	Experiment	Correlation	Experiment	Correlation	Experiment	Correlation
8	0.025	0.022	0.0236	0.0207	4.75	4.83
9	0.031	0.023	0.0205	0.0153	5.36	4.90
10	0.507	0.575	0.0959	0.1087	4.59	5.20
11	0.077	0.068	0.0309	0.0274	5.13	5.07
12	5.97	4.90	0.770	0.633	4.13	4.72
13	2.04	2.39	0.404	0.474	4.19	4.74
14	0.0168	0.0136	0.0163	0.0132	4.84	4.86

compressed slightly by the presence of the micro-beads (cataphote), but this effect disappears as the bed is expanded. Because the deviation was very small it is assumed that having one fluidized bed on top of another doesn't influence the fluidization of the lower bed. The expansion curve for the cataphote bed was not influenced at all by having the alundum bed fluidized below it. Thus single component data can be used to determine overall bed expansions for mixtures, provided the beds do not mix. Results pertaining to expansion curves for two components which do mix at certain porosities will be given in a later section.

The expansions of several of the water fluidized beds display an interesting behaviour. The expansion curve is composed of two sections of different slopes, and the expansion seems to proceed differently in the two regions, as seen in figures 27, 28 and 30. The bed expands at a greater rate with respect to velocity above porosities of about 55% than it does at porosities below 55%. This behaviour seems to depend on the d/D ratio, the velocity of the fluid, and the porosity of the bed. The phenomenum was not observed when particles were fluidized in polyethylene glycol solutions or when very large particles were fluidized in water. Diagrams based on visual observations of how beds appeared to fluidize and the particle flow patterns are given in figure 10. At porosities of about 55% bubbling and void wave formations begin to appear in the fluidized bed. The void waves grow as the bed expands. These are undoubtedly a cause for the change in slope of the expansion curve. Observations similar to the above were also noted by Cairns and Prausnitz (16) in their study of macroscopic mixing in fluidization.

Cairns and Prausnitz (17) also measured the line velocity profiles in water fluidized beds in a 2-inch column using a tracer technique. They found that the velocity profiles begin to change their shape from a

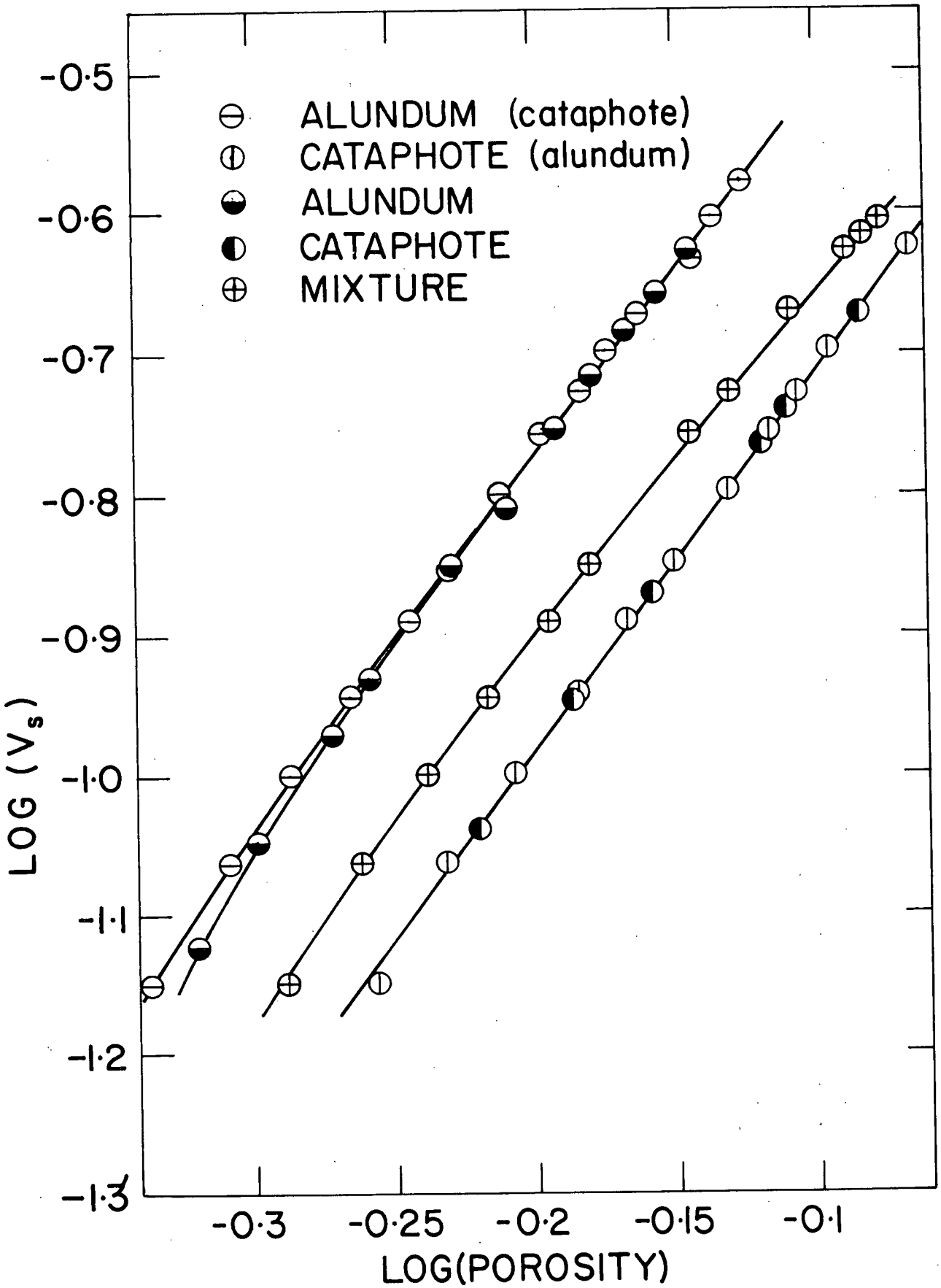

Figure 9. Plot of Alundum and Cataphote Bed Expansion, Individually and with Cataphote above Alundum.

radially flat profile and develop humps at 3 to 3.5 particle diameters from the wall, at porosities of about 55%. The height of the humps relative to the average velocity depends on the particle density.

There appears to be a limit to which a fluidized bed can be expanded before it becomes hydrodynamically unstable. On expansion of a bed slowly from a fixed to a dense and then a more dilute fluidized bed, the bed expanded uniformly until a porosity of 85%. The bed was stable, and disturbances which moved through it affected the quality of fluidization but did not cause any sustained oscillations. If a bed was expanded above 85% porosity, any disturbance beginning in the bed became amplified as it moved through the bed and set up continuous void waves and oscillations, which remained until the porosity of the bed was decreased. After decreasing the porosity, the oscillations slowly disappeared and the bed returned to a homogeneous fluidized state. According to Jackson (18), fluidized beds will remain stable and will not be affected by discontinuities unless the bed is expanded above a certain limit. Disturbances in a fluidized bed grow as they move up through the bed, but if a bed is not deep enough, the disturbance will have moved out of the bed before it has become large enough to disrupt it. Slis and Willemse (19) have also observed these disturbances and have developed a theory to account for their velocity of propagation.

The fluidization of particles in the polyethylene glycol solutions was much more uniform in appearance than with water. It was not until the bed was expanded to about 75% porosity that notable circulation of the particles occurred. There was some tendency for particle movement down the walls of the tube and up the centre, but it was not very pronounced. The particles, however, were continually coming together

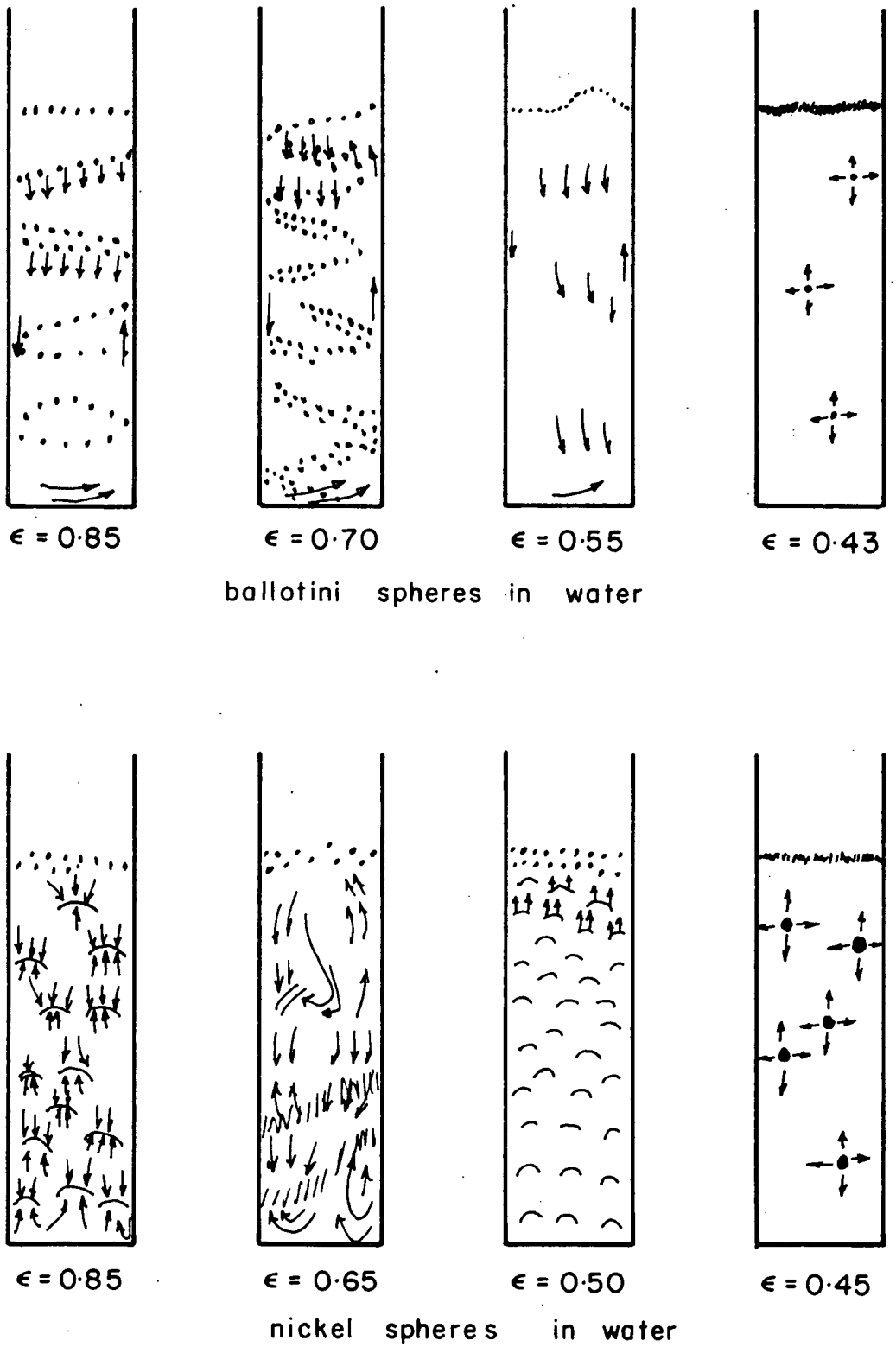

Figure 10. Visual Observation of Fluidization of Spheres.

in small groups, then falling through the bed as a group, dispersing, and rising again. This effect was particularly noticeable with nickel spheres, where 5 or 6 particles would fall as a vertical chain. For large particles, such as the lead and steel balls, there is evidence of mass movement of groups of particles, but in these runs the particle Reynolds' number was greater than 2.0. Particle flow consisted of a random eddying motion and there were fairly large variations in the local solids concentrations throughout the bed. However, disturbances similar to those observed in deep, water-fluidized beds were not present in beds fluidized by the polyethylene glycol solutions. Such beds could be expanded out the top of the column without large scale voids forming as they did in water-fluidized beds. Beds fluidized in polyethylene glycol segregated by size to a much greater extent than they did in water, and at high porosities several beds dispersed to the point that no interface between bed and fluid could be observed.

2. Differential Pressure Measurements.

Differential pressure measurements were made on beds fluidized with polyethylene glycol solution. Figures 11 and 12 are examples of these results. The results obtained are within 5% of the theoretical values for all porosities below 85%. At porosities greater than 85% the particles were sufficiently segregated by size that the porosity calculated from bed height was not representative of the bulk of the bed, and thus experimental results were significantly greater than the theoretical predicted values.

Further analysis of the results shows that for low porosities the experimental values of porosity are somewhat less than the theoretical values, while at high porosities the experimental results are larger than

the theoretical ones. This condition has been explained by Adler and Happel (20) as being caused by the nature of the entrance section. They have studied the effect of calming section packing and loose-packed bed height to diameter ratio on differential pressure drop across a fluidized bed. The results obtained indicate three trends. (1) With no packing in the calming section, the ratio of experimental differential pressure gradient to theoretical pressure gradient calculated from equation 26, known as the P ratio, is a function of the looser-packed bed height to diameter ratio and the porosity of the fluidized bed. (2) For packed calming sections, where the packing is above the support as in our case, the P ratio is only a function of the porosity of the fluidized bed. Also of importance is the fact that the P ratio varies from about 0.90 at porosities of 60% to about 1.10 at porosities of 90%. (3) When the packing was below the support screen the P ratios were always less than 1.0. This can be readily confirmed by observing Wilhelm and Kwauks' results (1).

When measuring the frictional pressure loss through the fluidized bed by the method used in this work, the pressure loss due to wall friction is also measured. The result obtained can be treated as the sum of the pressure loss due to the fluidized bed plus the pressure loss due to the wall. Calculations were made to determine the maximum error that the wall pressure loss could cause. The highest free settling particle velocities in water and in polyethylene glycol were used in the calculation. The maximum pressure loss per foot of column in the polyethylene glycol fluidized bed was computed to be 0.039 lb. force / ft^2 - ft, and in the water fluidized bed 0.002 lb. force / ft^2 ft. The measured frictional pressure losses in the fluidized bed were never less than 5 lb. force/ ft^2 - ft, and thus the error due to wall friction was never greater than 1%.

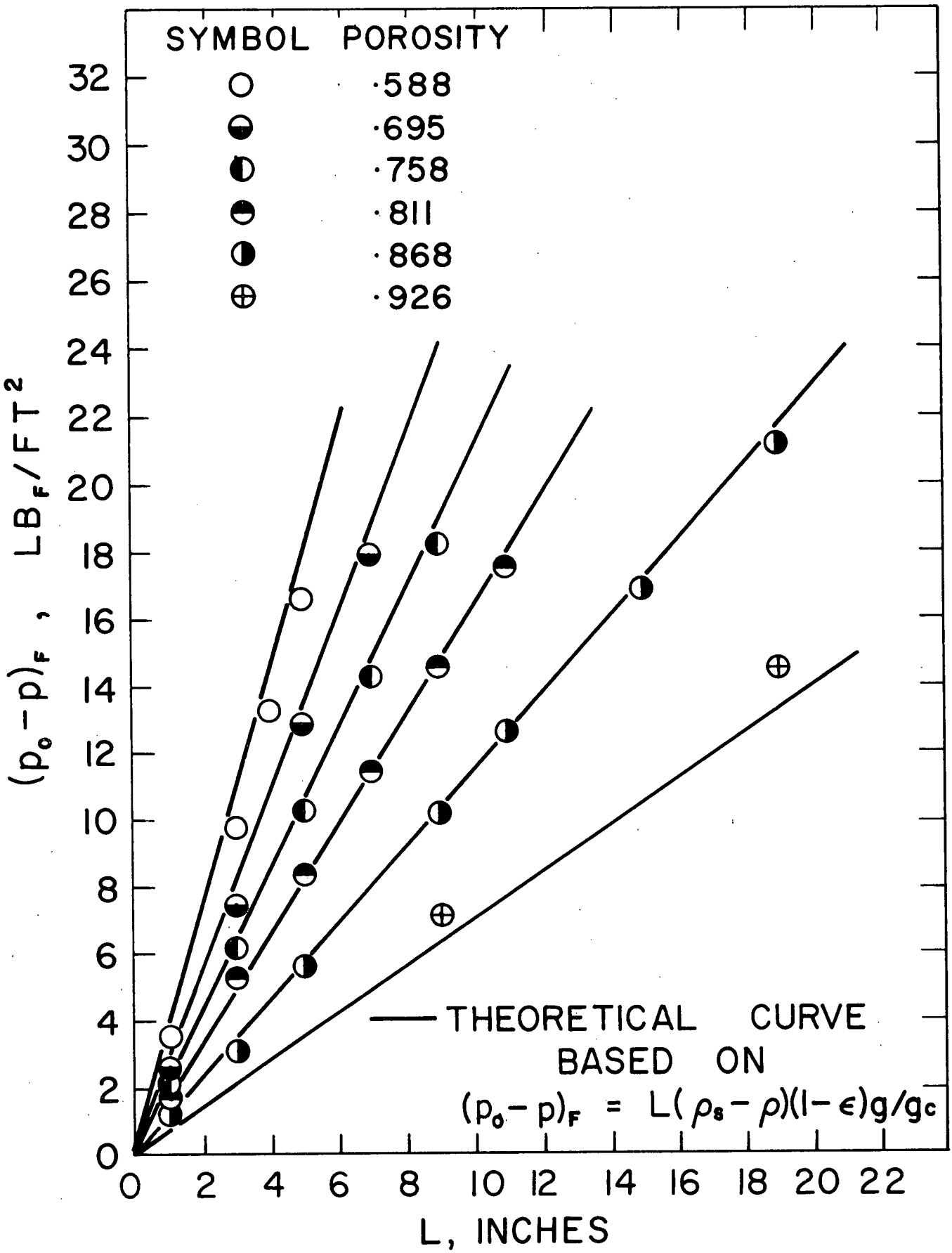

Figure 11. Frictional Pressure Drop Profiles in a Ballotini Bed Fluidized by Polyethylene Glycol.

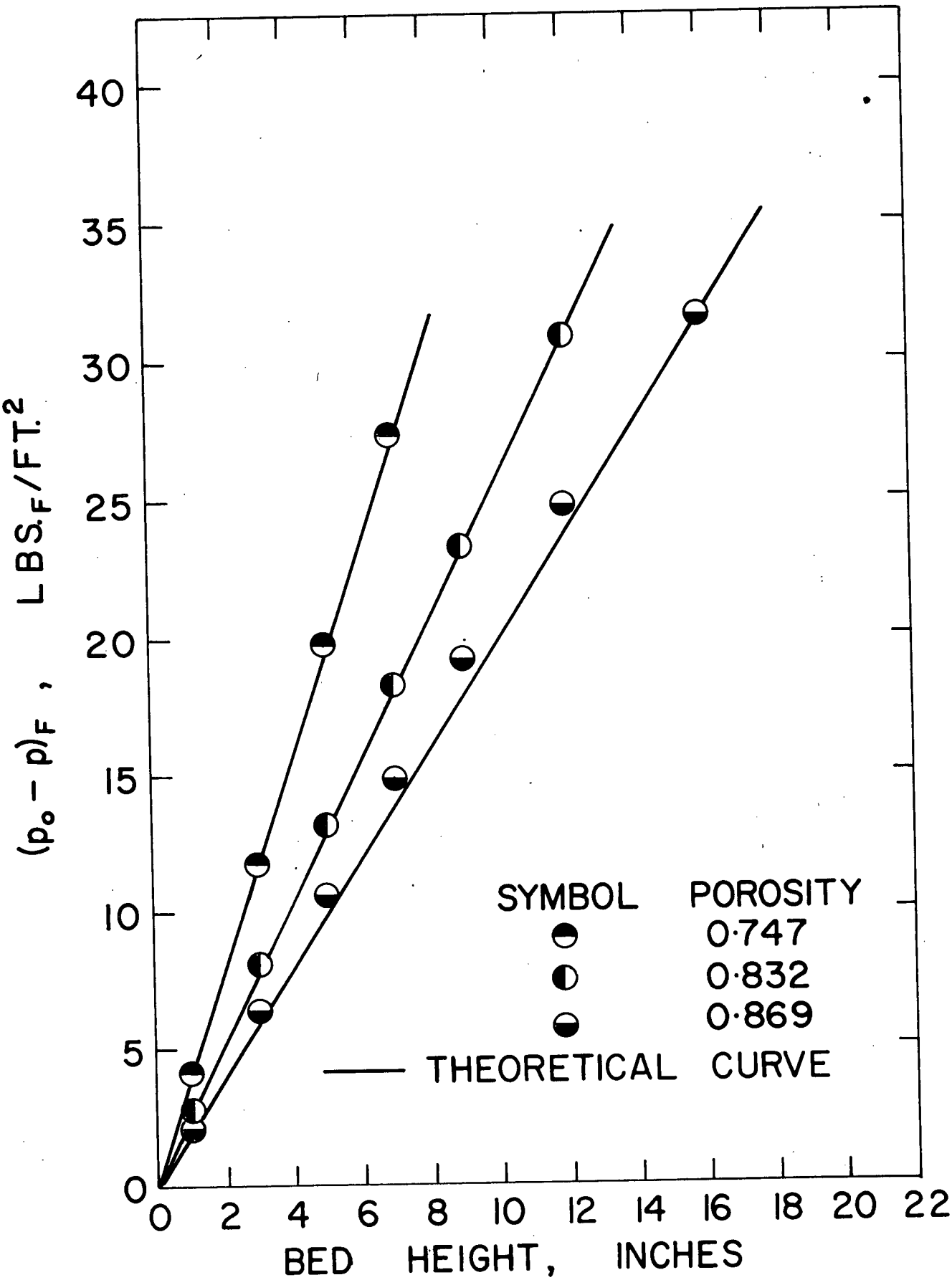

Figure 12. Frictional Pressure Drop Profiles in an Alundum Bed Fluidized by Polyethylene Glycol.

B. Experiments with two species.

1. Inversion of Mixtures.

Mixtures of two groups of particles, for which single component data had already been measured, were fluidized using polyethylene glycol solutions and water.

Many different mixtures were tested when the fluidizing medium was water, but no visible inversions were obtained. Most mixtures expanded in the following manner. At low velocities the bed was separated into two distinct sections and as the fluid velocity was increased the two components mixed together. The mixing increased as the fluid velocity increased until a homogeneous mixed bed was obtained. On further increase in fluid velocity no separation of the bed into two sections was observed. This was not unexpected as most practical inversions are predicted to occur at a porosity of about 85%, and in water fluidization the fluidized bed is very unstable at these porosities. It appears that macroscopic mixing in the water-fluidized beds masked the inversions, and that the driving force for segregation due to bulk density difference was not great enough to overcome the forces producing mixing affects and instabilities in the fluidized bed.

Binary mixtures of particles were also fluidized in polyethylene glycol solutions, and very detailed results were obtained for four mixtures. The results obtained appear in Tables 8 - 11, and are followed by a general analysis of two component fluidization.

The interpretation of data was as follows. Expansion data were plotted as logarithm (mean porosity) against logarithm (superficial liquid velocity). The experimental points obtained are given and the expansion curve predicted by equation (44), using single component data, is drawn as a bold line. The agreement between experimental and predicted expansions

is very good, as can be seen in Figures 13, 17, 21 and 24. The frictional pressure drop data were plotted as difference in pressure from a base position to a higher plane versus height L, which is the distance between the base position and the higher plane. The parameter is superficial liquid velocity. These data are displayed in Figures 14, 18 and 22. The differential pressure gradients for the individual components were obtained by measuring the slopes of the straight lines in the latter plots. The difference in bulk density of the two beds is numerically equal to the difference in differential pressure gradient for the beds. Development is given below.

$$(\Delta p_F/L)_1 = (1-\epsilon_1)(\rho_{s1}-\rho)g/g_c \qquad 26$$

$$(\Delta p_F/L)_1 - (\Delta p_F/L)_2 = (1-\epsilon_1)(\rho_{s1}-\rho)g/g_c - (1-\epsilon_2)(\rho_{s2}-\rho)g/g_c \qquad 51$$

The bulk density difference has already been shown to be given by

$$\rho_{B1} - \rho_{B2} = (1-\epsilon_1)(\rho_{s1}-\rho) - (1-\epsilon_2)(\rho_{s2}-\rho) \qquad 28$$

Thus

$$\rho_{B1} - \rho_{B2} = \left[(\Delta p_F/L)_1 - (\Delta p_F/L)_2\right] g_c/g \qquad 52$$

The measured differential pressure differences, which are thus equivalent to the bulk density differences, are plotted against the superficial liquid velocities in Figures 15, 19, 23 and 25. The bold line is the curve obtained by using single component expansion data and theoretical differential pressures to determine the inversion point, as follows. At a particular superficial liquid velocity ϵ_1 and ϵ_2 were read from the single component expansion curves, and these values were used in equation 51 to calculate the difference in differential frictional pressure gradient between the two components.

Table 8

Inversion Results for Nickel and Ballotini Mixture

Properties of Mixture Components	d, mm.	0.456	2.28
	ρ_s	8.90	2.73
	Material	Nickel	Ballotini
	Wt. of Sample	459.0 gm.	400.0 gm.
Buoyancy ratio γ		0.212	
Size ratio r		5.01	
Predicted inversion porosity (ϵ_m) by equation (39)		0.817	
Predicted inversion porosity (ϵ_m) using single component data.		0.842	
Experimental inversion porosity		0.783	
Flow régime		Stokes	

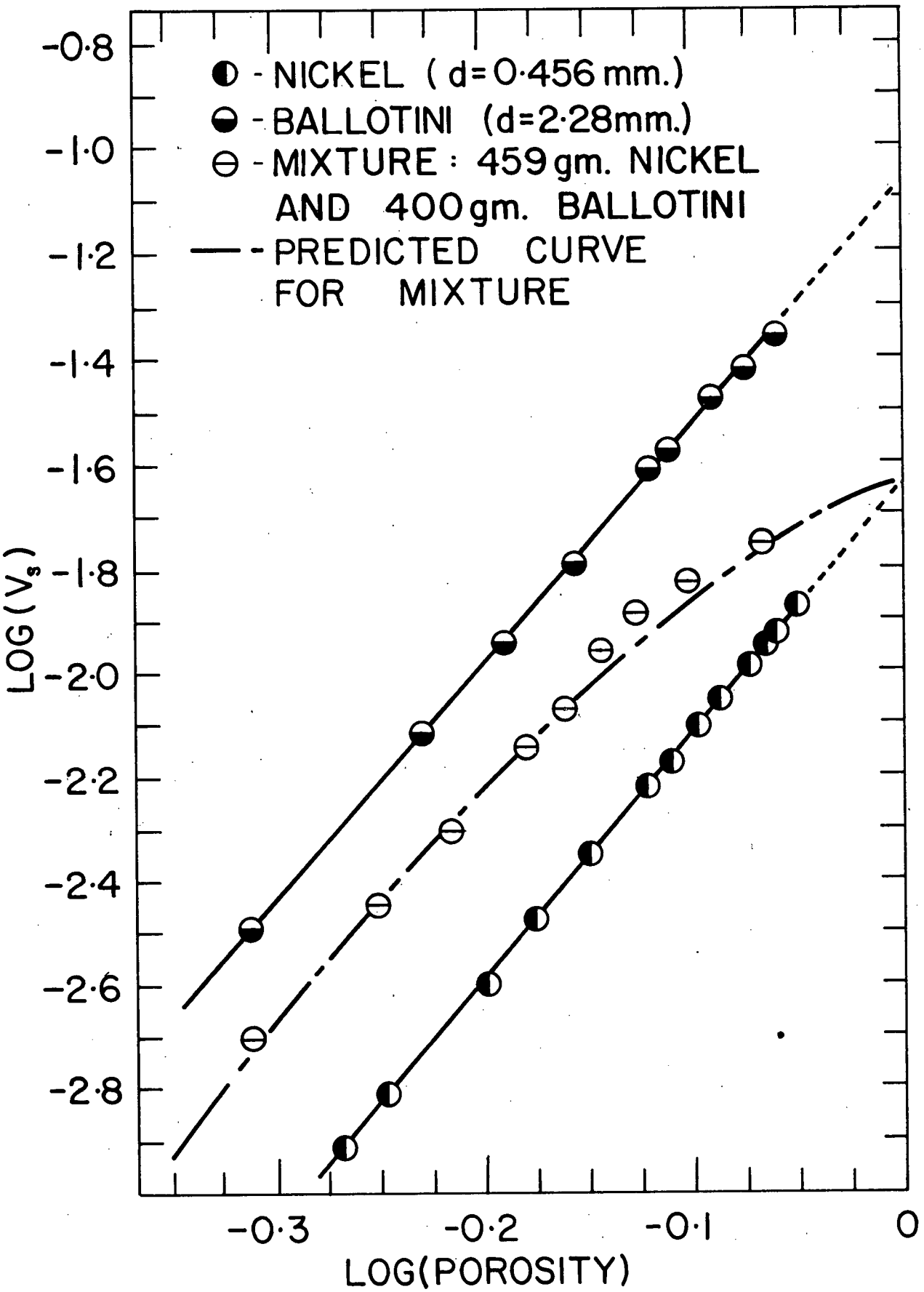

Figure 13. Plot of Nickel and Ballotini Bed Expansions.

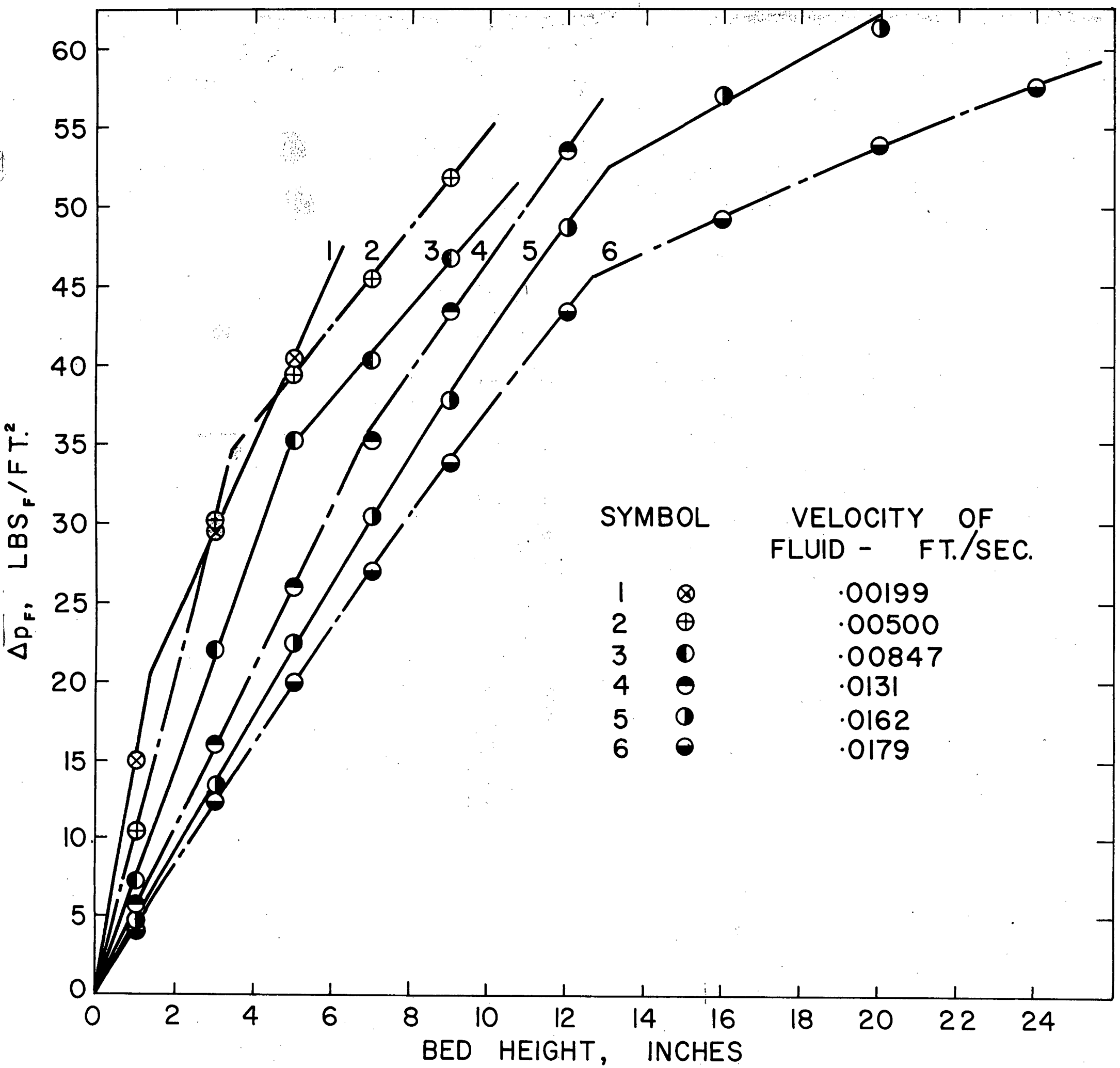

Figure 14. Differential Pressure Profiles in Nickel-Ballotini Bed.

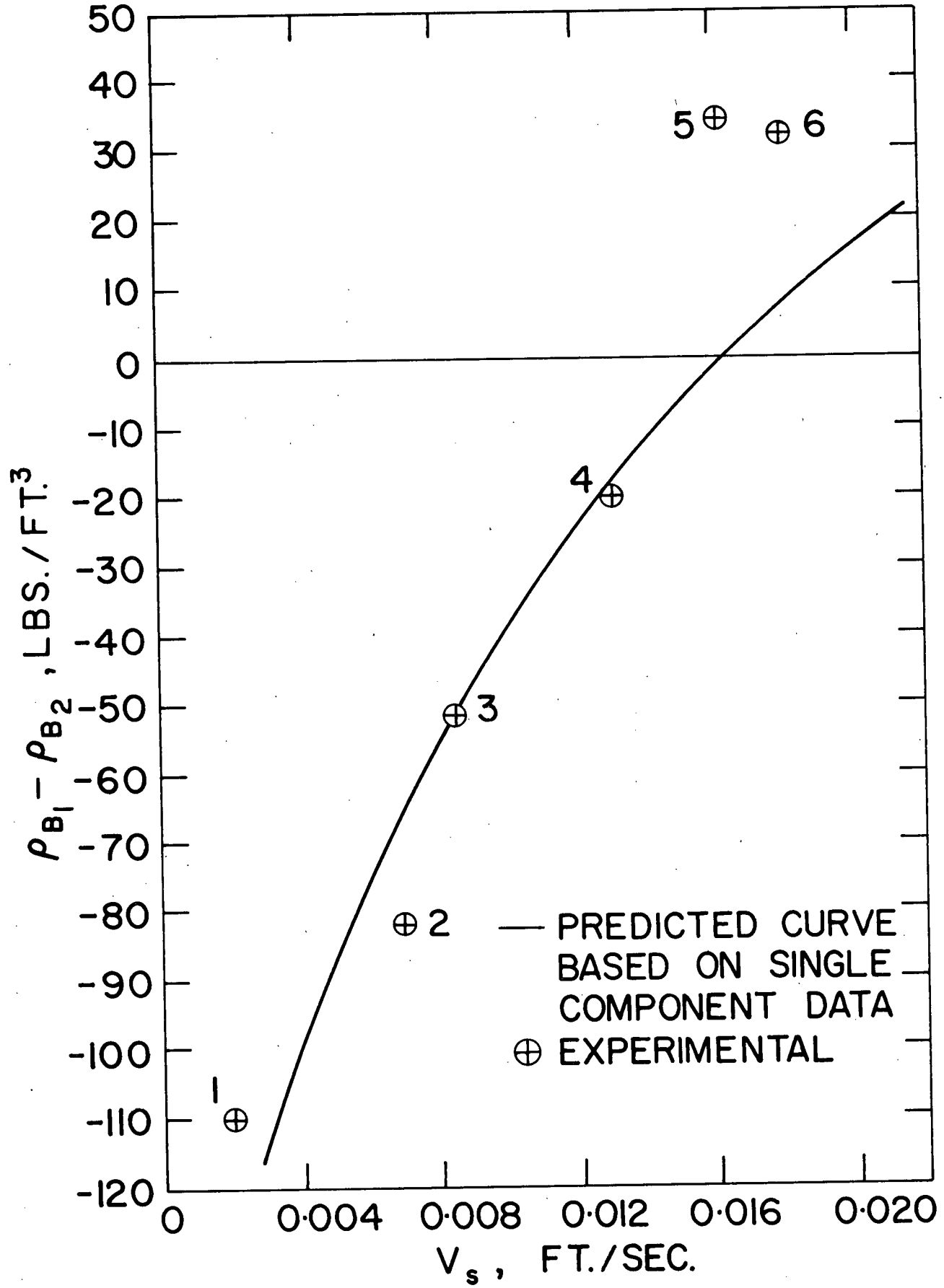

Figure 15. Plot of Bulk Density Difference and Velocity for the Nickel-Ballotini Bed.

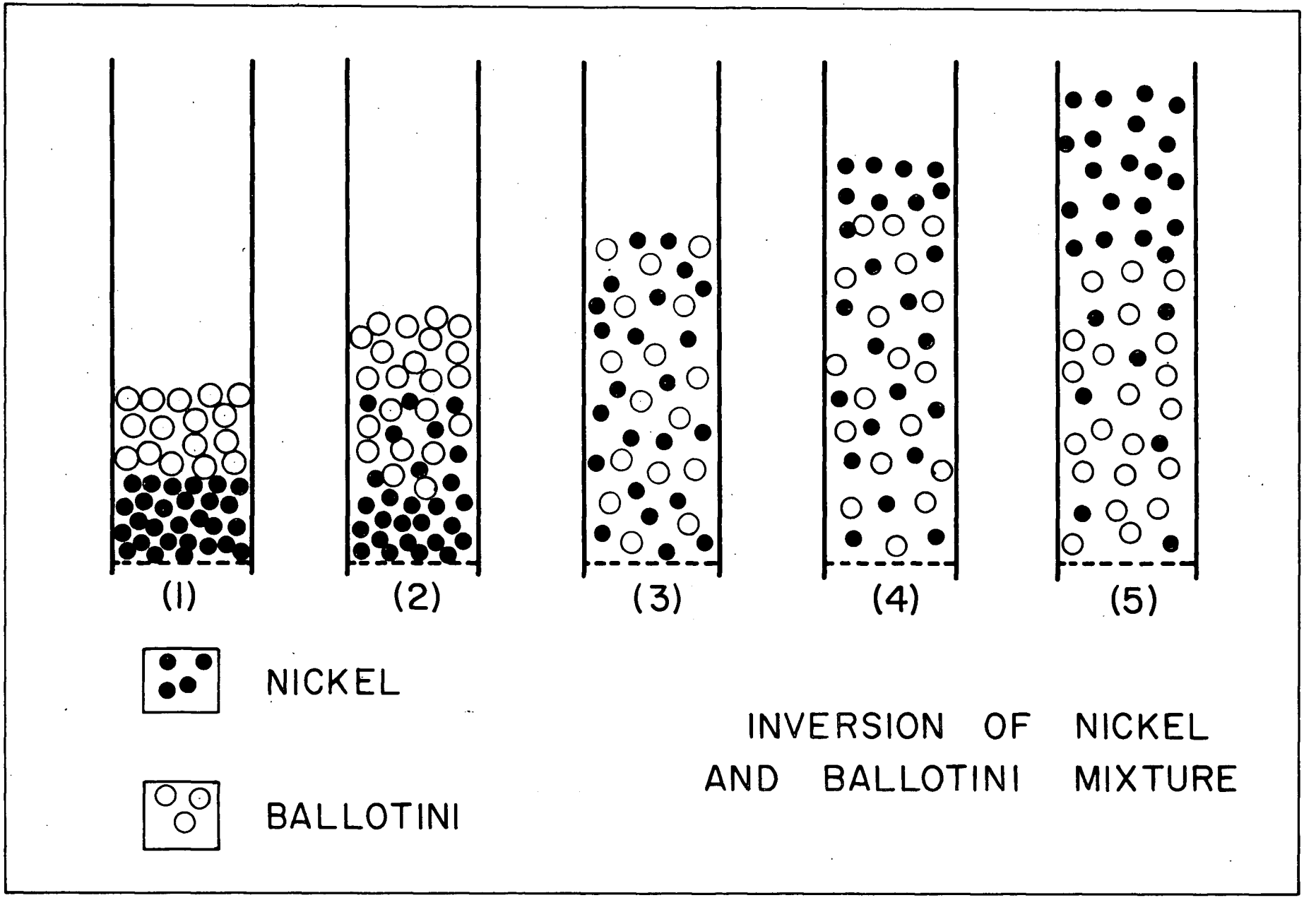

Figure 16. Schematic Diagram of how Inversion Proceeded.

Table 9

Inversion Results for
Alundum and Ballotini Mixture

Properties of Mixture Components	d, mm	0.645	1.08
	ρ_s	3.95	2.91
	Material	Alundum	Ballotini
	Wt. of sample	447.0 gm.	320.0 gm.
Buoyancy ratio	γ	0.640	
size ratio	r	1.675	
predicted inversion porosity (ϵ_m) by equation (39)		0.805	
predicted inversion porosity using single component data.		0.806	
experimental inversion porosity (ϵ_m)		0.763	
flow régime		Intermediate	

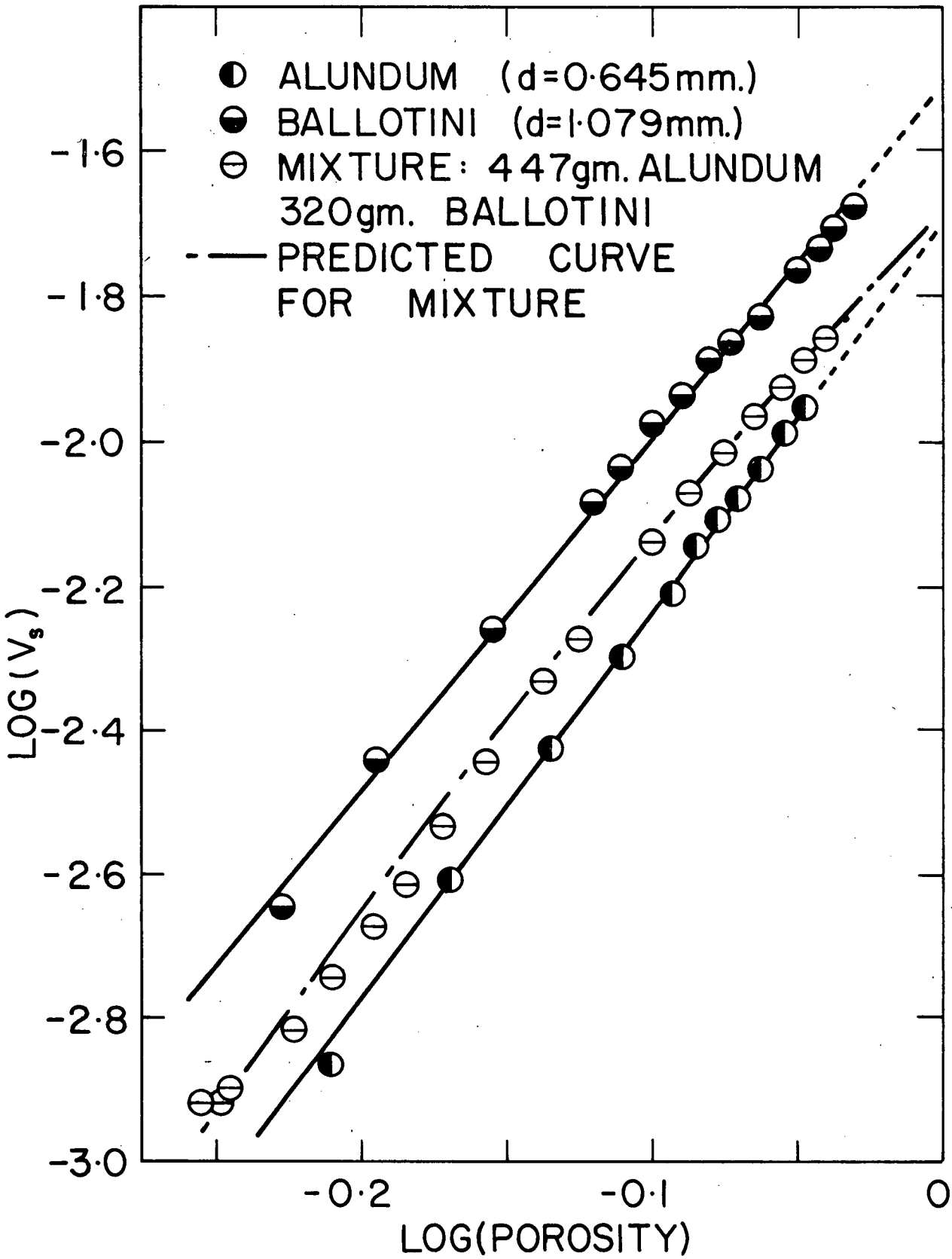

Figure 17. Plot of Alundum and Ballotini Bed Expansions in Polyethylene Glycol.

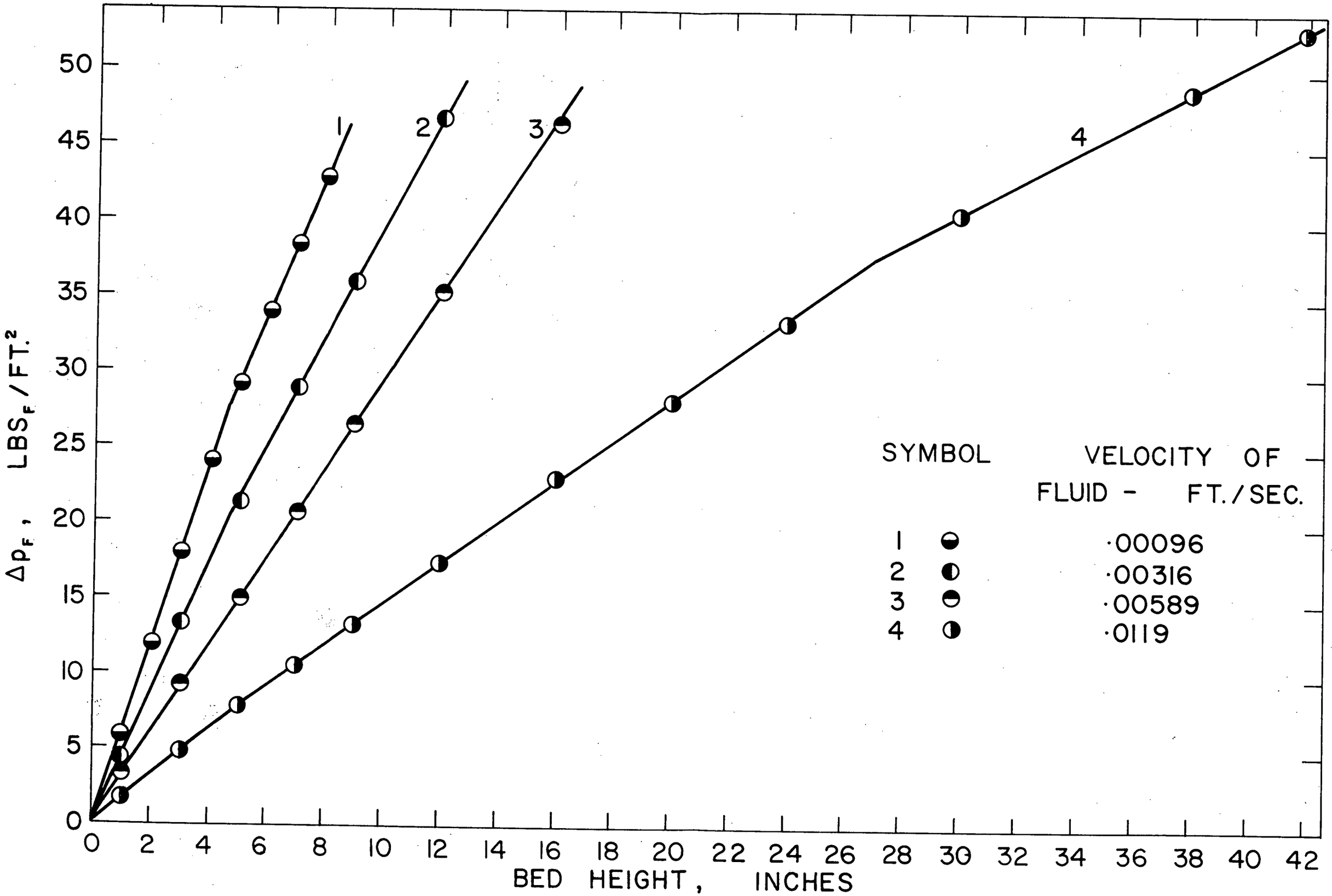

Figure 18. Differential Pressure Profiles in Alundum-Ballotini Bed.

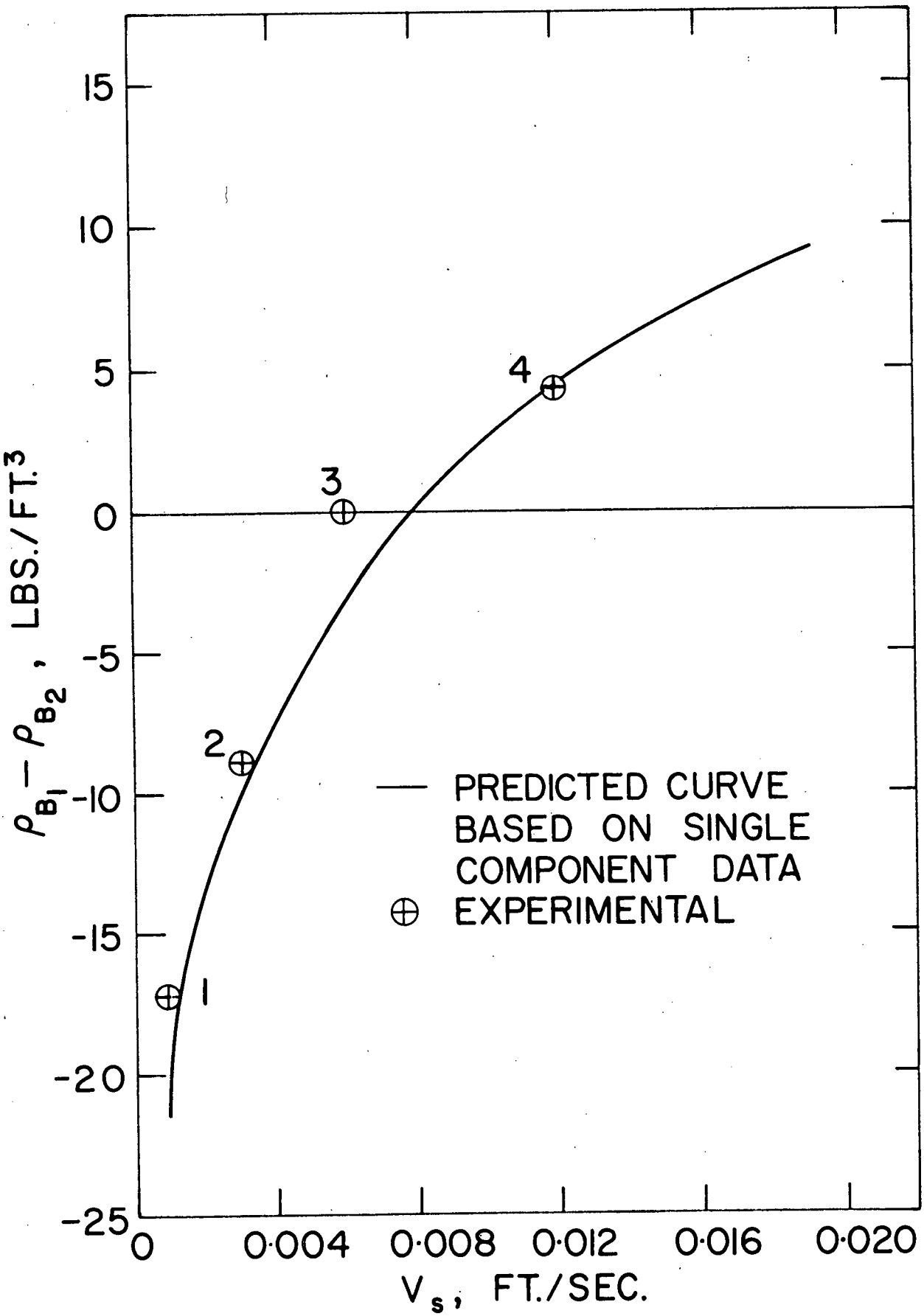

Figure 19. Plot of Bulk Density Difference and Velocity for Alundum-Ballotini Bed.

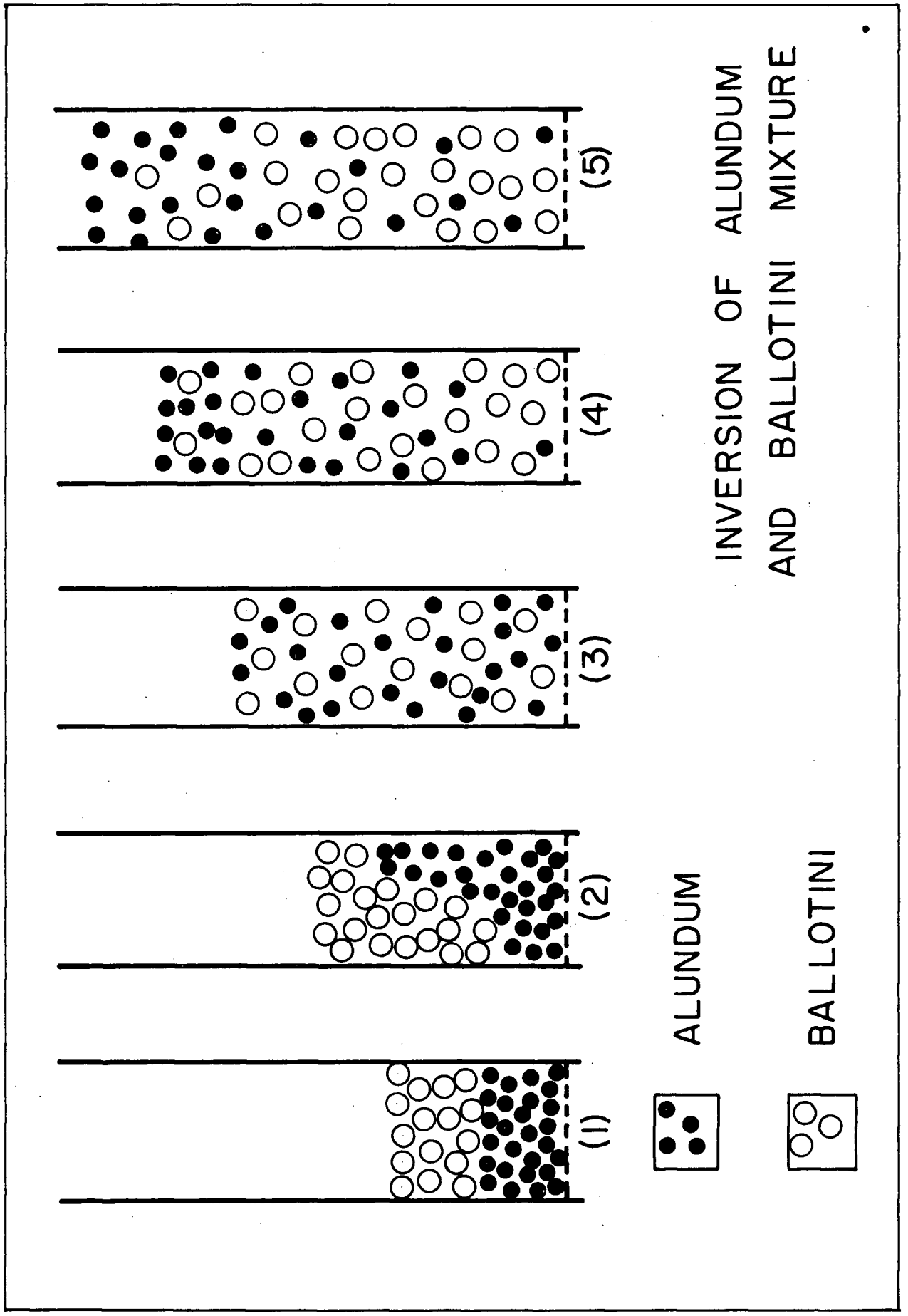

Figure 20. Schematic Diagram of how Inversion Proceeded.

Table 10

Inversion Results for Lead and Steel Mixture

Properties of Mixture Components	d,mm	3.15	2.05
	ρ_s	7.83	11.33
	Material	Steel	Lead
	Wt. of sample	800.0 gm.	900.0 gm.
buoyancy ratio	γ	0.659	
size ratio	r	1.536	
predicted inversion porosity (ϵ_m) by equation (39)		0.803	
predicted inversion porosity using single component data		0.688	
experimental inversion porosity (ϵ_m)		0.721	
flow regime		Intermediate	

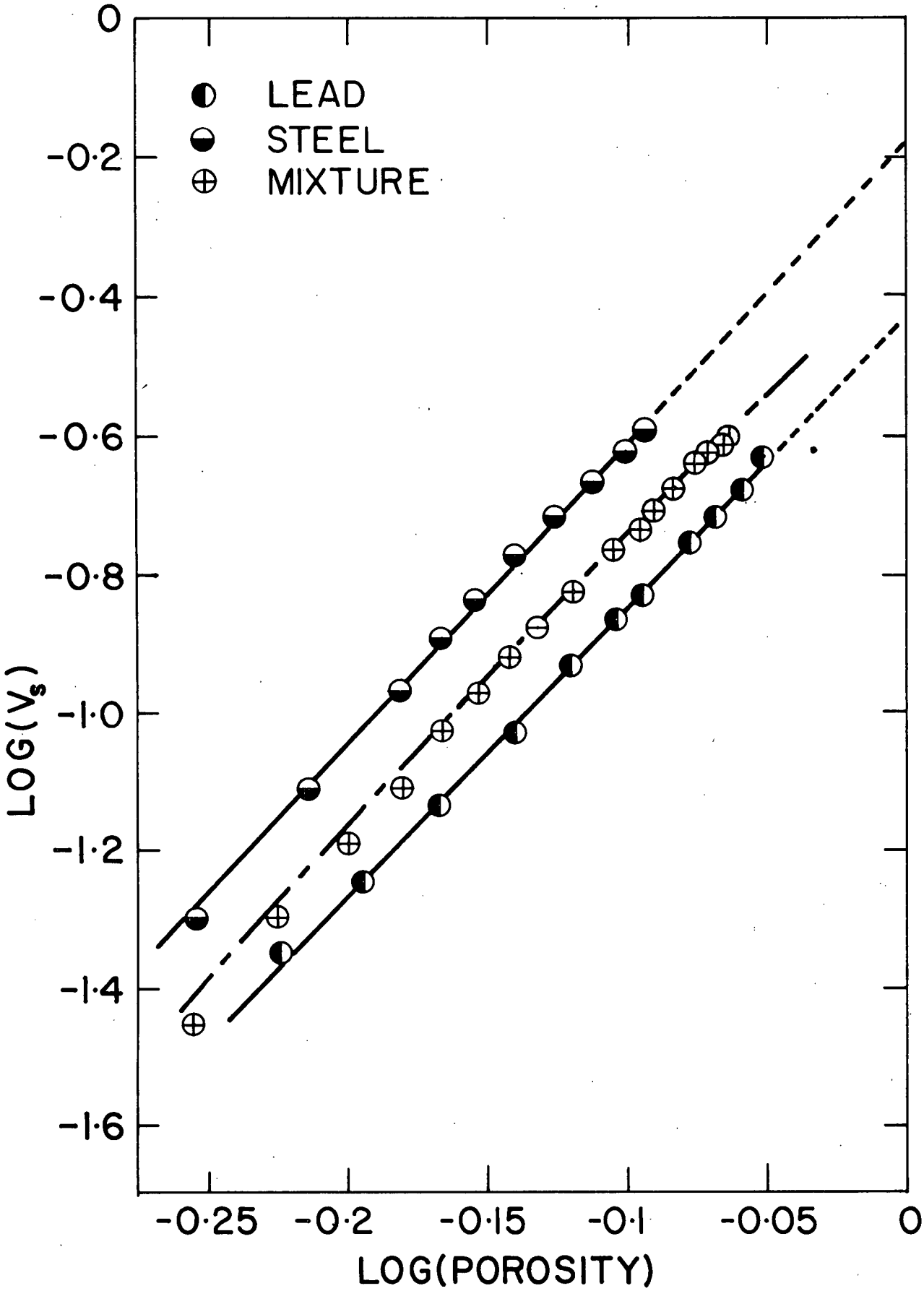

Figure 21. Plot of Lead and Steel Bed Expansions.

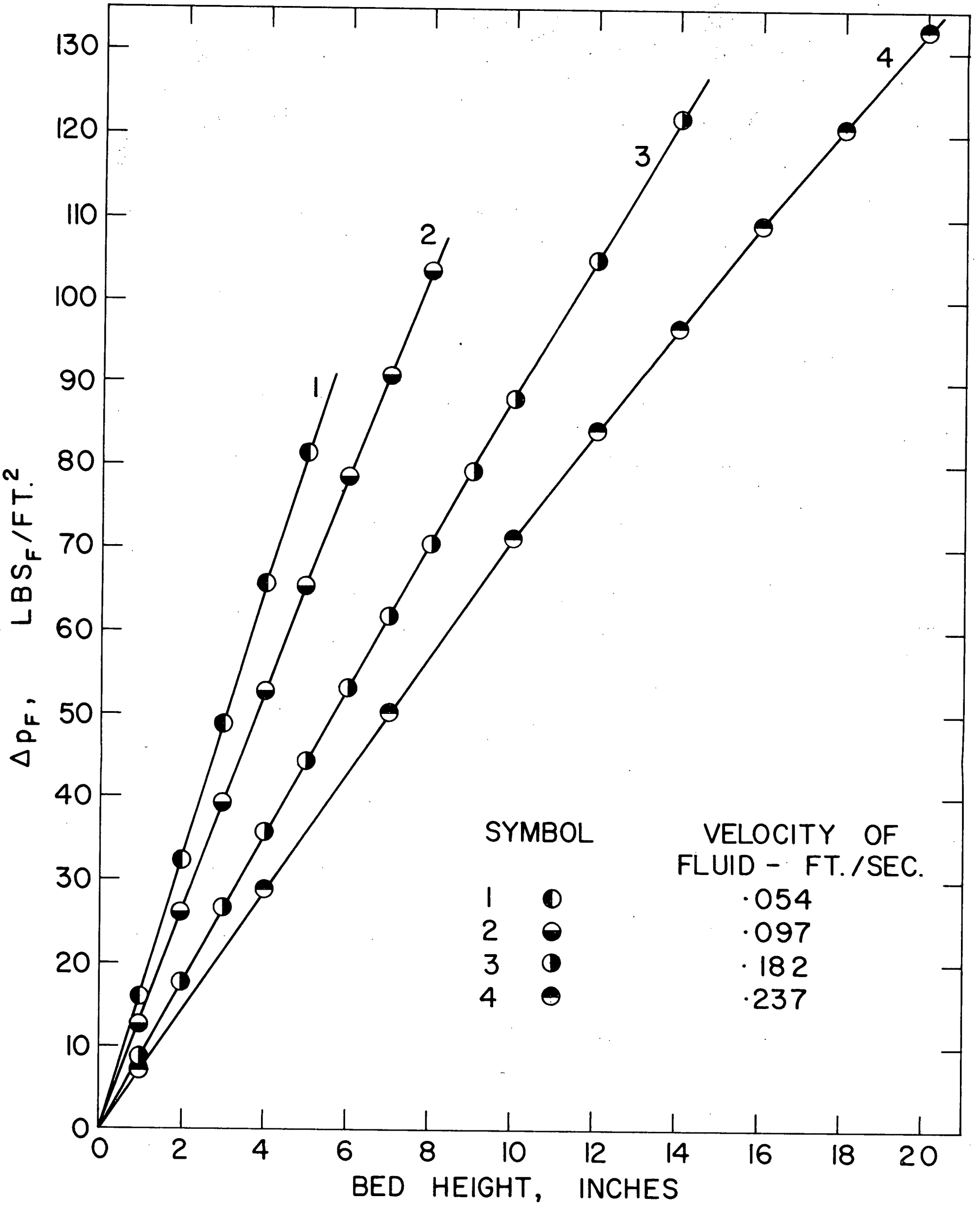

Figure 22. Differential Pressure Profiles in Lead-Steel Bed.

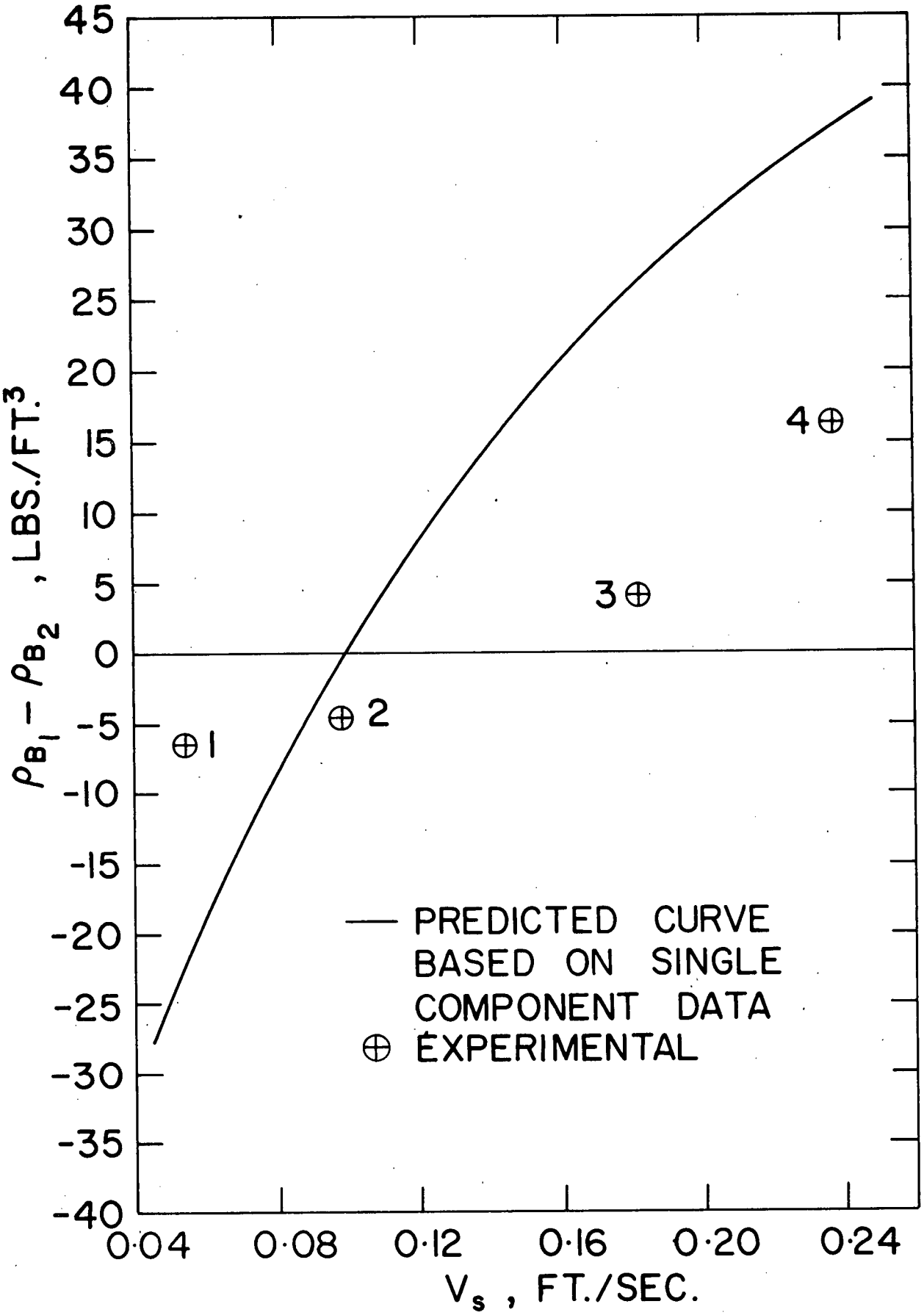

Figure 23. Plot of Bulk Density Difference and Velocity for the Lead-Steel Bed.

Table 11

Inversion Results for Nickel-Glass and Ballotini Mixture.

Properties of Mixture Components	d,mm	0.542	1.08
	ρ_s	4.50	2.91
	Material	Nickel-Glass	Ballotini
	Wt. of sample	296.0 gm.	290.0 gm.
buoyancy ratio	γ	0.537	
size ratio	r	1.99	
predicted inversion porosity (ϵ_m) by equation (39)		0.804	
predicted inversion porosity using single component data		0.841	
experimental inversion porosity		0.807	
flow régime		Stokes	

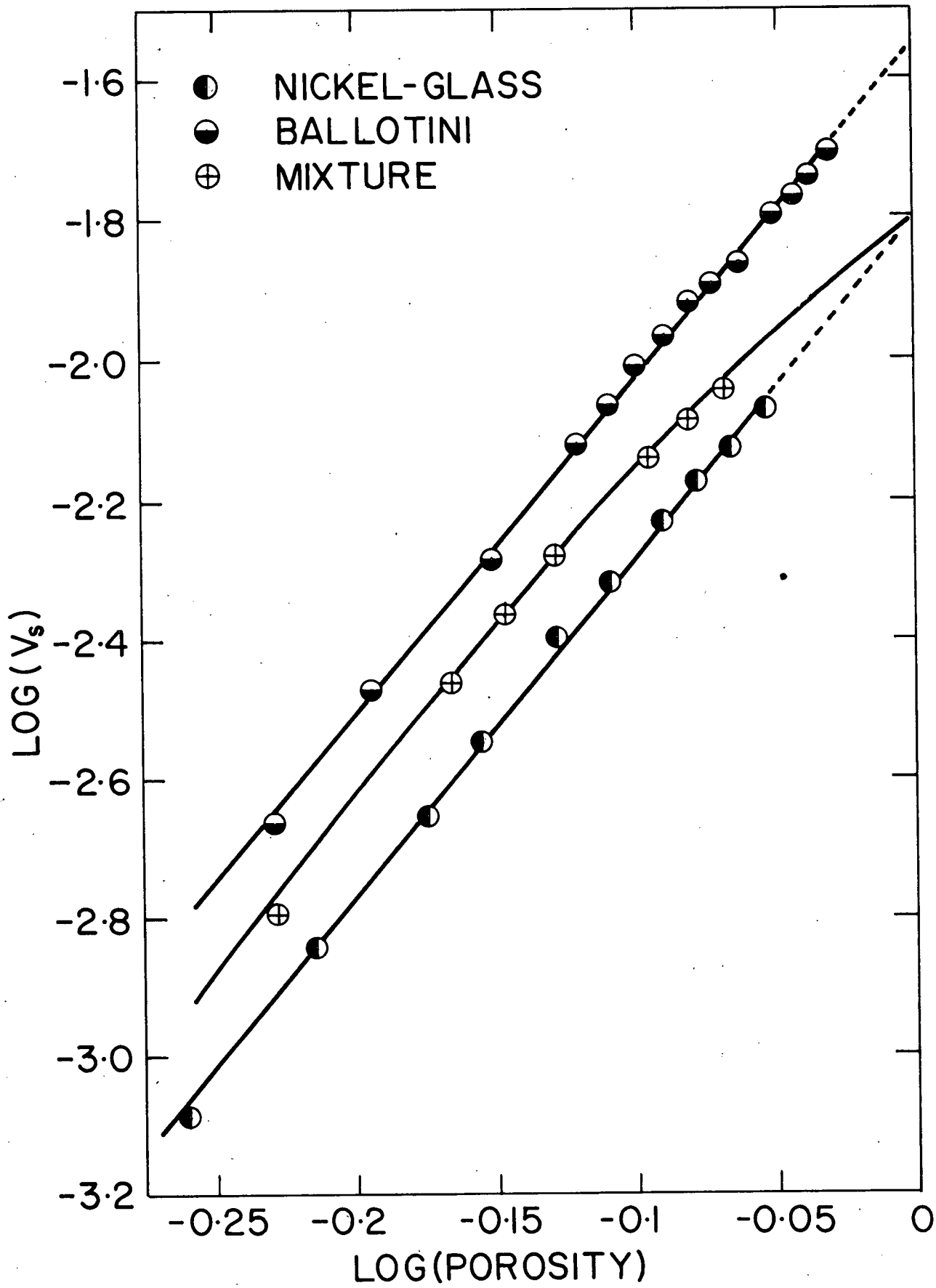

Figure 24. Plot of Nickel-Glass and Ballotini Bed Expansions in Polyethylene Glycol.

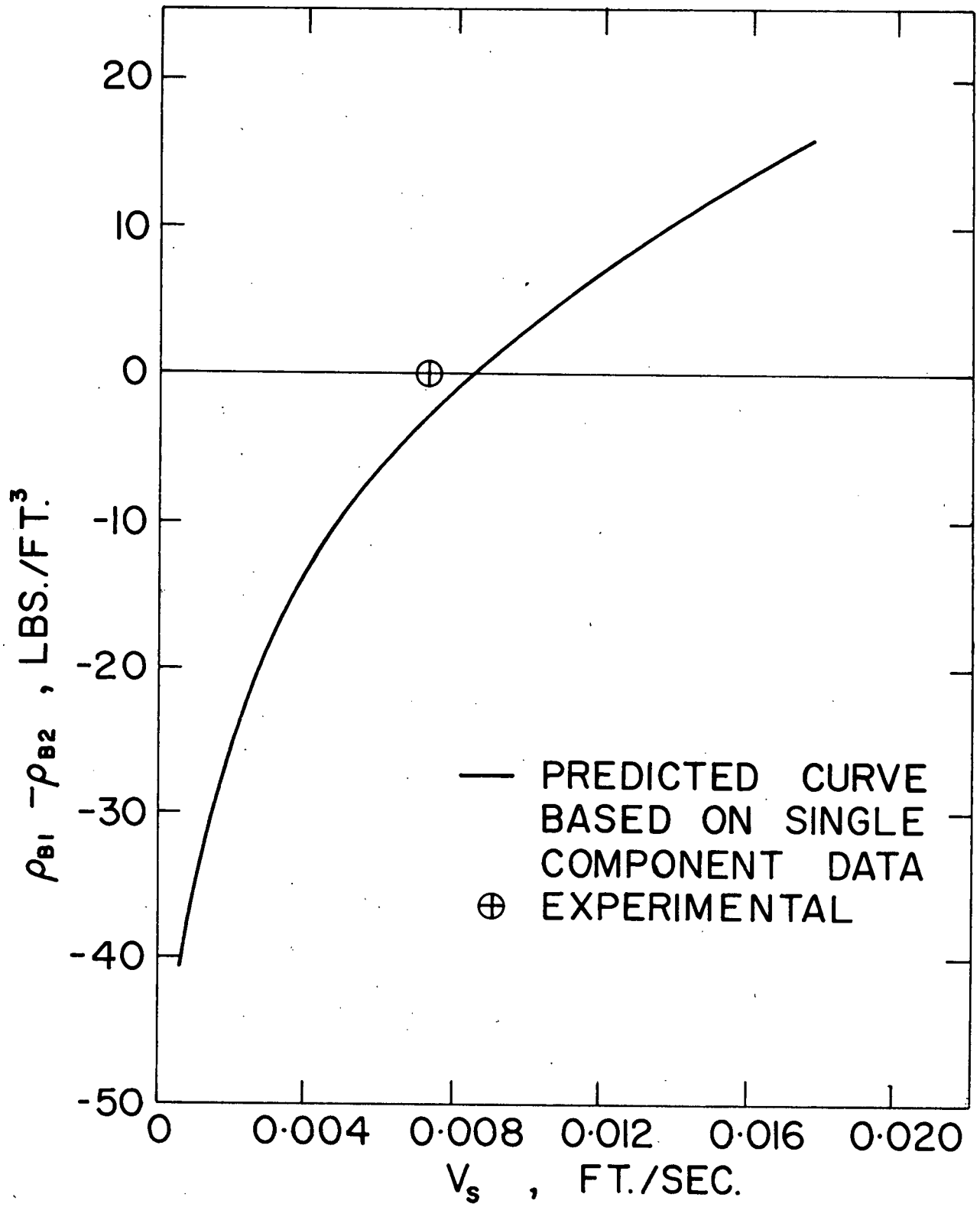

Figure 25. Plot of Bulk Density Difference and Velocity for Nickel-Glass - Ballotini Bed.

The superficial liquid velocity at which homogeneous fluidization occurred for the four mixtures was close to that predicted by equation (39) and that predicted from single component data. Visual observations showed a gradual transition from heavy component predominantly at the bottom to the heavy component predominantly at the top of the bed, as the velocity of the fluid was increased. An instantaneous flip-over of the component beds as described in the theory did not occur. The way in which the inversions proceeded is interesting. As the superficial liquid velocity was increased, mixing of the two components began at the interface between the two beds, producing a region of mixed bed. Further increase in velocity caused the mixed bed region to expand both upwards and downwards, until it engulfed the whole fluidized bed. Finally, as the velocity was increased further, the heavy small particles began to move out of the mixed bed and form a bed above the mixed bed. The mixed bed was slowly depleted of heavy small particles as the velocity was increased until the number of small particles left in the mixed bed was very small. Figures give a shcematic representation of the inversion of two mixtures.

The velocity interval over which the interface between beds was indistinguishable occurred between bulk density differences of approximately -15 and +4 lbs m/ft^3. In this region of small bulk density differences between the two components, the factors causing mixing, such as velocity distribution and particle size distribution, have a greater effect than the small bulk density gradients, and the beds remain mixed and do not segregate.

In order to have an almost instantaneous inversion, the region of small bulk density difference must correspond to a small change in superficial liquid velocity. For a sharp clear inversion the rate of change of bulk density with respect to velocity must be large. Considering

equation 28, the porosity is the only variable on the right hand side which is a function of velocity. Therefore the gradient of bulk density difference with respect to porosity must be directly related to the gradient of bulk density difference with respect to velocity. Thus

$$\rho_{B1} - \rho_{B2} = (\rho_{s1} - \rho)\left[(1 - \frac{1}{\gamma}) - \epsilon_1(1 - \frac{r^{(3-m)/mn}}{\gamma^{(mn-1)/mn}})\right] \qquad 28$$

Differentiating with respect to ϵ_1, we have

$$\frac{d(\rho_{B1} - \rho_{B2})}{d\epsilon_1} = (\rho_{s1} - \rho)\left[\frac{r^{(3-m)/mn}}{\gamma^{(mn-1)/mn}} - 1\right] \qquad 53$$

To have an inversion with $\gamma < 1$, it is necessary that $1 < r$ and thus

$$\frac{r^{(3-m)/mn}}{\gamma^{(mn-1)/mn}} > 1$$

Referring to equation 53, it is apparent therefore that for a large gradient of bulk density difference with respect to porosity, r must be large, $(\rho_{s1} - \rho)$ must be large and γ must be small. Analysis of the data shows that these factors do indeed have the predicted effect on the quality of inversion. A comparison of mixtures appears in table 12.

Table 12

Quality-of-Inversion Predictions

Mixture	Nickel-Ballotini	Nickel-Glass Ballotini	Alundum Ballotini
$\rho_{s1} - \rho$	1.84 gm/cc	1.84 gm/cc	1.84 gm/cc
r	5.01	1.99	1.67
γ	0.212	0.537	0.640
$d(\rho_{B1} - \rho_{B2})/d\epsilon_1$	10.6 gm/cc	2.21 gm/cc	1.44 gm/cc
Comments:	very good clear-cut inversion	fair inversion	mixed bed over most of fluidization region - poor inversion.

Particle size distributions affected the preciseness of the inversions and caused them to occur over a range of velocities. If a fluidized bed is composed of material of a range of sizes, there will be a porosity gradient through the fluidized bed which will cause a bulk density gradient. This has been shown to be so by Andrieu (10) and numerous other workers (4, 8, 9). Andrieu has also shown that the porosity gradation and thus the bulk density gradation increase as the overall average porosity is increased. Both components in the mixture have particle size distributions and thus both have bulk density distributions. Three cases arise. (1) The bulk density distributions of both beds is equal. (2) The bulk density distribution of the small heavy particles is greater than that of the large light particles. (3) The bulk density distribution of the heavy small particles is less than the bulk density distribution of the large particles. Case (2) is the most likely for two reasons. As small particles cannot be sized as well as large particles, the bulk density distribution will be greater for the small particle bed. Also, the small heavy particles will be at a higher porosity at inversion than the large light particles, so that the bulk density distribution will again be greater for the small heavy particles than for the large particles. Case (3) is very unlikely. As the density ratio and size ratio of the particles approach unity, the probability of case (1) increases.

As case (2) is the most likely, the way in which it affects the fluidized mixture will be discussed. The beds will begin to mix when the bulk density at the bottom of the top bed is equal to the bulk density at the top of the bottom bed. See figure 26a. As the bulk density variation in the small particle bed is greater than in the large particle bed, the small particles will begin to form a single component bed above the mixed bed before the average bulk density differences between the beds is zero.

This is illustrated in figure 26b, and accounts for the fact that the observed inversion point always fell to the left of the theoretical cross-over point in Figures 15, 19, 23 and 25. The components will finally separate completely into two beds when we have that situation which is shown in figure 26c. This was readily noticeable with the nickel-ballotini mixture, where the particle size distribution of the nickel particles was much larger than that of the ballotini particles. After the inversion point was reached and an apparent homogeneous fluidized bed appeared, as the superficial liquid velocity was increased a nickel bed began to form on top of the mixed bed. The nickel bed became larger but a mixed bed region remained until a much greater velocity than the inversion velocity was reached.

The case (1) situation would be similar to that of the alundum-ballotini mixture. Here, after the inversion point was reached, a ballotini bed began to form at the bottom of the mixed bed and an alundum bed at the top. As the superficial liquid velocity was increased, the region of mixed bed decreased until it disappeared at the centre of the bed. This is shown in figure 26d.

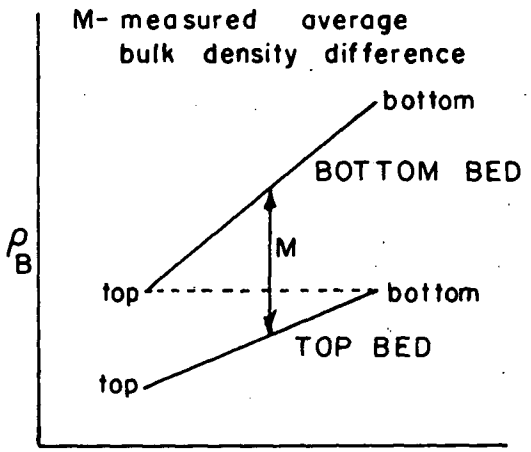

26a. beds beginning to mix.

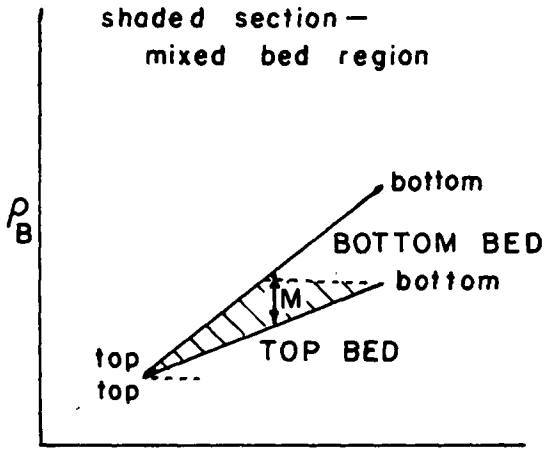

26b. initial bottom bed beginning to form bed at top of mixed bed.

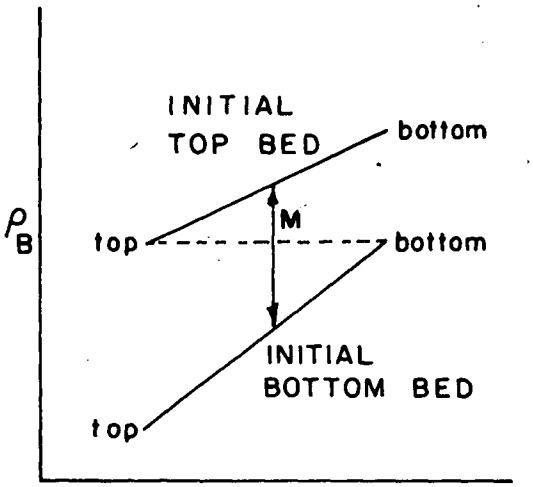

26c. initial bottom bed now on top - complete segregation.

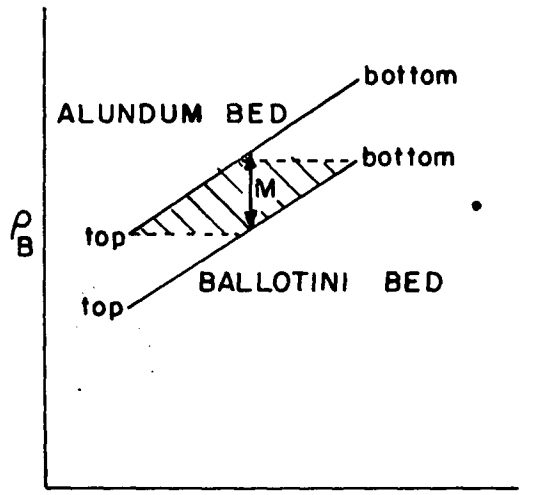

26d. alundum-ballotini mixture situation 1.

Figure.26. Effect of Particle Size Distributions on the Point of Inversion.

22 Prediction of Bed Expansion for Mixtures.

Equation 44, developed in an earlier section to predict bed expansions for mixtures of different materials, was tested for numerous mixtures in fluidizing media of water and polyethylene glycol solutions. The equation predicts the expansion of the mixed beds very well. In the inversion runs made with polyethylene glycol solutions, the experimental data cover the complete range of mixing of the two components, and equation 44 still predicts the expansion to a high degree of accuracy. Comparisons of experimental and predicted expansions in polyethylene glycol solutions are given in figures 13, 17, 21 and 24. In each case, the predicted expansion is represented by the dark bold line and the experimental data by the circular points.

Many runs of different materials were made in water-fluidized beds to test equation 44 thoroughly. Mixtures for which the γ ratio was large and the r ratio small, represented by figures 27, 28 and 29, and similarly mixtures with small γ ratios and large r ratios, represented by figures 30 and 31, were tested to determine the effect of these factors on how well the equation predicted the actual expansion. It was found that for large r ratios, the equation did not predict the expansion well at low porosities. In the region where one of the components is near the minimum porosity of fluidization, the predicted curve deviated from the experimental data. The latter fell much closer to the expansion line for that component which is near the minimum fluidization velocity than did the predicted results. This can be seen in Figure 31 .

A series of runs was made with various ratios of nickel-glass and ballotini to test equation 44 when there was large differences in the volume of each component present. The equation predicted the results fairly well for all ratios. Results are given in figure 32.

It is interesting that an equation which is based on the assumption that the two materials are completely segregated into two beds predicts the expansion even when the two components are partially or completely mixed. This seems to indicate that the building block theory of Happel (6), that a fluidized bed is made up of cells, each of which is associated with a particle, and that the size of the cells is dependent only on the particle and the slip velocity of the fluid, is sound. Thus the cells will be the same size whether they are in the mixture or in a completely segregated bed.

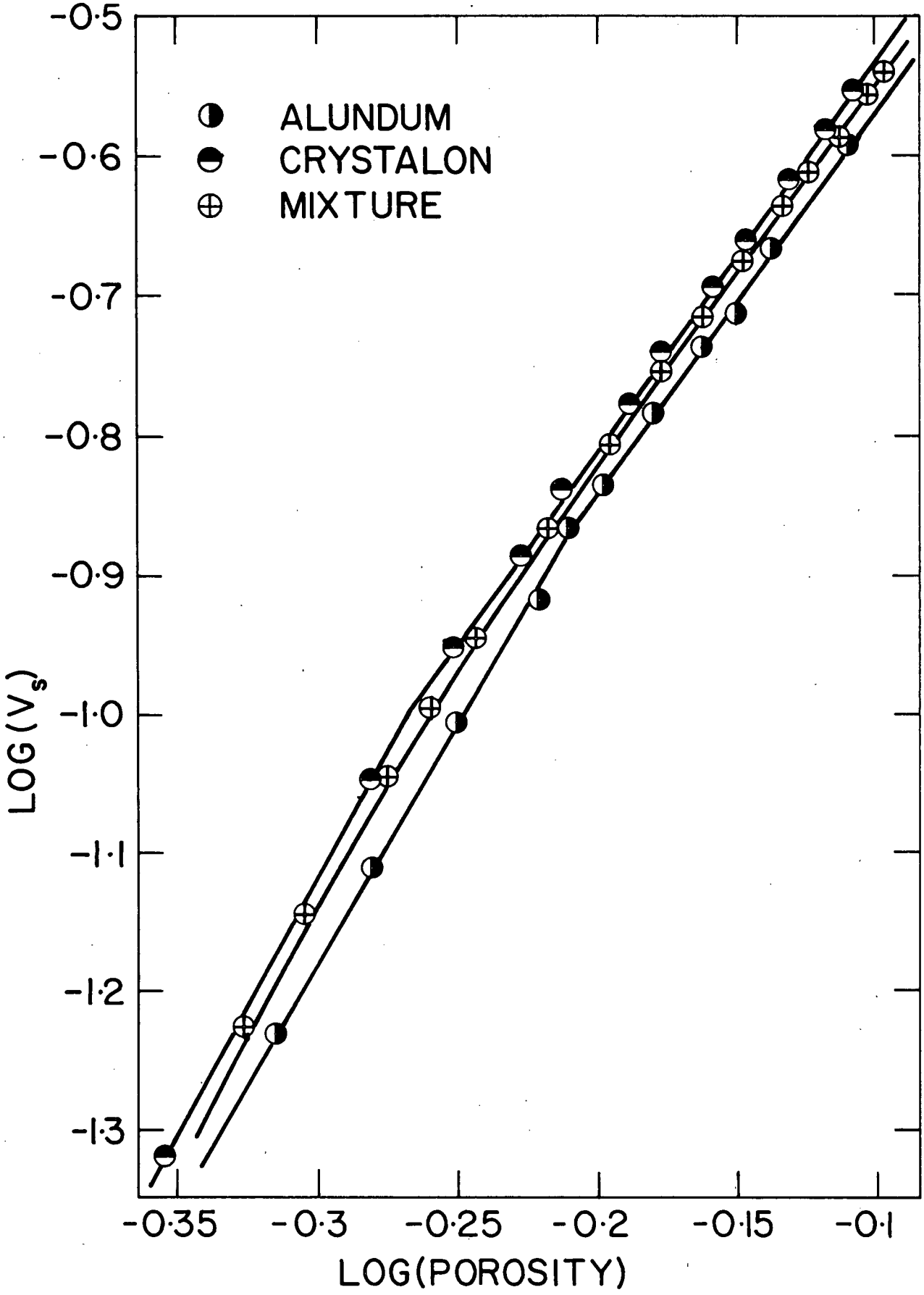

Figure 27. Plot of Alundum-Crystalon Run No.1.

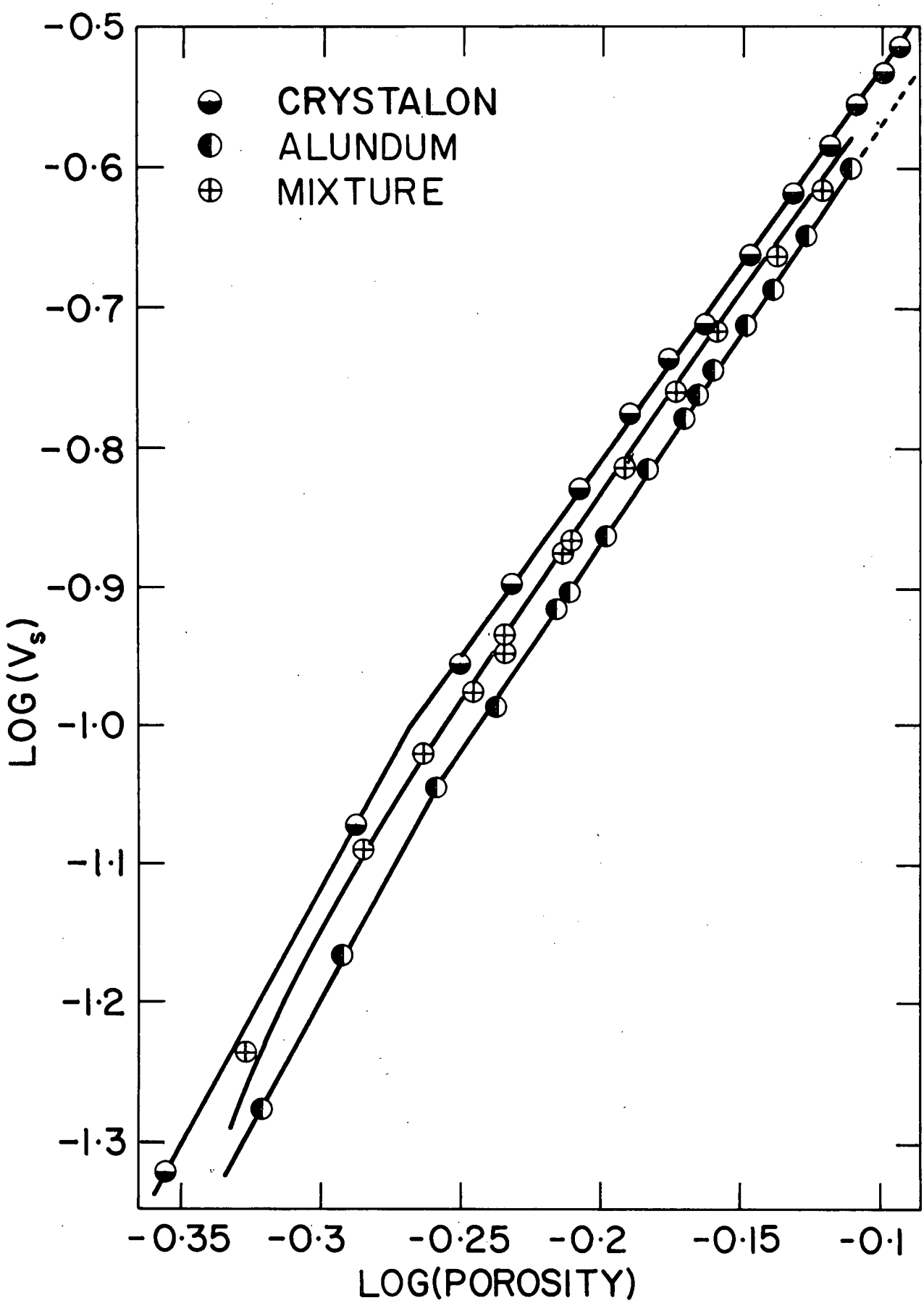

Figure 28. Plot of Alundum-Crystalon Run No.2.

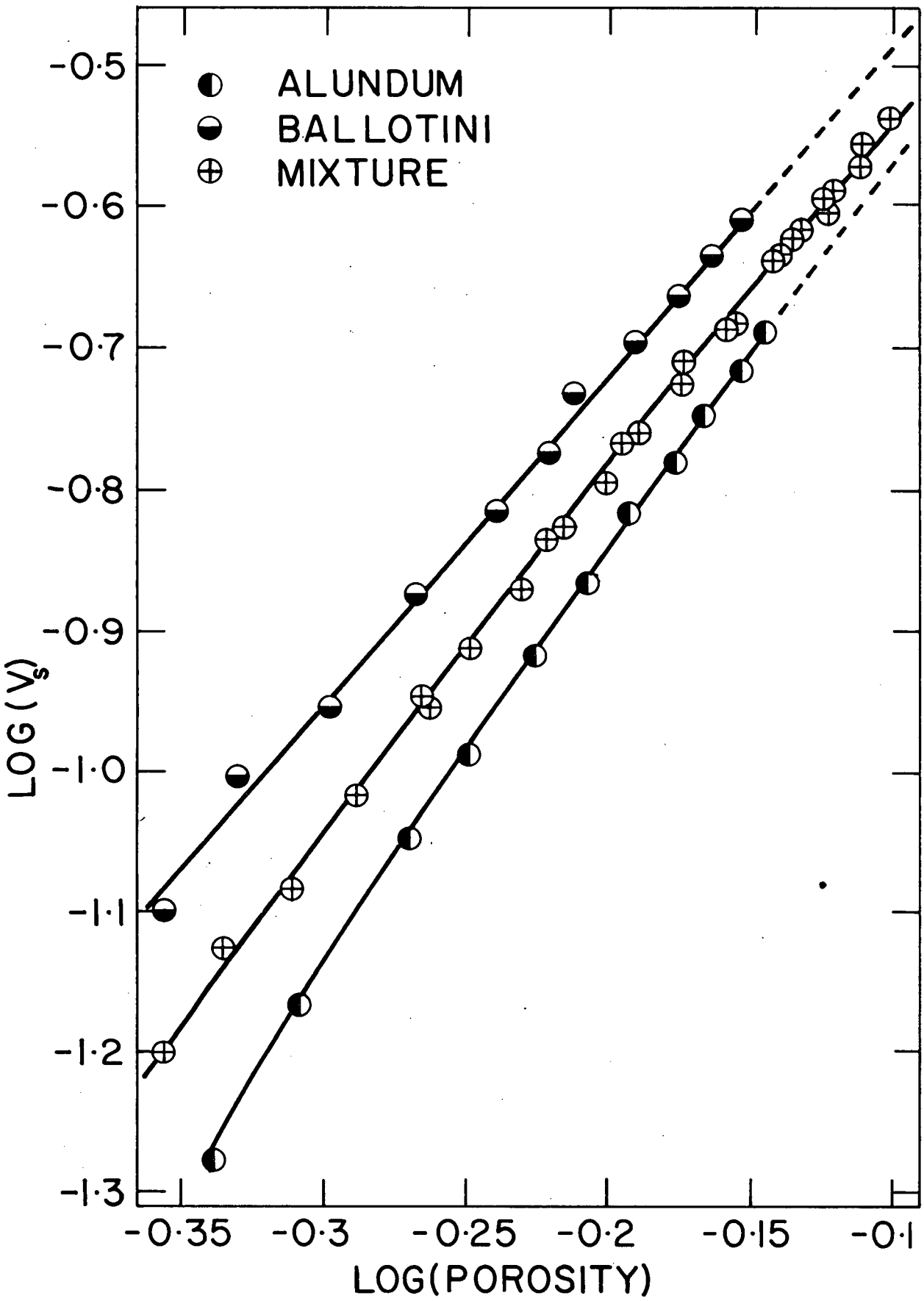

Figure 29. Plot of Alundum and Ballotini Bed Expansions in Water.

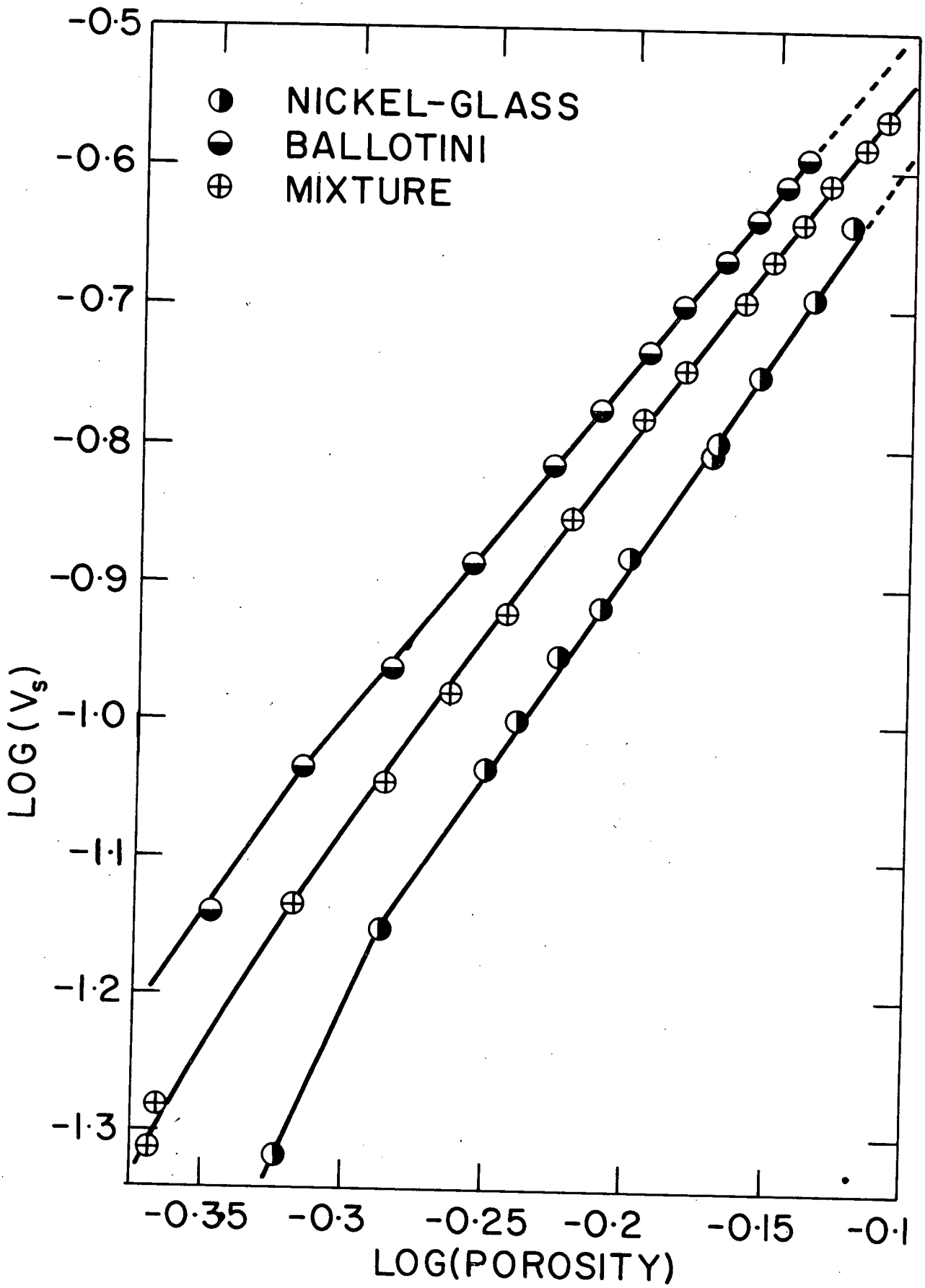

Figure 30. Plot of Nickel-Glass and Ballotini Bed Expansions in Water.

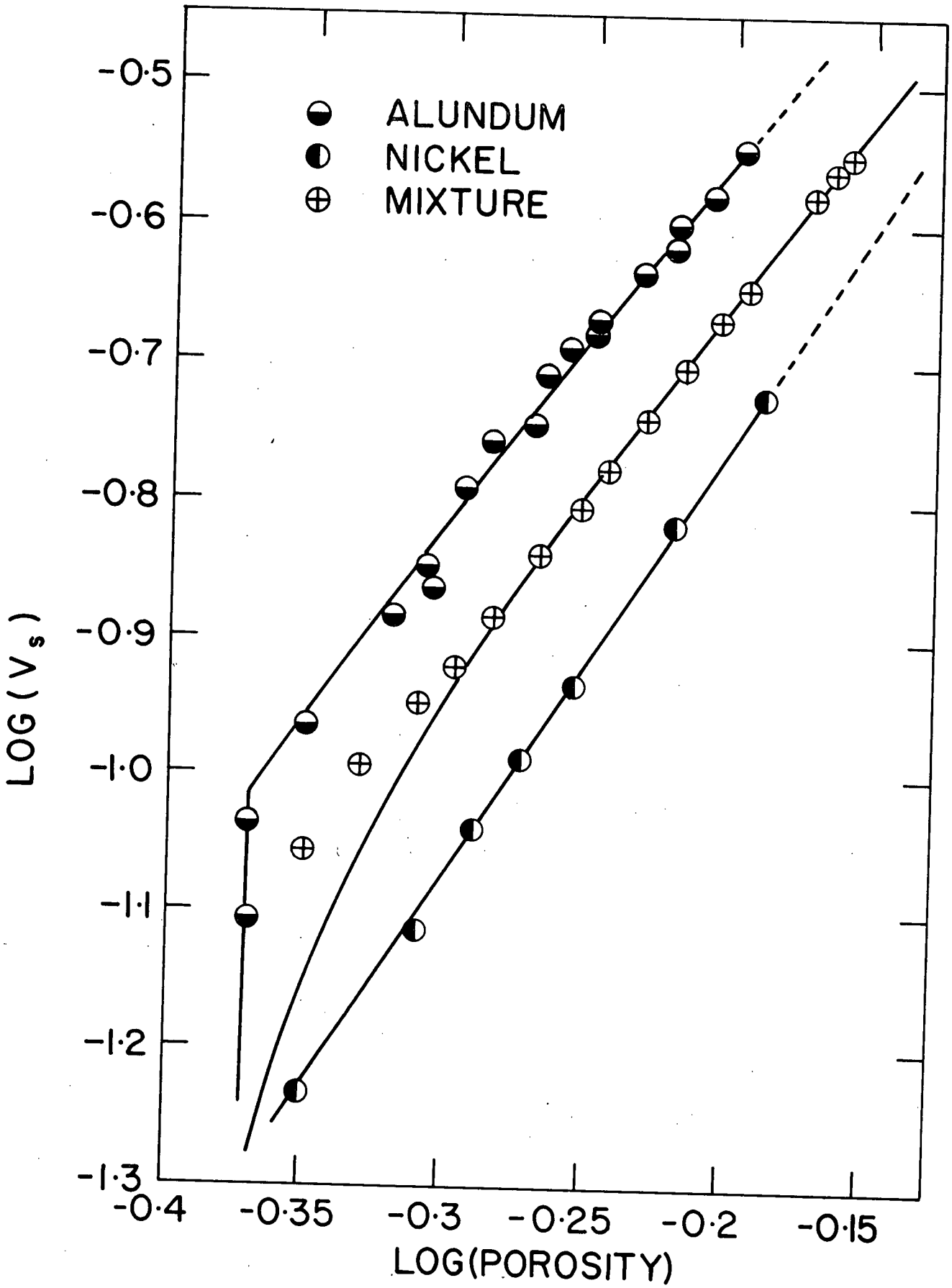

Figure 31. Plot of Nickel and Alundum Bed Expansion.

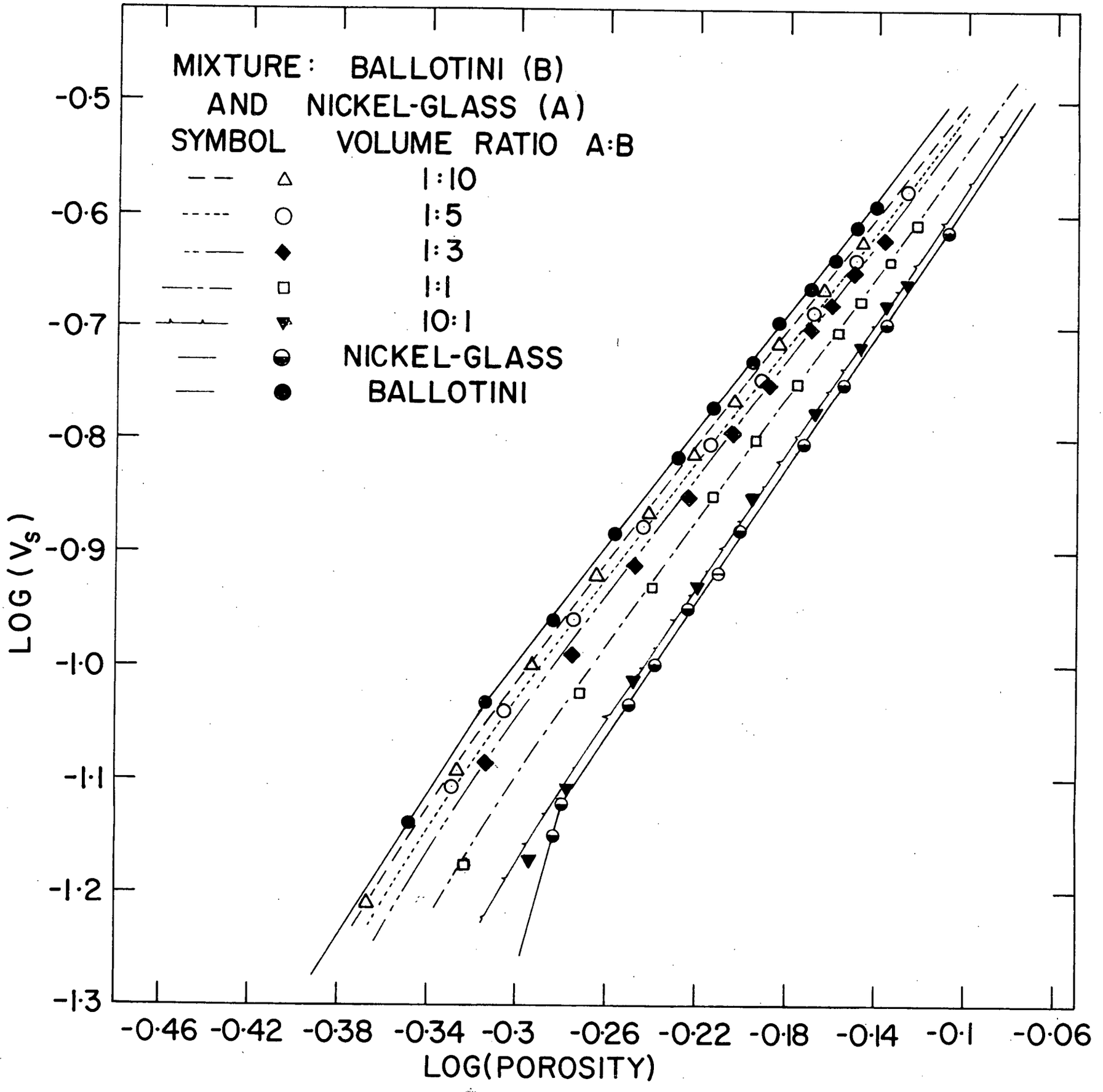

Figure 32. Plot of Nickel-Glass and Ballotini Bed Expansions with Different Volumes of Each Component.

CONCLUSIONS

1. The superficial liquid velocity which produces homogeneous fluidization of two species does so at a mean porosity for the fluidized mixture which is very close to that predicted by equation 39 and that predicted by single component data. Equation 39 is based on the following four assumptions: $n_1 = n_2$, $m_1 = m_2$, $k_{12} \equiv k_2$, and $(d_1 - d_2)/D_n$ is small. These conditions are satisfied approximately; each is in error by a small amount. Thus equation 39 can be expected to give only an approximate value for the inversion porosity, and corresponding velocity. The single component data also cannot predict inversion velocities precisely, because the porosity-velocity relationships obtained for the single component beds are average values over the whole bed. Point conditions in the fluidized bed describe the situation better than average values, especially when the particles are not perfectly uniform in size. Homogeneous mixing in the fluidized mixture is a function of the relative bulk density distribution in the single component beds.

2. The experimental mixture porosity at homogeneous fluidization is less than that predicted by single component data. This was analyzed and it was found that the only cause could be particle size distribution in the two single component beds. Also, the bulk density gradation in the small particle bed must be greater than that in the large particle bed. This would cause the point of homogeneous fluidization to be reached before that predicted from single component data. The two conditions which cause the bulk density gradation to be greater in the small particle bed are:

(1) the large particles can be sized better than the small particles;

(2) the small particles are at a higher average porosity, thus the effect of particle size distribution on the bulk density will be much greater

than for the large particles, which are at a much lower porosity.

3. For a clear-cut inversion in the fluidized bed the region of low bulk density differences, where mixing forces are predominant, must be traversed by a small change in velocity. This is accomplished by having a large value of r and a correspondingly small value of γ.

4. In contrast to beds fluidized by polyethylene glycol solutions, inversions in water-fluidized beds were not obtained because the extreme turbulence, particle circulation, and porosity distributions disrupted the bed too much. Bulk density gradients did not get a chance to develop, as mixing forces were much more predominant. The porosity of the small particle beds required to produce homogeneous fluidization was usually greater than 85%. At porosities in this range, water-fluidized beds are hydrodynamically unstable.

5. The prediction of mixed bed expansion based on single component data using equation 44 is very good. The equation predicts the expansion over the measured range of fluidization for mixtures which have volume ratios as great as 10:1. It also predicts the expansion very well for a wide range of γ and r ratios. The predicted values begin to deviate from the experimental values when one of the two components of the mixture is close to its minimum porosity for fluidization. Even though the equation is based on the assumption of no mixing of the component beds, it predicts the expansion of the four mixtures which passed through all stages of mixing as they were fluidized. This seems to indicate that the holdup in a fluidized bed is only a function of the individual particles and the superficial liquid velocity, and unaffected by particle interactions.

6. The Richardson and Zaki method of plotting data for single components appears to be excellent, as most data fell on a straight line having a slope very nearly equal to that predicted by the Richardson and Zaki equations.

The data began to tail off at very high porosities, but this is probably caused by size stratification in the fluidized bed.

7. Equation 23, developed by Richardson and Zaki for calculating the free settling velocity of the particles from the expansion lines velocity intercept at a porosity of 100%, gives answers which are often 10-20% different from those calculated using the drag coefficient-Reynolds' number plot for spheres. This could be caused by a number of factors, two of which may be the non-sphericity and non-uniformity of the particles. On the other hand, there is also the possibility that equation 23 does not adequately correct for the wall effect. Richardson and Zaki have assumed that the wall effect is only a function of the particle to column diameter ratio; and have ignored other possible variables such as fluid régime.

8. The frictional pressure drop equation based on a simple force balance, popularized by Wilhelm and Kwauk, predicts the experimental results well, except at very high porosities where there is a large amount of segregation by size of the particles. The average error is approximately 5%. The error due to assuming the wall pressure loss was negligible was found to be less than 1%. Also it has been shown that measurement of pressure loss profiles is an excellent method for determining longitudinal bulk density and porosity distributions in fluidized beds.

Recommendations for Further Work

1. Determination of the effect of particle size distribution on the inversion point is important. This may be accomplished by the following procedure:

(a) Fluidize a mixture of two materials of known properties and obtain expansion and differential pressure data for the mixture.

(b) At a velocity just less than the inversion velocity, remove separately the upper and lower portions of the bed. Measure the average particle diameter of the small heavy particles which were in the top bed. Do the same for the large particles which were in the small particle bed.

(c) With the small particles which were in the large particle bed and the large particles which were in the small particle bed removed, fluidize the remaining mixture. Expansion and differential pressure data should be obtained.

(d) At a velocity just greater than the inversion velocity, remove separately the upper and lower beds of the mixture. Measure the average particle diameter of the large particles which remained in the top bed and of the small particles which remained in the bottom bed.

If the particle size distribution was approximately Gaussian and if particle size distribution is important, the following results should be obtained. Figure 33 is a diagram of the particle size distribution in the small heavy particle bed and the large light particle bed. The average diameter of the small particles measured in part (b) should be in the shaded region A. The average diameter of the small particles measured in part (d) should be in the shaded region B. Similarly for the large particle bed, the average diameter of the particles removed in part (b) should be in the shaded region D, and the average diameter of the particles

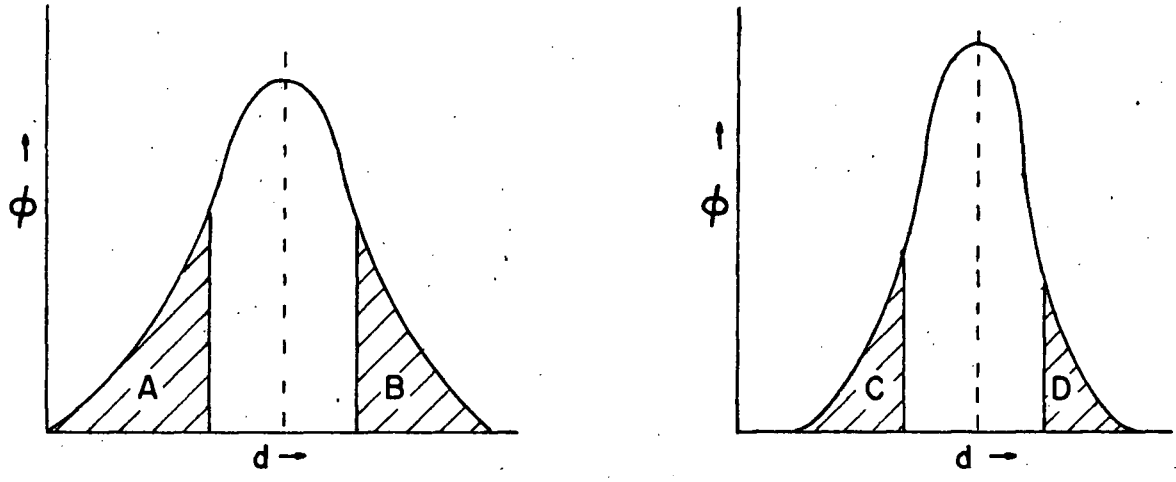

small heavy particle size distribution.

large light particle size distribution.

Figure 33. Particle Size Distributions

removed in part (d) should be in the shaded region C. If the above conditions are consistent with the experimental results for average particle diameters, then particle size distribution is a very important factor affecting inversions. The above procedure may be carried out a number of times until the inversion occurs over a very narrow velocity range.

2. Most mixtures subjected to inversion runs in the present research were approximately 50-50 mixtures by volume. Numerous experiments should be run where the initial amount of each component added is different from 50% by volume. If the results are similar to those obtained in the present report, it can be concluded that the relative proportions of each material has noteffect on the mixing and segregation in the fluidized mixture. If the inversions obtained are clear-cut, then runs made with very small amounts of one material added to another

can be used to measure rates of mixing. The time for the small amount of material to mix homogeneously in the component of large volume could be measured. This would be a measure of the random mixing of particles, because the driving force due to bulk density difference would then be negligible.

3. Experiments may be made to determine the experimental limits of density and size difference which can be tolerated in seeking an inversion.

4. Motion pictures of inversions may also be taken to record visually how an inversion takes place.

Literature Cited

1. Wilhelm, R.H., and Kwauk, M., Chem.Eng.Progr., 44, 201 (1948).
2. Hancock, R.T., The Mining Magazine, 55, 90 (1936).
3. Jottrand, R.J., Chem.Eng.Sci., 3, 12 (1954).
4. Richardson, J.F., and Zaki, W.N., Trans.Inst.Chem.Engrs. (London), 32, 35 (1954).
5. Leva, M., Fluidization, McGraw-Hill Book Co. Inc., New York, 1959.
6. Happel, J., A.I.Ch.E. Journal, 4, 197 (1958).
7. Hawksley, P.G.W., Paper No.7 in "Some Aspects of Fluid Flow", London, Edward Arnold and Co., 1951.
8. Lewis, E.W., and Bowerman, E.W., Chem.Eng.Progr., 48, 603 (1952).
9. Verschoor, H., Appl.Sci.Research, A2, 155 (1950).
10. Andrieu, R., Ph.D. thesis, University of Nancy, France, 1956.
11. Beare, J.W., B.A.Sc. thesis, University of British Columbia, 1958.
12. Hoffman, R.F., Lapidus, L., and Elgin, J.C., A.I.Ch.E. Journal, 6, 321 (1960).
13. De Verteuil, G.F., B.A.Sc. thesis, University of British Columbia, 1958.
14. A.S.T.M. Standards on Petroleum Products and Lubricants, Baltimore, 1958, page 201.
15. Pruden, B.B., M.A.Sc. thesis, University of British Columbia, 1964.
16. Cairns, E.J., and Prausnitz, J.M., A.I.Ch.E. Journal, 6, 554 (1960),
17. Cairns, E.J., and Prausnitz, J.M., Ind.Eng.Chem., 51, 1441 (1959).
18. Jackson, R.A., Trans.Instn. of Chem.Engrs. (London), 41, 13 (1963).
19. Slis, P.L., Willemse, T.W., Kramers, H., Appl.Sci.Res.Sec. A, 8, 209 (1959).
20. Adler, I.L., and Happel, J., Chem.Eng.Symposium Series, No.38, 58, 98 (1962).

APPENDIX I - BEARE'S PLOTS FOR PREDICTION OF INVERSION POROSITIES.

Below is presented Beare.'s plot for the laminar or Stokes' flow region. It relates inversion conditions with particular values of r and α. The plot is based on the simplifying assumptions that $n_2 = n_1 = 4.65$ in the Richardson-Zaki equations, and that the Stokes' law equation for free settling holds.

Thus

$$V_s = V_{o1}\epsilon^{n_1} = V_{o2}\epsilon^{n_2}$$

and

$$\frac{d_1^2(\rho_{s1}-\rho)g}{18\mu}\epsilon_1^{4.65} = \frac{d_2^2(\rho_{s2}-\rho)g}{18\mu}\epsilon_2^{4.65} \qquad (A)$$

The bulk density difference at inversion equals zero.

Therefore

$$\rho_{B1} - \rho_{B2} = \rho_{s1}(1-\epsilon_1) + \rho\epsilon_1 - \rho_{s2}(1-\epsilon_2) - \rho\epsilon_2 = 0$$

or

$$(1-\epsilon_1)(\rho_{s1}-\rho) = (1-\epsilon_2)(\rho_{s2}-\rho)$$

whence

$$\frac{1-\epsilon_1}{1-\epsilon_2} = \frac{\rho_{s2}-\rho}{\rho_{s1}-\rho}$$

Define

$$\alpha = \frac{1}{\gamma} = \frac{\rho_{s2}-\rho}{\rho_{s1}-\rho} > 1 \qquad r = \frac{d_1}{d_2} > 1$$

Then

$$\frac{1-\epsilon_1}{1-\epsilon_2} = \alpha \qquad (B)$$

and from equation A above,

$$r^2 = \alpha \left[\frac{\epsilon_2}{\epsilon_1} \right]^{4.65} \qquad (C)$$

Manipulating equations B and C,

$$\epsilon_1 = \frac{\alpha - 1}{\alpha^{3.65/4.65} r^{2/4.65} - 1}$$

and

$$\epsilon_2 = \epsilon_1/\alpha + (\alpha - 1)/\alpha$$

Using the two equations given above, a chart was developed by Beare to give the porosities of the two beds at inversion for any particular combination of r and α. The chart appears in figure 33.

A similar chart was also developed by the present author for the Newton region. The assumptions used are: (1) $n_1 = n_2 = 2.39$ and (2) Newton's law for free settling holds. The inversion porosities are then

$$\epsilon_1 = \frac{\alpha - 1}{\alpha^{3.78/4.78} r^{1/4.78} - 1}$$

and

$$\epsilon_2 = \epsilon_1/\alpha + (\alpha - 1)/\alpha$$

These equations were used to develop the chart, which works on the same principle as Beare's chart and appears in figure 34.

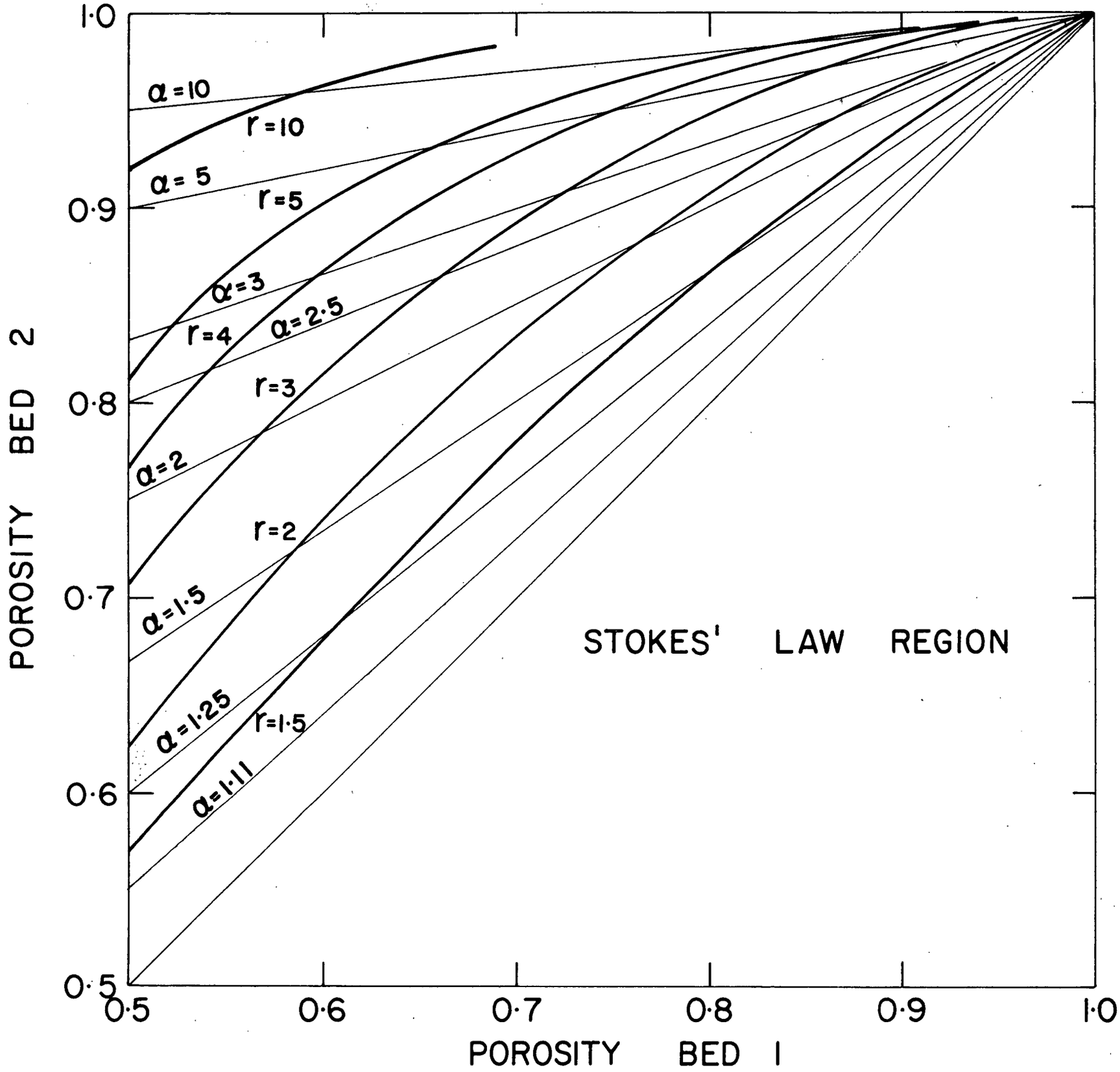

Figure 34. Beare Plot for Stokes' Law Region.

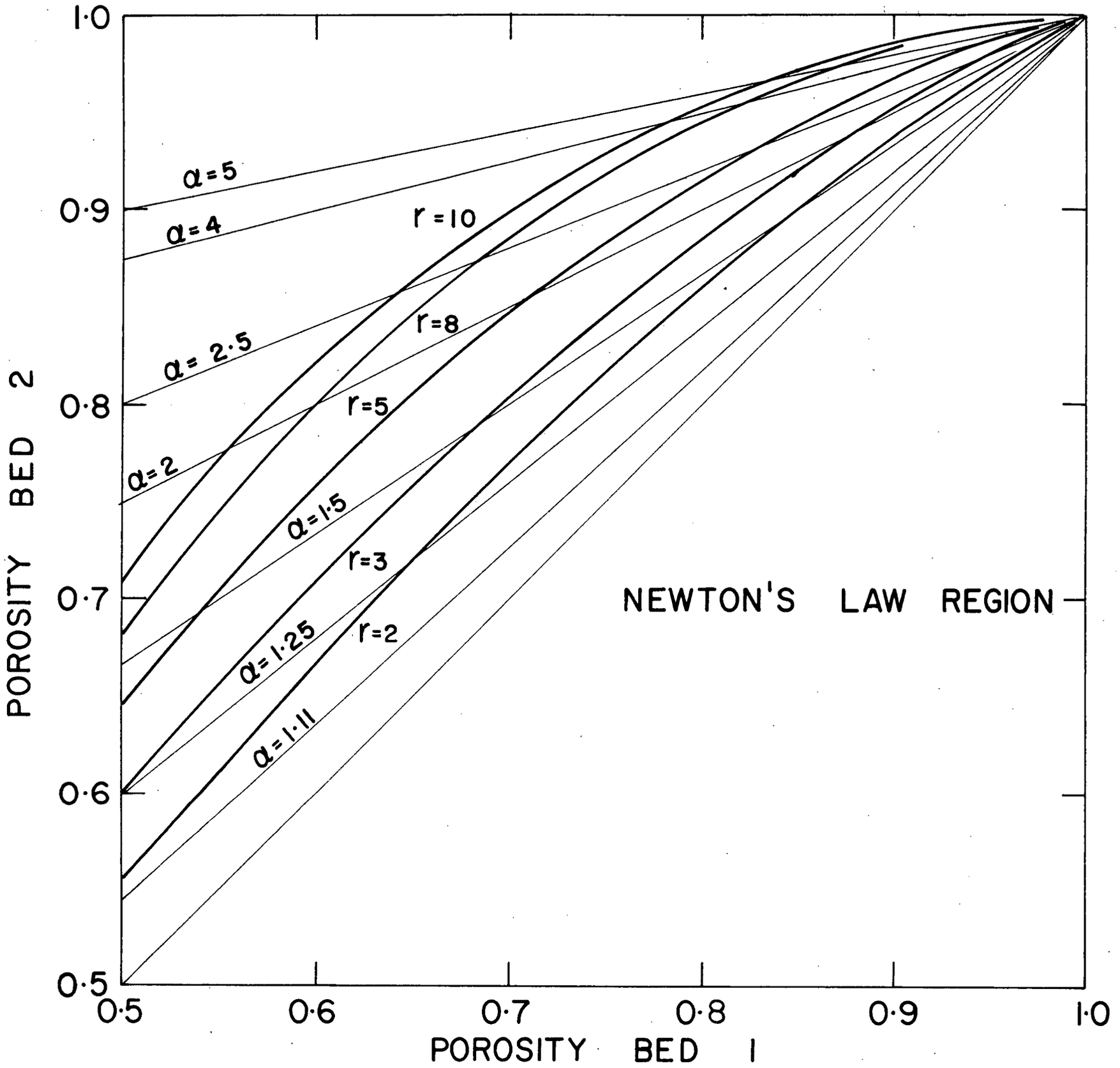

Figure 35. Beare Plot for Newton's Law Region.

APPENDIX II

SAMPLE CALCULATION AND ERROR ANALYSIS

Reference Literature Data:

Density of Mercury.
Perry, J.H., editor, Chemical Engineers' Handbook, Third Edition, McGraw-Hill Book Co.Inc., New York, 1950, p.176.

Density of Carbon Tetrachloride.
Riddick, J.A. and Toops, Jr., E.E., Organic Solvents, Volume 7, Second Edition, Interscience Publishers, Inc., New York, 1955, p.194.

Drag Coefficient - Reynolds' number data.
Zenz, A.F., and Othmer, D.F., Fluidization and Fluid-Particle Systems, Reinhold Publishing Corporation, New York, 1960, p.203.

Density of Water.
Chemical Engineers' Handbook, p.175, complete reference above.

Viscosity of Water.
Chemical Engineers' Handbook, p.374, complete reference above.

A. Porosity of Bed.

$H = 20.0 \pm 0.5$ cm. ; $\rho_s = 4.00 \pm 0.05$ gm./cc.

$W = 400.0 \pm 1.0$ gm. ; $A = 20.26 \pm 0.18$ cm^2.

$\epsilon = 1 - 400.0/(20.0 \times 20.26 \times 4.00)$

$= 0.724$

$$1 - \epsilon = W/\rho_s H A$$

$$= \frac{1}{400} + \frac{0.05}{4.00} + \frac{0.5}{20.0} + \frac{0.18}{20.26}$$

maximum error in $(1 - \epsilon) = (0.0487)(0.276)$

= maximum error in ϵ

maximum percent error in $\epsilon = \frac{(0.0487)(0.276)}{0.724} \times 100\%$

$= \pm 1.86\%$

B. Calculation of Pressure Loss in a Fluidized Bed.

$$\frac{\Delta p_F}{L} = 0.394 \frac{x}{L} (\rho_M - \rho_F) g/g_c \quad \text{lb force/ft.}^3$$

$x = 10.0 \pm 0.2$ cm. ; $\rho_M = 100.0 \pm 0.3$ lbs./ft.^{3} ;

$\rho_F = 67.0 \pm 0.6$ lbs./ft.^{3}; $L = 3.0 \pm 0.31$ inches.

$$(\rho_M - \rho_F) = (100.0 - 67.0) \pm 0.9 \text{ lbs./ft.}^3$$

maximum percent error in $\Delta p_F / L$ =

$$= \left(\frac{0.2}{10.0} + \frac{0.9}{33.0} + \frac{0.0313}{3.0} \right) 100\% = 5.77\ \%$$

C. Velocity of Fluid.

$V = f(Re)$

$D = 2.0 \pm 0.31$ inches ; $\rho_F = 66.6 \pm 0.6$ lbs./ft.^{3}

μ = 0.090 $\pm$ 0.002 lbs./ft.sec.

Re - taken from correlation chart, for which the mean error is $\pm$ 2.8%

maximum error in V = $2.8\% + \left(\frac{0.0313}{2.0} + \frac{0.6}{66.6} + \frac{0.002}{0.090} \right) 100\%$.

= 7.48%

APPENDIX III - MATERIALS USED

Material	Particle Shape	Density gm./cc.	Average Diameter mm.	Appendix IV Run No.
Alundum	granular, jagged	3.95	0.645	3
			0.645	2*
			0.767	2
			0.912	4
			1.52	11
Ballotini	glass spheres	2.91	1.08	1
			1.08	2*
			1.83	5
		2.73	2.28	1*
Cataphote	glass micro-beads	2.47	0.767	9
Crystalon	granular	3.50	1.08	6
Lead	shot, spherical	11.30	2.05	3*
Nickel	spherical	8.91	0.456	1*
			0.384	10
Nickel-Glass	nickel coated glass spheres	4.50	0.542	
Steel	ball bearings	7.80	3.15	3*

* polyethylene glycol solution run numbers

APPENDIX IV - ORIGINAL DATA

APPENDIX IV - INDEX

All original data for the expansion runs and the frictional pressure runs are included in this section. Explanations of table headings are as follows:

Ave. Diameter - the average diameter of the particles based on the arithmetic average of the screen sizes.

From Run - refers to the particular run in which the single component data for the material appears.

Across Taps - the frictional pressure gradient reading was measured across the following two pressure taps.

Run 1 (Polyethylene Glycol) - a run in which the fluidizing medium is the polyethylene glycol solution; similarly for water runs (water).

$\frac{1}{2}$" Meter (Mercury), etc. - refers to the particular flow meter and manometer fluid used to make that particular reading.

Run 1 (Polyethylene Glycol)
Material: Glass Ballotini — Ave. Diameter: 2.28mm.
Wt. of Sample: 400 gms. — Density: 2.73 gm./cm^3.

Manometer Reading arm 1	in.	arm 2	in.	Temperature column °F	Temperature Bed Room °F	Height cm.
9.15	*	6.95		70.8	70.1	23.6
14.00	*	10.75		71.0	71.0	29.8
0.60		4.60		72.5	73.4	38.3
3.90		4.30		71.0	71.6	54.6
5.50		7.00		71.0	71.4	96.6
4.55	*	3.15		69.5	69.6	17.5
2.20	*	1.00		70.2	70.8	14.1
6.60	*	4.80		70.4	70.9	20.2
15.10	*	11.65		70.6	71.0	31.8
4.15		2.25		70.7	71.0	45.3
6.10		4.00		71.0	70.9	71.8

- $\frac{1}{4}$" Meter (Mercury) - $\frac{1}{2}$" Meter (Air)

Run 1 (Polyethylene Glycol)
Material: Nickel — Ave. Diameter: 0.456 mm.
Wt. of Sample: 447 gms. — Density: 8.92 gm./cm^3.

Manometer Reading arm 1	in.	arm 2	in.	Temperature column °F	Temperature Room °F	Bed height	cm.
0.90		0.25		74.0	73.2	5.4	
1.10		0.35		73.9	73.4	5.7	
1.60		0.70		74.0	73.8	6.7	
2.05		1.10		74.0	73.6	7.4	
2.60		1.60		74.0	73.9	8.5	
3.40		2.30		73.9	73.6	10.1	
3.75		2.60		73.9	73.7	11.0	
4.40		3.10		73.8	73.8	12.3	
4.85		3.50		73.8	73.7	13.7	
5.65		4.10		73.8	73.8	16.0	
6.15		4.50		73.8	73.4	17.8	
6.50		4.85		73.8	73.4	19.5	
7.25		5.45		73.8	73.6	23.0	

$\frac{1}{4}$" Meter (Mercury)

Run 1 (Polyethylene Glycol)
Material: Glass Ballotini — Ave. Diameter: 2.28 mm.
Wt. of Sample: 400.0 gm. — Density: 2.73 gm./cc.
From Run

Manometer Reading arm 1 cm	arm 2 cm	Temp Column °F	Temp Room °F	Bed Height cm	Across Taps
59.0	61.4	70.8	70.1	23.5	1-2
56.8	63.7	70.8	71.1		1-4
54.3	66.2	71.0	71.0		1-6
52.0	68.6	71.0	71.0		1-8
59.2	61.2	71.0	71.0	29.8	1-2
57.3	63.0	71.0	71.0		1-4
55.5	65.0	72.0	72.5		1-6
53.7	66.9	72.0	72.5		1-8
51.9	68.8	72.0	73.2		1-10
52.6	68.5	72.5	73.4	38.3	1-12
53.6	67.1	73.0	73.8		1-10
55.0	65.6	72.4	73.3		1-8
56.4	64.2	72.4	73.3		1-6
50.7	55.6	71.2	71.2		1-4
52.3	53.9	71.0	71.5		1-2
52.6	53.7	71.0	71.6	54.6	1-2
51.7	54.5	71.0	71.8		1-4
50.5	55.7	71.0	71.6		1-6
47.4	57.8	71.0	71.4		1-10
47.3	59.0	71.0	71.5		1-12
45.4	61.0	71.2	71.5		1-16
43.5	63.0	71.0	71.4		1-20
42.3	64.3	71.0	71.4	96.6	1-36
44.1	62.4	71.0	71.1		1-28
46.5	59.9	71.5	71.2		1-20
49.8	56.4	71.2	71.4		1-10
51.4	54.6	69.5	69.6	17.5	1-2
48.5	57.5	69.6	69.8		1-4
48.5	57.5	70.0	70.4		2-5
51.5	54.7	70.0	70.7		4-5

Run 1 (Polyethylene Glycol)

Materials:	Glass Ballotini	Nickel
Wt. of Samples	400.0 gm.	459.0 gm.
From Run	1	1

Manometer Reading arm 1 in.	arm 2 in.	Temperature column °F	Temperature Room °F	Bed Heights cm. Ni	glass
0.40	1.55	71.8	72.0	8.4 *	21.5 *
1.10	2.35	71.7	72.6	10.6	25.0
1.80	3.10	71.6	72.6	12.2	28.0
2.65	4.10	71.8	72.8	14.5	31.5
3.35	4.95	71.5	72.8	16.0	34.1
4.50	6.35	71.6	72.9	-	37.2
5.60	7.45	70.5	70.6	-	40.2
6.30	8.55	70.3	71.6	39.6	48.0
6.70	9.05	71.8	73.5	37.5	59.0
7.30	9.90	72.5	74.0	36.0	70.0
4.50	6.50	71.0	73.1	-	36.3
8.20	5.85	71.0	73.2	39.6	40.5

$\frac{1}{4}$" Meter (Mercury)

* - Subtract 2.80 from all valves in column.

Run 1
Viscosity and Density

Temperature °F	Viscosity 16/ft.sec.	Temperature °F	Density gm./cc.
70.0	0.096	75.0	66.55
75.0	0.087	78.4	66.52
80.0	0.079	63.8	66.73

Run 1 (Polyethylene Glycol)

Materials:	Glass Ballotini	Nickel
Wt. of sample:	400.0 gm.	459.0 gm.
From Run	1	1

Bed Height cm.	Manometer Reading arm 1 cm.	arm 2 cm.	Temp. Column °F	Temp. Room °F	Across Taps
18.7	46.1	60.0	71.8	72.0	2-3
	39.7	66.6	71.9	72.4	2-5
	34.2	72.0	71.6	72.5	2-7
25.2	28.1	77.8	71.6	72.6	2-11
	31.8	74.3	71.5	72.4	2-9
	35.0	71.1	71.6	72.5	2-7
	39.1	67.2	71.6	72.5	2-5
	48.3	58.3	71.6	72.6	2-3
31.3	49.9	56.6	71.5	72.8	2-3
	42.9	63.4	71.7	72.8	2-5
	37.3	69.0	71.7	72.9	2-7
	34.3	71.8	71.8	73.0	2-9
	31.3	74.8	71.8	73.0	2-11
37.4	27.8	77.6	70.5	70.6	2-14
	32.8	72.9	70.6	71.1	2-11
	36.6	69.3	70.3	71.4	2-9
	41.0	65.1	70.4	71.6	2-7
	45.7	60.6	70.2	71.4	2-5
	50.9	56.6	70.5	71.5	2-3
56.2	30.4	75.7	71.8	73.5	2-14
	26.5	79.6	72.0	73.4	2-18
	24.6	81.5	72.0	73.4	2-22
	35.7	70.8	72.0	73.4	2-11
	39.1	67.4	72.0	73.5	2-9
	42.8	63.7	71.9	73.3	2-7
	47.0	59.5	72.0	73.8	2-5
	51.1	55.6	72.0	73.9	2-3
33.5	26.7	79.2	71.0	73.1	2-14
	31.4	74.6	71.0	73.0	2-11
	34.8	71.3	71.0	73.0	2-9
	38.8	67.5	71.0	73.1	2-7
	44.3	62.1	71.0	72.8	2-5
	50.2	56.4	71.0	73.2	2-3

Run 1 (Polyethylene Glycol)

Materials:	Glass Ballotini	Nickel
Wt. of Sample:	400.0 gm.	459.0 gm.
From Run	1	1

Bed Height cm.	Manometer Reading arm 1 cm.	arm 1 cm.	Temp. Column °F	Temp. Room °F	Across Taps
37.7	50.8	55.8	71.0	73.2	2-3
	45.9	60.6	71.0	73.4	2-5
	41.3	65.0	71.0	73.4	2-7
	37.1	69.1	71.0	73.4	2-9
67.2	51.4	55.2	72.5	74.0	2-3
	47.5	59.0	72.0	73.6	2-5
	43.9	62.5	71.8	73.6	2-7
	40.6	65.7	71.5	73.4	2-9
	37.4	68.8	71.5	73.3	2-11
	32.8	73.2	71.4	73.2	2-14
	30.1	75.9	71.4	73.3	2-18
	27.9	78.1	71.3	73.4	2-22
	26.2	79.7	71.3	73.4	2-26
	25.1	80.8	71.3	73.2	2-32

Run 2 (Polyethylene Glycol)
Material: Glass Ballotini Ave. Diameter 1.08 mm.
Wt. of Sample 320 gm. Density 2.91 gm./cm^3.

Manometer Reading arm 1 in.		arm 2 in.	Temperature Column °F	Temperature Room °C	Bed Height cm.
2.60	*	2.25	75.6	24.0	9.6
5.50	*	5.30	76.0	24.0	10.8
8.05		5.50	74.5	24.0	40.6
7.00		4.65	74.7	24.2	32.8
5.80		3.70	74.7	24.3	26.7
4.65		2.75	75.0	24.3	22.4
3.35		1.60	75.0	24.5	18.1
2.47		0.80	75.2	24.6	15.1
12.40	*	13.50	75.6	24.6	13.3
9.15		6.40	74.9	24.7	49.4
10.25		7.30	74.8	24.9	66.5
11.05		7.90	74.8	24.8	82.8
9.65		6.80	74.6	24.6	58.6
7.40		5.00	75.0	24.6	35.8
6.35		4.10	75.0	25.0	29.4
5.20		3.15	75.3	25.0	24.1

* $\frac{1}{4}$" Meter (Air) $\frac{1}{4}$" Meter (Mercury)

Run 2 (Polyethylene Glycol)
Material: Alundum Ave. Diameter: 0.645 mm.
Wt. of Sample: 440 gm. Density: 3.95 gm./cm^3.

Manometer Reading arm 1 in.	arm 2 in.	Temperature Column °F	Temperature Room °F	Bed Height cm.
4.40	2.75	71.3	71.2	31.1
4.75	3.00	71.1	71.0	33.5
5.10	3.20	71.3	71.4	36.6
5.50	3.60	71.3	70.9	40.6
6.05	4.10	71.3	71.2	47.0
6.50	4.45	71.4	71.5	53.5
3.85	2.25	71.3	71.2	28.5
3.25	1.70	71.3	71.0	24.4
2.60	1.10	71.3	71.2	20.6
1.95	0.50	71.3	71.3	17.1
1.35	0.00	71.3	71.4	13.8

$\frac{1}{4}$" Meter (Mercury)

Run 2 (Polyethylene Glycol)
Material: Alundum — Ave. Diameter 0.645 mm.
Wt. of Sample: 440.gm. — Density 3.95 gm./cc.

Manometer Reading arm 1 in.	arm 2 in.	Temp. Column °F	Temp. Room °F	Bed Height cm.	Across Taps
52.3	55.2	71.1	71.1	32.6	1-2
49.7	57.7	71.0	70.9		1-4
47.4	59.9	71.0	71.0		1-6
45.1	62.2	71.0	71.2		1-8
42.8	64.5	71.2	71.2		1-10
39.3	67.9	71.3	71.4		1-13
40.9	66.3	71.4	70.9	21.1	1-8
44.5	62.9	71.5	71.2		1-6
48.1	59.4	71.5	71.2		1-4
51.7	55.6	71.2	70.2		1-2
52.5	54.9	71.5	70.6	42.0	1-2
50.5	56.9	71.7	70.8		1-4
48.6	58.8	71.6	71.0		1-6
46.7	60.6	71.6	71.1		1-8
44.8	62.4	71.6	70.9		1-10
42.0	65.2	71.7	71.2		1-13
38.8	68.2	71.7	71.5		1-17

Run 2 (Polyethylene Glycol)

Materials:	Glass Ballotini	Alundum
Wt. of Sample:	320.0 gm.	447.0 gm.
From Run	2	2

Manometer arm 1		Reading arm 2	Temperature Column °F	Temperature Room °C	Bed Height cm.
7.20	*	7.40	73.5	22.0	25.5
7.00	*	6.90	74.0	22.2	24.8
6.50	*	7.50	73.1	22.0	25.4
8.30	*	9.30	73.5	22.4	27.4
9.90	*	10.85	73.7	22.6	28.9
11.70	*	12.70	73.8	22.3	30.5
13.45	*	14.50	73.8	22.3	31.9
2.20		0.50	73.7	22.3	33.6
2.50		0.80	73.7	22.4	36.4
3.05		1.25	73.5	22.4	40.7
3.35		1.55	73.6	22.5	44.1
3.85		2.00	73.9	22.6	48.2
4.30		2.40	73.4	22.4	53.4
4.95		2.90	73.4	22.4	61.1
5.50		3.40	73.2	22.2	69.7
6.10		3.90	73.0	22.1	80.7
6.70		4.35	73.1	22.6	92.8
7.25		4.80	73.0	22.5	108.6
7.75		5.25	73.1	22.7	125.4

* $\frac{1}{4}$" Meter (Air) $\frac{1}{4}$" Meter (Mercury)

Run 2
Viscosity and Density

Temperature °F	Viscosity lb./ft.sec.	Temperature °F	Density gm./cc.
70.0	0.079	70.0	66.67
75.0	0.087	75.0	66.61
80.0	0.096	80.0	66.55

Run 2 (Polyethylene Glycol)

Materials:	Glass Ballotini	Alundum
Wt. of Samples	315.0 gm.	440.0 gm.
From Run	2	2

Manometer Reading arm 1 cm.	arm 2 cm.	Temp. Column °F	Temp. Room °F	Bed Height cm.	Across Taps
31.6	43.9	72.3	72.5	34.0	1-4
27.9	47.6	71.9	72.2		1-6
24.4	51.1	71.7	72.4		1-8
21.1	54.4	71.7	72.0		1-10
16.0	59.4	71.7	72.0		1-13
16.1	59.2	71.2	71.8	45.9	1-17
21.4	54.1	71.2	71.8		1-13
25.5	50.1	71.2	71.2		1-10
28.3	47.4	71.5	72.2		1-8
30.9	44.8	71.5	71.3		1-6
33.6	42.1	71.5	71.1		1-4
36.5	39.5	71.5	71.6		1-2
35.1	40.6	73.8	72.8	24.5	1-2
29.4	46.1	73.8	72.9		1-4
24.2	51.3	73.9	73.9		1-6
19.8	55.6	73.9	74.0		1-8
15.4	59.9	73.9	74.2		1-10
32.6	43.7	74.3	74.3		1-3
27.1	49.5	74.9	74.9		1-5
22.5	54.2	74.8	75.0		1-7
18.4	58.3	74.8	74.8		1-9
37.1	38.6	73.5	72.8	100.0	1-2
35.7	40.1	73.5	73.2		1-4
34.2	41.5	73.2	72.9		1-6
32.9	42.6	73.0	72.8		1-8
31.6	43.9	73.2	73.2		1-10
29.8	45.8	73.3	73.6		1-13
27.1	48.4	73.2	73.0		1-17
24.6	50.7	73.2	72.5		1-21
22.1	53.2	73.2	72.6		1-25
18.8	56.6	73.0	72.5		1-31
14.9	60.3	73.2	72.9		1-39
13.1	62.1	73.1	73.0		1-43

Run 3 (Polyethylene Glycol)
Material: Lead Ave. Diameter 2.05 mm.
Wt. of Sample: 900.0 gm. Density 11.33gm./cc.

Manometer arm 1 in.		Reading arm 2 in.	Temperature Column °F	Temperature Room °F	Bed Height cm.
2.20	*	3.50	73.9	73.4	8.5
4.30	*	5.20	73.8	73.4	9.7
7.20	*	7.80	73.9	73.4	10.9
0.40		1.50	74.0	73.6	12.3
1.00		2.10	74.0	73.4	14.3
1.70		2.80	74.0	73.4	16.3
2.45		3.70	73.9	73.4	18.5
3.05		4.40	73.9	73.4	20.4
4.15		5.80	74.0	73.4	24.2
4.95		6.75	74.0	73.4	27.1
5.80		7.80	74.1	73.6	31.1
6.70		8.85	74.0	73.6	35.3

* ½" Meter (Air) ½" Meter (Mercury)

Run 3 (Polyethylene Glycol)
Material: Steel Ave. Diameter 3.15mm.
Wt. of Sample: 800 gm. Density 7.83 gm./cc.

Manometer arm 1 in.		Reading arm 2 in.	Temperature Column °F	Temperature Room °F	Bed Height cm.
1.30	*	2.80	74.0	73.2	10.1
4.90	*	5.80	73.9	73.2	11.6
1.55		0.55	73.9	73.2	13.0
2.50		1.40	73.9	73.2	14.7
3.35		2.20	73.9	73.4	15.8
4.15		2.85	73.9	73.5	16.9
5.30		3.80	73.9	73.5	18.3
6.60		4.90	74.1	73.4	20.0
8.15		6.10	74.2	73.3	22.1
9.95		7.60	74.2	73.3	24.6
11.10		8.60	74.1	73.4	26.1

* ½" Meter (Air) ½" Meter (Mercury)

Run 3 (Polyethylene Glycol)

Material:	Lead	Steel
Wt. of Sample:	900.0 gm.	800.0 gm.
From Run	3	3

Manometer arm 1 in.	Reading arm 2 in.	Temperature Column °F	Temperature Room °F	Bed Height cm.
14.30 **	11.10	72.6	74.4	18.6
2.45 *	3.70	73.7	72.6	20.2
5.60 *	6.30	74.0	72.8	22.1
9.70 *	9.90	74.3	73.0	24.4
13.50 *	13.20	74.3	73.0	26.4
2.05	1.00	73.8	72.8	28.1
2.50	1.40	73.6	73.0	30.1
3.00	11.80	73.5	72.8	32.1
3.50	2.25	73.6	73.0	34.1
4.30	2.95	74.0	73.0	37.4
5.55	4.00	74.0	73.2	42.1
6.45	4.70	74.0	73.4	45.6
6.95	5.15	74.0	71.2	47.3
7.85	5.90	74.0	71.0	51.6
8.65	6.50	73.8	71.2	56.1
9.15	6.90	73.5	70.8	59.6
9.80	7.40	73.2	70.8	63.8
10.30	7.80	73.3	71.0	67.4
10.70	8.15	73.3	71.0	71.6
11.20	8.55	73.3	71.0	75.1

* $\frac{1}{2}$" Meter (Air) $\frac{1}{2}$" Meter (Mercury)
** $\frac{1}{4}$" Meter (Mercury)

Run 3
Viscosity and Density

Temperature F	Viscosity lb./ft.sec.	Temperature °F	Density lb./ft.^{3}
70.0	0.081	70.0	66.64
75.0	0.088	75.0	66.60
80.0	0.099	80.0	66.49

Run 3 (Polyethylene Glycol)

Material:	Lead	Steel
Wt. of Sample:	900.0 gm.	800.0 gm.
From Run	3	3

Manometer arm 1 cm.	Reading arm 2 cm.	Temperature Column °F	Temperature Room °F	Bed Height cm.	Across Taps
42.5	66.8	73.0	71.2	28.8	2-4
48.9	60.7	73.0	71.4		2-3
48.7	61.0	73.0	71.4		3-4
48.5	60.8	73.0	71.4		4-5
48.5	61.0	73.0	70.9		5-6
48.8	60.4	73.0	71.0		6-7
48.6	60.8	73.0	71.2		7-8
48.8	60.2	73.3	71.0		8-9
48.8	60.6	73.3	71.2		9-10
50.4	58.6	75.0	73.7	44.6	2-3
50.4	58.8	74.7	73.5		3-4
50.3	58.7	75.0	74.3		4-5
50.4	58.7	73.9	72.9		5-6
50.5	58.4	73.8	72.5		6-7
50.4	58.7	74.0	73.2		7-8
50.5	58.4	74.1	73.4		8-9
50.5	58.6	73.9	72.3		9-10
50.4	58.4	74.0	72.8		10-11
50.4	58.7	74.0	73.0		11-12
46.6	62.4	74.3	72.7		12-14
46.7	62.4	74.3	72.6		14-16
49.0	59.8	73.3	71.4	60.1	22-20
49.2	60.0	73.5	71.6		20-18
48.7	60.3	73.6	71.8		18-16
48.8	60.5	73.5	72.0		16-14
48.4	60.5	73.8	72.0		14-12
45.0	64.5	73.8	72.2		12-9
44.8	64.4	73.8	72.3		9-6
44.6	64.8	73.5	72.0		6-3
51.1	57.9	73.5	71.9		3-2
46.9	61.8	73.5	71.7	22.7	2-3
47.1	62.2	73.7	71.7		3-4
46.8	62.1	73.8	71.8		4-5
46.9	62.5	74.0	71.8		5-6
47.2	61.8	74.0	72.0		6-7
49.2	60.1	74.1	72.1		7-8

Run 4 (Polyethylene Glycol)
Material: Nickel Glass — Ave. Diameter 0.542 mm.
Wt. of Sample: 296.0 gm. — Density 4.50 gm/cc.

Manometer arm 1 in.	Reading arm 2 in.	Temperature Column °F	Temperature Room °F	Bed Height cm.
0.30	0.50	75.0	73.4	7.2
0.60	0.80	75.0	73.6	8.4
1.00	1.15	75.1	74.0	9.8
1.35	1.45	74.9	73.6	10.8
1.95	1.95	74.8	73.6	12.7
2.35	2.35	74.9	73.8	14.6
2.95	2.85	74.8	73.6	17.3
3.40	3.20	74.9	73.6	20.1
3.80	3.50	74.9	73.8	23.3
4.30	4.00	74.9	73.6	28.3

$\frac{1}{4}$" Meter (Mercury)

Run 4 (Polyethylene Glycol)
Material: Glass Ballotini — Nickel Glass
Wt. of Sample: 290.0 gm. — 296.0 gm.
From Run 1 — 4

Manometer arm 1 in.	Reading arm 2 in.	Temperature Column °F	Temperature Room °F	Bed Height cm.
0.35	0.50	76.7	74.8	16.8
0.70	0.85	76.8	74.8	19.9
1.20	1.30	76.4	74.4	22.9
1.65	1.70	75.8	74.1	25.7
2.10	2.10	75.6	74.3	28.5
2.60	2.55	75.3	74.2	32.0
3.15	3.00	75.4	74.4	36.3
* 3.65	3.40	75.4	74.2	41.5
4.20	3.85	75.5	74.3	48.3
4.65	4.20	75.6	74.4	56.3

$\frac{1}{4}$" Meter (Mercury)
* Homogeneous Mixing Point

Run 1 (Water)
Material: Glass Ballotini Ave. Diameter 1.08 mm.
Wt. of Sample: 400.0 gm. Density 2.91 gm./cc.

Manometer Reading arm 1 in.	arm 2 in.	Temperature Column °F	Temperature Room °C	Bed Height cm.
3.40	1.30	78.9	24.3	15.80
2.65	0.65	78.8	24.3	14.60
2.05	0.05	78.8	24.3	13.40
1.45	0.45	78.7	24.3	11.90
4.15	2.00	78.7	24.3	17.00
4.80	2.60	78.7	24.2	17.00
5.35	3.05	78.7	24.2	18.7
5.90	3.45	78.7	24.2	19.4
6.50	4.00	78.7	24.2	20.3
7.10	4.50	78.7	24.2	21.0
7.85	5.10	78.7	24.2	22.1
8.50	5.65	78.7	24.0	22.9
9.05	6.10	78.7	24.0	23.6
10.15	7.00	78.7	24.0	25.2
11.40	8.00	78.7	24.0	26.8
12.65	9.00	78.7	24.0	28.6
13.85	9.95	78.7	24.0	30.3
15.10	10.95	78.7	24.0	32.1

$\frac{1}{2}$" Meter (Mercury)

Run 2 (Water)
Material: Alundum — Ave. Diameter 0.767 mm.
Wt. of Sample: 500.0 gm. — Density: 3.95 gm/cc.

Manometer Reading arm 1 in.	arm 2 in.	Temperature Column °F	Temperature Room °C	Bed Height cm.
0.25	0.55	69.5	22.5	12.0
0.55	0.85	69.5	22.5	13.0
0.95	1.20	69.5	22.5	14.0
1.35	1.55	69.5	22.5	14.8
1.90	2.05	69.5	22.5	15.9
2.35	2.40	69.5	22.6	16.7
2.95	2.95	69.2	22.6	17.8
3.45	3.35	69.2	22.6	18.6
4.05	3.85	69.1	22.6	19.5
4.60	4.30	69.1	22.6	20.5
5.20	4.80	69.0	22.6	21.4
5.95	5.40	69.0	22.6	22.6
6.70	6.00	69.0	22.6	23.8
7.20	6.45	69.0	22.6	24.7
7.95	7.00	69.0	22.6	25.9

½" Meter (Mercury)

Run 5 (Water)
Material: Glass Ballotini — Ave. Diameter 1.83 mm.
Wt. of Sample: 400.0 gm. — Density 2.91 gm/cc.

Manometer Reading arm 1 in.	arm2. in.	Temperature Column °F	Temperature Room °C	Bed Height cm.
0.85	1.05	70.2	23.0	11.0
1.95	2.00	70.2	23.0	12.0
3.40	3.30	70.1	23.0	13.3
4.60	4.25	70.1	23.0	14.1
5.90	5.30	70.1	23.0	15.0
6.90	6.10	70.1	23.0	15.6
8.10	7.00	70.1	23.0	16.2
9.45	8.00	70.1	23.0	16.9
10.60	9.05	70.1	23.0	17.6
11.80	10.00	70.1	23.0	18.2
13.10	11.00	70.1	23.0	18.7

½" Meter (Mercury)

Run 3 (Water)
Material: Alundum Ave. Diameter 10.645 mm.
Wt. of Sample: 500.0 gm. Density 3.95 gm/cc.

Manometer Reading arm 1 in.	arm 2 in.	Temperature Column °F	Temperature Room °C	Bed Height cm.
0.25	0.50	70.0	23.2	12.6
0.65	0.95	70.0	23.2	14.0
1.10	1.30	70.0	23.2	15.3
1.50	1.70	70.0	23.2	16.2
1.95	2.05	70.0	23.2	17.3
2.35	2.40	70.0	23.0	18.1
2.80	2.80	70.0	73.0	19.0
3.45	3.35	70.0	23.0	20.3
4.10	3.90	70.0	23.0	21.5
4.80	4.45	70.0	23.0	22.7
5.50	5.05	70.0	23.0	24.3
6.15	5.55	70.0	23.0	25.6
6.50	6.00	71.1	23.0	26.3
7.45	6.60	71.1	23.0	28.4
8.10	7.10	71.1	23.0	29.6

½" Meter (Mercury)

Run 4 (Water)
Material: Alundum Ave. Diameter 0.912 mm.
Wt. of Sample: 500.0 gm. Density 3.95 gm/cc.

Manometer Reading arm 1 in.	arm 2 in.	Temperature Column °F	Temperature Room °C	Bed Height cm.
0.30	0.50	74.2	22.6	11.4
0.80	1.00	74.2	22.6	12.8
1.20	1.35	74.2	22.6	13.7
1.95	2.00	74.2	22.6	14.9
2.55	2.50	74.3	22.6	15.8
3.20	3.10	74.2	22.6	16.7
3.80	3.60	74.2	22.6	17.5
4.45	4.10	74.2	22.6	18.3
5.15	4.70	74.3	22.6	19.2
5.80	5.20	74.3	22.6	20.0
6.70	5.95	74.3	22.6	21.1
7.70	6.75	74.3	22.6	22.4

½" Meter (Mercury)

Run 6 (Water)
Material: Crystalon Ave. Diameter 1.08 mm.
Wt. of Sample: 350.0 gm. Density

Manometer Reading arm 1 in.	arm 2 in.	Temperature Column °F	Temperature Room °C	Bed Height cm.
10.80 *	10.60	70.0	19.6	11.3
3.10 *	3.20	70.0	19.6	9.8
0.20	2.85	70.0	19.7	12.5
0.75	3.30	70.0	19.7	13.3
1.55	4.00	70.0	19.7	14.4
2.50	4.75	70.0	19.4	15.5
3.35	5.45	70.0	19.6	16.5
4.30	6.20	70.0	19.9	17.6
5.50	7.20	70.1	19.8	19.2
7.20	8.60	70.1	19.6	21.2
8.80	9.80	70.1	19.7	23.2
10.30	11.00	70.2	19.8	25.2
11.70	12.15	70.3	19.9	27.1

* ½" Meter (Air) ½" Meter (Mercury)

Run 13
Material: Alundum Crystalon
Wt. of Sample: 350.0 gm. 350.0 gm.
From Run 3 Run 6

Manometer Reading arm 1 in.	arm 2 in.	Temperature Column °F	Temperature Room °C	Bed Height cm.
14.00 *	13.60	70.4	19.8	21.7
0.05	2.70	70.5	20.0	22.9
0.40	3.00	70.6	20.0	23.7
1.00	3.55	70.7	20.0	25.6
1.80	4.20	70.6	20.0	27.7
2.80	5.00	70.7	19.9	30.1
3.80	5.80	70.7	20.0	32.6
5.45	7.10	70.8	20.0	36.7
7.20	8.50	70.8	20.0	41.3
9.40	10.25	71.4	20.0	47.3
10.60	11.25	70.9	20.0	51.7
11.95	12.30	71.0	19.9	56.0
13.60	13.75	70.8	20.0	63.0

* ½" Meter (Air) ½" Meter (Mercury)

Run 7 (Water)
Material: Glass Ballotini — Ave. Diameter 1.08 mm.
Wt. of Sample: 320.8 gm. — Density 2.91

Manometer arm 1 in.	Reading arm 2 in.	Temperature Column °F	Temperature Room °C	Bed Height cm.
4.60 *	3.20	71.8	22.9	9.1
8.70 *	6.60	71.8	22.9	9.9
14.50 *	11.50	71.9	23.0	10.6
0.15	2.80	71.9	22.9	11.4
0.90	3.40	72.1	22.8	12.3
1.80	4.20	72.3	22.9	13.4
2.60	4.85	72.3	22.9	14.2
3.50	5.55	72.4	22.9	15.2
4.40	6.30	72.3	22.9	16.0
5.45	7.20	72.3	23.0	17.1
6.45	7.90	72.4	23.0	18.1
7.50	8.80	72.5	23.0	19.2
8.40	9.50	72.5	23.0	20.1

* ½" Meter (Air) ½" Meter (Mercury)

Run 7 (Water)
Material: Nickel-Glass — Ave. Diameter 0.542 mm.
Wt. of Sample: 334.0 gm. — Density 4.50 gm/cc.

Manometer arm 1 in.	Reading arm 2 in.	Temperature Column °F	Temperature Room °C	Bed Height cm.
3.10 *	3.40	67.2	19.6	7.0
7.10 *	7.30	67.7	19.5	7.6
12.70 *	12.80	67.3	19.5	8.4
0.20	2.85	67.4	19.6	9.1
0.90	3.45	67.6	19.6	10.0
2.00	4.35	67.8	19.8	11.3
3.10	5.25	68.1	20.0	12.3
4.50	6.40	68.3	20.0	13.8
6.50	8.00	68.3	19.7	15.0
2.10	4.50	68.4	19.6	11.4
0.50	3.10	68.5	19.6	9.6
0.10	2.55	68.6	19.5	8.7

* ½" Meter (Air) ½" Meter (Mercury)

Run 7 (Water) Mixture	Glass Ballotini	Nickel Glass
Wt. of Sample:	320.0 gm.	49.5 gm.
From Run	7	7

Manometer arm 1 in.	Reading arm 2 in.	Temperature Column °F	Temperature Room °C	Bed Height cm.
3.10 *	4.90	70.6	22.0	10.1
4.80 *	6.30	70.5		10.5
8.80 *	10.30	70.3		11.3
0.05	2.50	70.3		12.2
0.50	3.05	70.2		13.1
1.15	3.60	70.2		14.1
1.90	4.20	70.2		15.0
2.70	4.95	70.2		16.1
3.90	5.90	70.3		17.4
5.45	7.15	70.2		19.2
7.00	8.40	70.2		21.1
9.20	10.05	70.2		23.5
10.10	10.80	70.2		24.7
12.50	12.80	70.2		27.5

* ½" Meter (Air) ½" Meter (Mercury)

Run 7 (Water) Mixture	Glass Ballotini	Nickel-Glass
Wt. of Sample:	320.0 gm.	99.0 gm.
From Run	7	7

Manometer arm 1 in.	Reading arm 2 in.	Temperature Column °F	Temperature Room °C	Bed Height cm.
2.70 *	4.90	70.4	22.0	11.1
11.20 *	13.00	70.5	22.0	13.0
0.20	2.80	70.5	22.0	14.1
1.00	3.50	70.3	22.0	15.4
2.15	4.45	70.3	22.0	17.0
3.20	5.30	70.3	22.0	18.4
4.40	6.25	70.3	22.1	20.0
5.50	7.20	70.3	22.2	21.4
6.80	8.20	70.3	22.2	23.2
7.90	9.10	70.3	22.1	24.6
9.45	10.40	70.3	22.2	26.7
11.20	11.80	70.3	22.2	29.3

* ½" Meter (Air) ½" Meter (Mercury)

Run 7 (Water)

Material:	Glass Ballotini	Nickel Glass
Wt. of Sample:	320.0 gm.	165.0 gm.
From Run	7	7

Manometer arm 1 in.	Reading arm 2 in.	Temperature Column °F	Temperature Room °C	Bed Height cm.
3.70 *	6.30	70.8	22.4	12.6
7.60 *	10.10	70.9	22.3	13.6
11.30 *	13.60	70.8	22.3	14.3
0.15	2.75	70.7	22.3	15.5
1.00	3.50	70.7	22.3	17.0
2.00	4.30	70.6	22.4	18.6
3.20	5.30	70.6	22.3	20.4
4.60	6.40	70.7	22.3	22.4
6.15	7.70	70.7	22.3	24.7
7.15	8.50	70.7	22.4	26.3
8.80	9.70	70.6	22.5	28.5
10.30	11.00	70.6	22.5	31.0

* $\frac{1}{4}$" Meter (Air) $\frac{1}{4}$" Meter (Mercury)

Run 7 (Water)

Material:	Glass Ballotini	Nickel Glass
Wt. of Sample	320.0 gm.	247.5 gm.
From Run	7	7

Manometer arm 1 in.	Reading arm 2 in.	Temperature Column °F	Temperature Room °F	Bed Height cm.
3.10 *	6.00	71.0	22.6	14.3
8.40 *	11.50	71.0	22.7	15.9
0.00	2.60	71.0	22.6	17.4
0.65	3.20	71.0	22.5	18.8
1.30	3.75	70.9	22.5	20.2
2.10	4.45	70.9	22.6	21.6
3.10	5.20	71.0	22.7	23.3
4.30	6.20	71.0	22.7	25.3
5.00	6.75	71.0	22.8	26.5
5.85	7.40	71.0	22.8	28.1
7.10	8.50	71.0	22.9	30.3

* $\frac{1}{4}$" Meter (Air) $\frac{1}{4}$" Meter (Mercury)

Run 7 (Water)		
Material:	Glass Ballotini	Nickel Glass
Wt. of Sample:	194.0 gm.	300.0 gm.
From Run	7	7

Manometer Reading arm 1 in.	arm 2 in.	Temperature Column °F	Temperature Room °C	Bed Height cm.
2.80 *	3.60	69.7	23.0	11.6
6.70 *	7.30	70.0	23.0	12.7
13.30 *	13.50	69.8	23.0	14.2
0.40	3.00	69.7	23.0	15.6
1.25	3.75	69.7	23.0	17.1
2.05	4.40	69.5	23.0	18.4
3.05	5.20	69.6	23.1	20.0
4.20	6.15	69.6	23.0	21.8
5.05	6.80	69.5	23.0	23.1
6.20	7.70	69.6	23.0	24.9
7.75	8.90	69.5	23.0	27.3

* $\frac{1}{4}$" Meter (Air) $\frac{1}{4}$" Meter (Mercury)

Run 7 (Water)		
Material:	Glass Ballotini	Nickel -Glass
Wt. of Sample:	38.8 gm.	300.0 gm.
From Run	7	7

Manometer Reading arm 1 in.	arm 2 in.	Temperature Column °F	Temperature Room °C	Bed Height cm.
6.40 *	6.70	70.0	22.9	8.0
8.70 *	8.90	70.0	23.0	8.4
14.20 *	14.20	69.8	23.0	9.1
0.45	3.00	69.7	23.0	10.0
1.30	3.70	69.7	23.0	11.0
2.50	4.75	69.6	23.0	12.4
3.90	5.80	69.5	23.0	13.8
4.90	6.65	69.4	23.0	14.9
5.60	7.20	69.4	23.0	15.7

* $\frac{1}{4}$" Meter (Air) $\frac{1}{4}$" Meter (Mercury)

Run 7 (Water)

Material:	Glass Ballotini	Nickel Glass
Wt. of Sample:	300.0 gm.	19.4 gm.
From Run	7	7

Manometer Reading arm 1 in.	arm 2 in.	Temperature Column °F	Temperature Room °C	Bed Height cm.
4.70 *	4.70	68.9	22.2	7.1
8.00 *	7.80	68.8	22.2	7.6
11.90 *	11.60	68.8	22.2	8.1
0.05	2.65	68.7	22.3	8.7
0.55	3.10	68.7	22.2	9.4
1.45	3.90	68.6	22.2	10.4
2.35	4.60	68.6	22.3	11.4
3.50	5.55	68.7	22.3	12.5
4.50	6.35	68.7	22.4	13.6
5.35	7.00	68.7	22.4	14.3

* $\frac{1}{4}$" Meter (Air) $\frac{1}{4}$" Meter (Mercury)

Run 8 (Water)

Material:	Glass Ballotini	Nickel Glass
Wt. of Sample:	320.8 gm.	334.0 gm.
From Run	7	7

Manometer Reading arm 1 in.	arm 2 in.	Temperature Column °F	Temperature Room °C	Bed Height
3.20 *	3.40	69.8	20.0	15.9
7.90 *	7.80	69.0		17.6
12.20 *	12.20	69.2		18.9
0.0	2.70	69.4		20.1
0.50	3.10	69.5		21.3
1.25	3.75	69.5		23.1
2.20	4.55	69.6		25.1
3.20	5.30	69.5		27.0
4.40	6.30	69.7		29.5
5.40	7.10	69.9		31.4
6.35	7.85	70.0		33.3
7.45	8.75	69.8		35.7
8.80	9.80	69.9		38.3
9.90	10.70	70.0		41.3

* $\frac{1}{2}$" Meter (Water) $\frac{1}{2}$" Meter (Mercury)

Run 9 (Water)
Material: Alundum Ave. Diameter 0.912 mm.
Wt. of Sample: 400.0 gm. Density 3.95 gm/cc.

Manometer arm 1 in.	Reading arm 2 in.	Temperature Column °F	Temperature Room °C	Bed Height cm.
-0.15	0.55	73.0	23.0	8.5
-0.70	2.05	73.0	23.0	9.9
-0.45	2.35	72.7	23.0	10.4
0	2.80	72.6	23.0	11.1
0.35	3.05	72.5	23.0	11.5
1.25	3.80	72.5	23.0	12.6
1.90	4.40	72.5	23.0	13.5
2.95	5.20	72.7	23.0	14.4
3.80	5.90	72.7	23.0	15.3
4.70	6.70	72.7	23.0	16.2
5.65	7.40	72.6	22.6	17.1
6.70	8.20	72.6	23.0	18.1
7.80	9.05	72.7	23.0	19.2
8.90	10.05	72.6	22.9	20.5
* Above run without cataphote bed on top				
Below - 300.0 gm. of cataphote on top				
-0.50	2.25	67.6	20.0	10.2
-0.15	2.55	67.6	20.0	10.7
0.25	2.95	67.8	20.2	11.3
0.75	3.40	67.9	20.2	12.0
1.25	3.85	68.0	20.2	12.6
2.05	4.45	68.1	20.3	13.4
2.85	5.15	68.8	20.3	14.2
3.60	5.70	68.9	20.3	15.0
4.25	6.25	69.0	20.3	15.6
5.15	6.90	69.1	20.3	16.5
5.95	7.60	69.2	20.3	17.4
6.70	8.20	69.2	20.3	18.2
7.30	8.70	69.8	20.3	18.8
7.80	9.10	69.9	20.3	19.4

½" Meter (Mercury)

Run 9 (Water)
Material: Cataphote Ave. Diameter 0.767 mm.
Wt. of Sample: 300.0 gm. Density 2.47 gm/cc.

Manometer arm 1 in.	Reading arm 2 in.	Temperature Column °F	Temperature Room ° C	Bed Height cm.
-0.50	2.25	67.6	20.2	15.0
-0.15	2.55	67.6	20.2	16.3
0.25	2.95	67.8	20.2	17.8
0.75	3.40	67.9	20.3	19.4
1.25	3.85	68.0	20.3	21.1
2.05	4.45	68.1	20.3	23.7
2.85	5.15	68.8	20.3	26.3
3.60	5.70	68.9	20.3	28.9
4.25	6.25	69.0	20.3	31.5
5.15	6.90	69.1	20.3	35.2
5.95	7.60	69.2	20.3	39.1
6.70	8.20	69.2	20.3	43.3
7.30	8.70	69.8	20.3	46.7
7.80	9.10	69.9	20.3	49.9

½" Meter (Mercury)

Run 10 (Water)
Material: Nickel Ave. Diameter 0.384 mm.
Wt. of Sample: 800.0 gm. Density 8.92 gm/cc.

Manometer Reading arm 1 in.	arm 2 in.	Temperature Column °F	Temperature Room °C	Bed Height cm.
6.60 *	3.10	72.2	22.5	8.0
10.60 *	6.90	72.3	22.5	8.6
14.60 *	10.60	72.4	22.5	9.1
0.0	2.60	72.5	22.6	9.5
0.40	3.00	72.4	22.7	10.0
1.90	4.20	72.7	22.7	11.2
4.10 *	0.70	72.6	22.8	7.6
2.40 *	1.00	72.5	22.6	7.1

* ½" Meter (Air) ½" Meter (Mercury)

Run 10 (Water)
Material: Alundum Nickel
Wt. of Sample: 400.0 gm. 800.0 gm.
From Run 10 10

Manometer Reading arm 1 in.	arm 2 in.	Temperature Column °F	Temperature Room °C	Bed Height cm.
1.50 *	3.30	71.2	22.8	15.5
4.50 *	6.10	71.6	23.0	15.9
7.00 *	8.50	71.7	23.0	16.2
11.00 *	12.50	71.7	23.0	17.0
0.05	2.6	71.7	23.3	17.7
0.30	2.90	72.0	23.4	18.5
0.50	3.10	72.1	23.4	19.0
0.95	3.40	72.3	23.2	19.7
1.45	3.90	72.3	23.3	20.5
2.00	4.35	72.3	23.3	21.4
2.50	4.70	72.3	22.8	22.0
3.30	5.40	72.5	23.0	23.0
4.30	6.20	72.6	23.3	24.1
5.40	7.00	72.7	23.2	25.2
6.35	7.85	72.7	23.1	26.3
7.25	8.55	72.6	23.0	27.2
8.20	9.35	72.8	23.0	28.3
9.00	10.00	72.7	23.0	29.2

* ½" Meter (Air) ½" Meter (Mercury)

R 10 (Water)

Material:	Alundum	Ave. Diameter	1.52 mm.
Wt. of Sample:	500 gm.	Density	3.95 gm/cc.

Manometer Reading arm 1 in.	arm 2 in.	Temperature Column °F	Temperature Room °C	Bed Height cm.
-0.30	2.30	23.4	65.0	10.9
0.15	2.75	23.4	65.2	11.3
0.85	3.40	23.7	65.5	12.0
1.35	3.35	23.5	65.7	12.4
3.20	5.30	23.4	65.7	13.5
4.95	6.75	23.5	65.8	14.4
7.30	8.60	23.5	66.0	15.7
9.00	10.00	23.5	66.3	16.5
10.80	11.40	23.5	66.5	17.3
8.10	9.20	23.6	66.5	15.8
5.30	7.00	23.6	66.5	14.4
4.10	6.00	23.6	66.5	13.7
2.85	5.05	23.4	66.6	13.0
1.10	4.05	23.4	67.0	12.3
6.50	8.00	23.3	67.2	15.1

$\frac{1}{2}$" Meter (Mercury)

Run 11 (Water)

Material:	Alundum	Crystalon
Wt. of Sample:	350.0 gm.	350.0 gm.
From	Run 2	Run 6

Manometer Reading arm 1 in.	arm 2 in.	Temperature Column °F	Temperature Column °C	Bed Height cm.
1.30 *	8.80	71.6	22.0	18.6
4.00 *	11.30	71.6	22.0	19.5
0.35	2.30	71.5	22.0	21.0
-0.10	2.60	71.7	22.0	21.9
0.30	2.90	71.8	22.0	23.0
1.10	3.60	72.3	22.1	25.1
2.00	4.35	72.5	22.1	27.1
3.00	5.15	72.5	22.2	29.5
3.90	5.90	72.6	22.0	31.5
5.10	6.90	72.6	22.0	34.2
6.60	8.00	72.7	23.7	37.3
7.40	8.80	71.9	23.7	39.8
8.35	9.90	71.9	23.5	43.0
10.20	11.00	71.9	23.4	46.7
11.30	11.80	72.0	23.1	49.3

* $\frac{1}{2}$" Meter (Air) $\frac{1}{2}$" Meter (Mercury)

Run 12 (Water)				
Material: ;		Glass Ballotini	Alundum	
Wt. of Sample:		320.8 gm.	450.0 gm.	
From		Run 1	Run 3	
Manometer arm 1 in.	Reading arm 2 in.	Temperature Column °F	Temperature Room °C	Bed Height cm.
-0.90	1.80	67.8	20.3	20.5
-0.55	2.15	68.2	20.5	22.4
-0.25	2.45	68.3	20.2	23.7
0.20	2.90	68.3	20.2	25.3
0.55	3.20	68.6	20.2	26.4
1.00	3.60	68.9	20.2	27.9
1.60	4.05	69.0	20.2	29.4
2.15	4.50	69.2	20.2	30.9
2.80	5.05	69.5	20.2	32.7
3.60	5.75	69.8	20.3	34.8
4.70	6.60	70.0	20.3	37.5
5.60	7.30	70.0	20.3	39.8
6.40	8.00	70.0	20.3	42.0
7.20	8.55	70.0	20.4	43.9
7.80	9.10	70.2	20.5	45.9
8.90	10.00	70.2	20.5	48.7
9.65	10.50	70.3	20.6	51.0
10.30	11.00	72.0	20.8	48.0
11.40	12.00	72.3	21.0	49.5
10.80	11.40	71.9	21.0	49.0
10.30	11.00	71.9	21.0	47.0
9.00	10.00	71.9	21.0	47.7
7.75	9.00	72.2	20.7	45.0
6.35	7.95	72.0	21.0	41.2
5.20	6.95	71.9	21.0	38.2
4.00	6.00	71.9	21.0	35.0
2.70	5.00	71.9	21.0	31.8
1.50	4.00	72.1	21.0	28.7
0.25	2.95	72.0	21.0	28.7
-0.70	2.00	72.0	21.0	21.3

½" Meter (Mercury)

APPENDIX V - MEASUREMENT OF LONGITUDINAL PARTICLE CONCENTRATION (PROPOSED METHOD)

An informative method of measuring longitudinal particle concentration gradients, and hence segregation by size, is a plot of P ratio vs. vertical position in the column, using average porosity of the bed as a parameter. Such a plot is shown in Figure 36 for the fluidization of 2.28 mm. glass ballotini by the polyethylene glycol solution. The curves obtained give a measure of the fraction solids at a particular position relative to the average fraction solids in the bed, as can be seen by analyzing the following equations

$$\frac{(\Delta p/L)_i}{(\Delta p/L)_{theory}} = P = \frac{(1-\epsilon)_i(\rho_s - \rho)}{(1-\epsilon)_m(\rho_s - \rho)} \qquad (A)$$

or

$$(1-\epsilon)_i = (1-\epsilon)_m \cdot P \qquad (B)$$

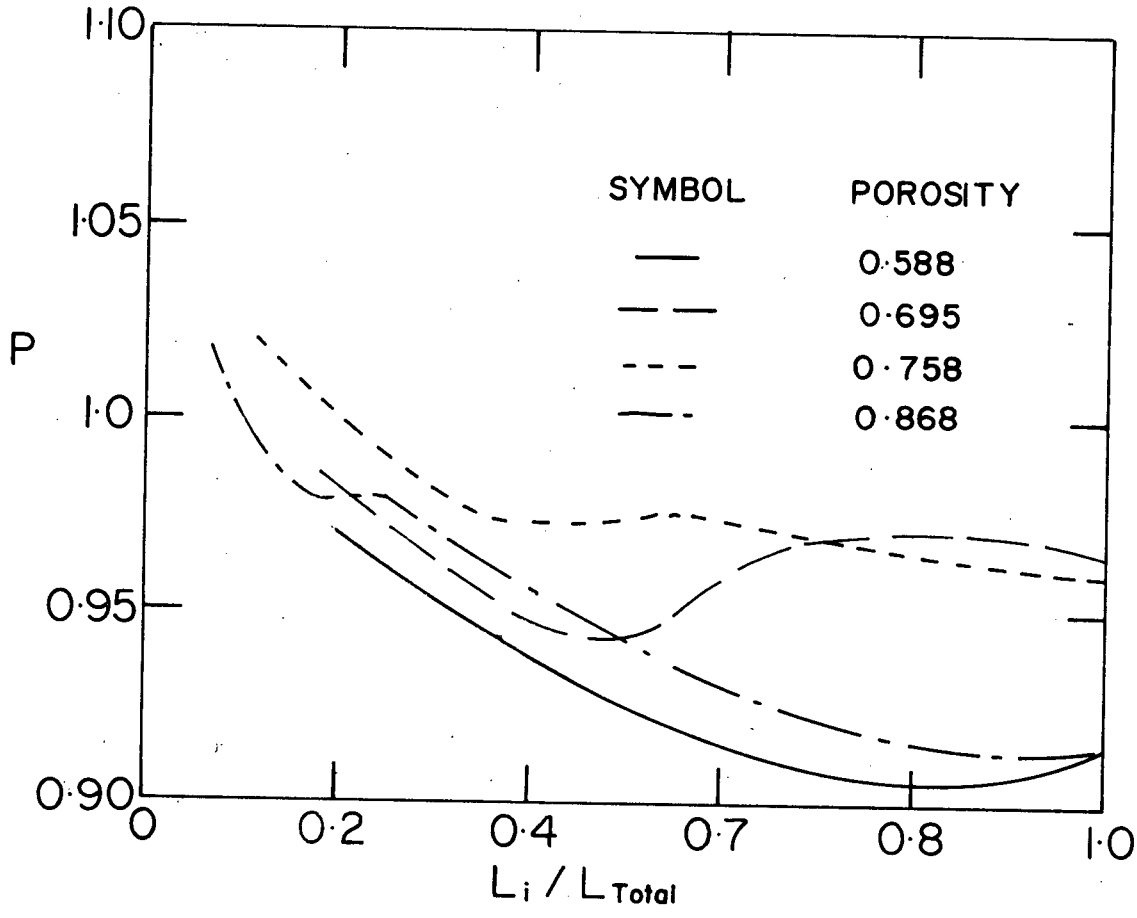

Figure 36. Plot of P Ratio Profiles at Various Average Porosities.